POLITECHNIKA LUBELSKA

António Gaspar-Cunha

Polymer Processing

Plasticizing in Single Screw Extruders

Lublin 2021

PODRĘCZNIKI

Polymer Processing

Plasticizing in Single Screw Extruders

Podręczniki – Politechnika Lubelska

Politechnika Lubelska
Wydział Mechaniczny
ul. Nadbystrzycka 36
20-618 LUBLIN

António Gaspar-Cunha

Polymer Processing

Plasticizing in Single Screw Extruders

Wydawnictwo
Politechniki Lubelskiej

Reviewers:

Wiesław Frącz, DSc, PhD, Eng., Associate Prof. Rzeszow University of Technology,

This book was written in the framework of the ULAM project, financed by NAWA, the Polish National Agency for Academic Exchange, under grant PPN/ULM/2020/1/00125, from which the author was the beneficiary.

Publication approved by the Rector of Lublin University of Technology

ISBN: 978-83-7947-460-8

Publisher: Wydawnictwo Politechniki Lubelskiej
www.biblioteka.pollub.pl/wydawnictwa
ul. Nadbystrzycka 36C, 20-618 Lublin
tel. (81) 538-46-59

Printed by: DjaF – 30-092 Kraków, ul. Kmietowicza 1/1
www.djaf.pl

Table of contents

1. Introduction

In polymer processing one of the most important steps is plasticization, which consists of transforming the raw material, initially in the solid state (in the form of granules or powder), into a viscous fluid. In the plastics processing industry, practically all polymers go through a plasticization process, where one or more screws force the solid material to pass through heated areas of a cylinder where it melts [TAD 70, RAU 86, AGA 96, WHI 90, STE 95, TAD 06, GAS 09]. This thermomechanical process occurs in injection molding, blow-molding, single-screw and twin-screw extrusion and even the raw material (in sheet form) used in the thermoforming is manufactured using an extruder.

Due to the unique characteristics of polymers, especially their thermal, physical and rheological properties, the study of the plasticization process is not trivial, and it is therefore necessary to study the influence that these properties may have on the performance of the process. On the other hand, the geometry of the system also plays an important role in this same performance, since, of course, it will not be indifferent to use a single-screw extruder, with or without barrier screws and/or mixing sections, or a twin-screw extruder, counter or co-rotating, or even multi-screw extruders. Finally, it is also important to mention that the processing conditions defined in the machine have a decisive influence on the plasticization performance [TAD 70, RAU 86, WHI 90].

From the above, it can be said that the performance of a plasticization process depends on variables related to the properties of the polymers, the geometry of the system and the processing conditions. In order to develop methodologies capable of predicting the behavior of polymer plasticization systems, scientific, experimental and theoretical studies were carried out that allowed to relate the process variables to their performance, thus enabling the development of mathematical models, later transformed into computational models, capable of helping the Polymer Engineer to predict the behavior of the systems [TAD 70, RAU 86, WHI 90, O'BR 92, GAS 09].

This text intends to present the mathematical models developed for the calculation of the performance predictions of single-screw extruders (including barrier screws, mixing sections and grooved cylinders) according to the properties of the polymers, the geometry of the system and the operating conditions. It is also intended that these notes serve to support the Polymer Processing Engineering courses. In this sense, in the following chapters the basic concepts necessary to understand the process, the relevant properties, and how they can be quantified in the models presented, and the mathematical models developed will be presented. In the final part of some chapters, practical exercises will be proposed.

Finally, this book was written in the framework of the an ULAM project financed by NAWA, the Polish Agency for research. The present book is one of the results of the work done by the author during the stay at Lublin University of Technology (LUT) to carry out the ULAM project from which was the beneficiary. The project was settled down in different aspects, scientific and pedagogical. In what concerns the later, two different parts were addressed, writing the present pedagogical book and giving classes in the field of polymer processing. Specifically, the book and the software previously developed are the main basis for the course taught.

2. Polymer processing

2.1. Overview

The processing of polymers involves a sequence of steps, and the path to get from the raw material (polymers and additives) to the final product is not unique, it depends on the material, the processing technique and the product to be manufactured. The steps usually present in this process are: a) preparation of the material; b) processing and c) manufacturing and finishing operations [TAD 06].

Several techniques are available that allow the material to be prepared for processing. Of these, the following stand out: the incorporation and mixing of additives, the mixing of polymers, the modification of polymers, the incorporation of recycled materials and the homogenization and granulation. In most cases, and in industrial practice, the raw material is purchased already ready to be processed, so there is no need for any preparation stage.

After the raw material is prepared, it will be necessary to transport it to the processing machine, considering that there are several technologies available to make the transformation of the raw material into the desired product. The most relevant are: extrusion, injection molding, thermoforming, blow-molding, rotational molding, calendaring and compression and/or transfer molding. The choice of the technique to use depends fundamentally on the characteristics intended for the final product. These characteristics determine, in most practical cases, the choice of polymer and processing technique.

Finally, due to several reasons, mainly related to the processing technique used, an additional step may be necessary where some manufacturing and finishing operations are performed. For example, in the case of injection molding it may be necessary to separate runners and excess material. In other cases, the final product will only be completely ready after carrying out some operations, such as: welding, machining, surface treatment, printing and/or painting.

Figure 1 shows schematically the sequence of the steps usually present and referred to above. At this point it is important to say that the steps presented are the current practice of the processing industry. Of course, additional steps will be required that involve the production of the polymers and additives themselves. These tasks are carried out by large chemical companies that promote the polymerization of different polymers in large chemical reactors, which are outside the scope of these notes.

Thus, there are different possibilities with regard to operations carried out within the scope of polymer processing: i) post-reactor processing, where granules are produced from the monomers and additives for the final manufacturers; ii) composition of polymers, in which granules are produced from virgin material and additives; iii) reactive extrusion, in which the base polymers can be chemically modified and materials are produced for the final manufacturer or composers; iv) mixture of polymers, where two polymers are made compatible with the aim of obtaining mixtures of polymers with special properties; v) manufacturers of plastic products, which with the raw material of other suppliers produce the final parts [TAD 06].

Figure 1 shows the fundamental steps of a manufacturer of final products. As can be seen in the figure, there are several paths that can be taken. You can enter the system by composing polymers with additives using mixers or twin-screw extruders. Then, the raw material stored abroad will be transported to the machines by solid transport systems. In the following steps the plasticization of the plastic occurs, that is, its transformation into a homogeneous fluid.

Plasticization involves (as will be seen in more detail below) the transport of solids in the hopper and screw, the melting, mixing and pumping of the melt. During this process, the necessary pressure is created so that the molten polymer is able to pass through the die, in the case of extrusion, or the mold channels, in the case of injection molding. The last fundamental step is to cool the polymer after it has acquired its final shape. In the case of extrusion, there is a set of equipment, called an extrusion line, which allows the tasks necessary for the production of the final product. While in the case of injection molding, the part is cooled inside the mold cavity, the heat being removed by cooling channels where water flows [TAD 70]. As previously mentioned, this text will be dedicated to plasticization in the single screw extrusion process.

The term extrusion identifies polymer processing techniques where the molten polymer is forced to pass through an orifice (the die) that gives it its final shape. The pressure required for the polymer to pass through the die is obtained with the help of one or more screws rotating inside a heated cylinder.

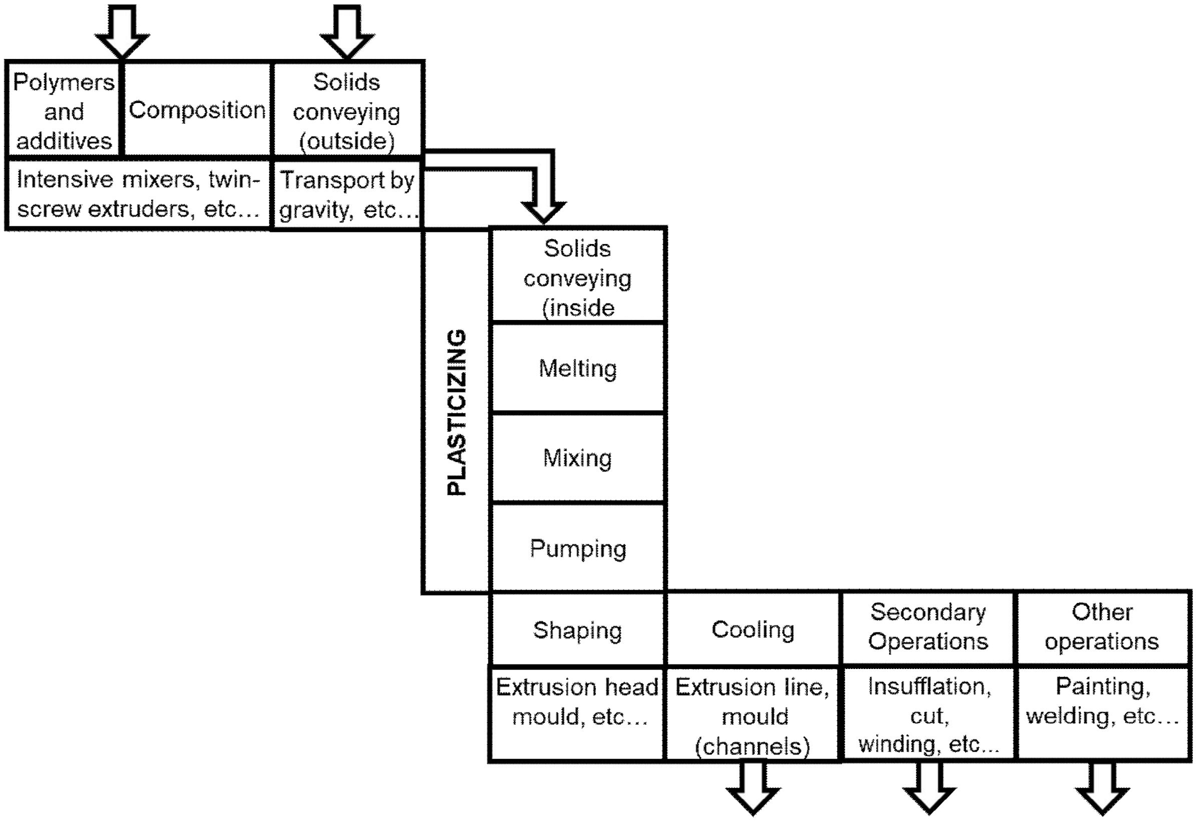

Figure 1- Polymer processing steps

Figure 2 shows a diagram of the of a single screw extruder operation. The solid polymer is introduced into the hopper which, by gravity, falls into the cylinder (or barrel, these two words will e used indifferently). An Archimedes type screw rotates (at a constant speed, *N*) inside a cylinder heated by heating bands. Due to this rotation speed, the solid polymer is transported to the heated zone of the cylinder where it melts. Then, the molten polymer is mixed, homogenized and pressurized. Due to the pressure thus generated, the molten polymer is forced to pass through the die that gives it its final shape.

Thus, an extruder, for the plastics industry, must ensure the performance of five basic functions: i) transporting the solid material; ii) melt the solid material; iii) mix and homogenize the components of the raw material; iv) homogenize the temperature of the material to be extruded; v) pump the melt through the die at a constant rate [TAD 70, TAD 06, CHU 10, GAS 09].

However, it is important to note that in the manufacture of products by extrusion, additional equipment is needed that complements the functions of the extruder and that varies with the type of product to be extruded. That is, the production of extruded products is carried out on an extrusion line, which consists of one or more extruders, an extrusion head and calibration, cooling and manipulation systems of the extrudate.

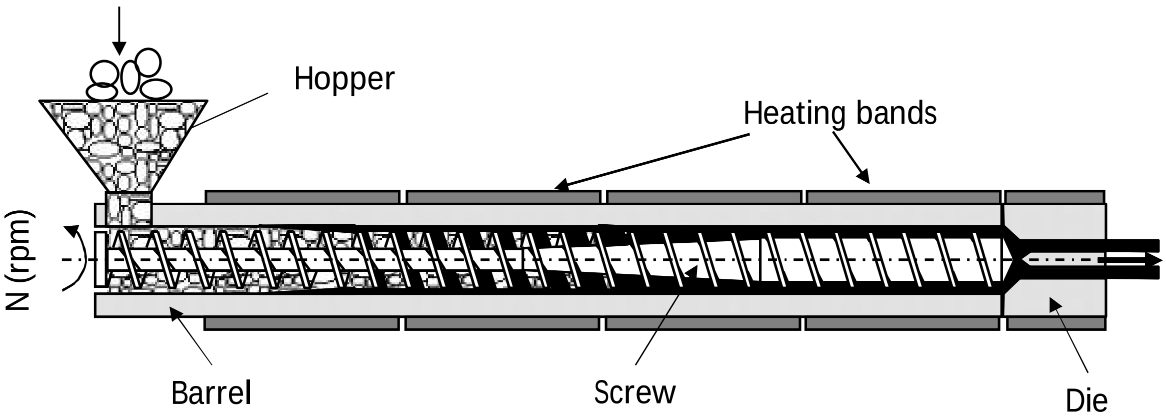

Figure 2- Scheme of operation of an extruder

The purpose of the extruder is to send a homogeneous melt under pressure to the extrusion head (in addition to the functions mentioned above). For its realization it is necessary to be able to transport the solid material, mix, homogenize and pressurize the melt, in order to pump it at a constant rate to the die. Details on thermomechanical phenomena, referred to as the plasticization process, are the object of study in this text, which will be presented in detail in the following chapters.

The differentiation between the various extrusion techniques starts at the extrusion head, which consists of a filtration system and the die. The objective is to filter out any impurities and give shape to the melt, respectively. The extrusion process is only complete after the extruded material passes through a set of accessory equipment, which carries out a series of operations until obtaining a solid product. These operations include: calibration and cooling, insufflation, drawing, cutting and winding and, eventually, secondary forming may be induced.

The different extrusion lines (Figure 3) can produce: profiles, tubes, monofilaments, flat film and sheet, blown film and insulating conductors.

<table>
<tr><th>EXTRUDER</th><th>EXTRUSION HEAD</th><th>AUXILIARY EQUIPMENT</th></tr>
<tr><td>Single screw
Twin-Screw:
Co-rotating
Counter-rotating
Co-extrusion
Other</td><td colspan="2">Profile
Pipes
Wire and cable extrusion
Monofilaments
Flat film/sheet
Blow film</td></tr>
<tr><td colspan="3">EXTRUSION LINE</td></tr>
</table>

Figure 3- Scheme for extrusion lines

2.2. Plasticizing process

Figure 4 schematically illustrates the thermomechanical phenomena that occur in the plasticization process in a single-screw extruder. Taking into account the basic functions of an extruder, mentioned above, it appears in this process that there are zones where the flow of solid and molten material occurs separately and an intermediate zone where there is the flow of polymer in the solid and molten states simultaneously.

Maddock and Street carried out, for the first time, specific experiments to visualize the process in order to discover what was going on in the area from the passage from solid to melt. These experiences consisted of [MAD 59]:

1) Put the extruder into operation until it reaches steady state,

2) Suddenly stop the process,

3) Quickly cool the heated cylinder area,

4) Extract the screw with the polymer.

These experiments, carried out with different polymers, processing conditions and screw geometries, made it possible to observe three distinct functional zones, corresponding, sequentially, to the presence of solids, melts and the coexistence of both. It was found that in the initial part of the screw, the granules are progressively compressed, forming a block (or a plug) with a certain cohesion. It was also verified that the solids zone could be subdivided in two, the first corresponding only to the flow of solid material and the second to the flow of the solid plug partially surrounded by a melt film next to the cylinder. In the melting zone, the solid and melt flow towards the channel but separate and, as the melting progresses, the melt width increases and the solids width decreases. Finally, in the pumping zone, the channel is full of melt [MAD 59, TAD 70].

These studies allowed us to conclude that plasticization develops in six sequential stages, as shown in Figure 4 [TAD 70, CHU 10]:

1) Transport of solids in the hopper: where the flow takes place by the force of gravity;

2) Transport of solids in the screw: which consists of dragging a block of solids along the screw channel due to the existence of friction between the polymer and the walls of the screw and cylinder;

3) Delay in melting: zone corresponding to the existence of a flow of a block of solids surrounded by a melt film next to the cylinder, which may later extend to the surfaces of the screw channel;

4) Mixing: where a specific mixing mechanism takes place;

5) Melt pumping: where the flow occurs due to the difference in pressure generated and the viscous drag of the melted polymer caused by the cylinder wall;

6) Flow of melt in the die: due to the pressure generated in the screw of the extruder.

Each of the functional zones identified in Figure 4 will be analyzed mathematically in the next chapter. In order to integrate the different individual models developed for each of the stages, it will be necessary to take into account appropriate boundary conditions: i) the pressure calculated at the base of the hopper will be the initial value required in the solid transport zone on the screw; ii) the start of the delay zone occurs when the material temperature at the solid plug interface of the cylinder wall reaches the melting temperature of the material, in the case of semi-crystalline polymers, or an adequate softening temperature, in the case of amorphous polymers (in this case about 50-60ºC above the glass transition temperature); iii) the beginning of the melting zone occurs when melt films are formed next to the screw walls and the width of the film next to the active flank begins to increase; iv) the end of the melting zone occurs when the material is fully melted; v) the flow rate of the extruder will be determined taking into account the counter pressure exerted by the die [GAS 09].

The mathematical and computational models developed from the process parameters (system geometry, polymer properties and processing conditions) should provide some measures regarding the performance of the process, such as: flow rate, mechanical power consumption required to rotates the screw, melt temperature, temperature homogeneity, degree of mixing induced, length required for melting, ability to generate pressure and viscous dissipation [GAS 09].

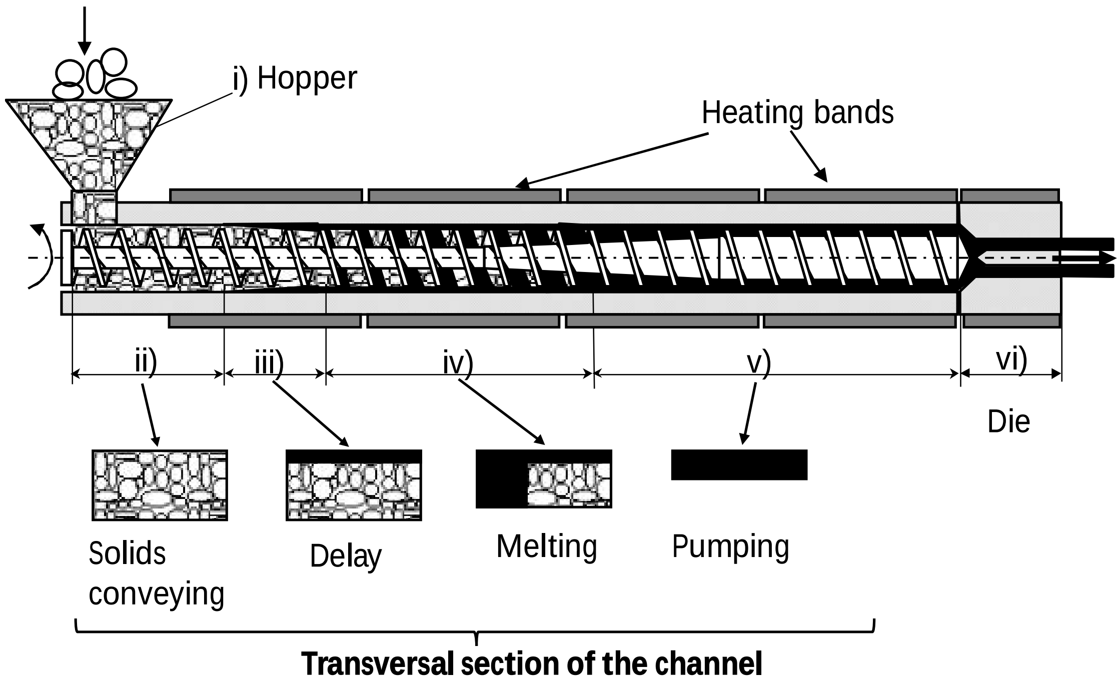

Figure 4- Functional steps in plasticization

In order to facilitate the study of the process, *i.e.*, to allow visualization and theoretical study of the thermomechanical phenomena that occur in plasticizing, two simplifications related to the geometry of the screw were considered [TAD 70, RAU 86].

First, and as shown in Figure 5, the polymer is considered to flow in a rectangular channel that results from the unwinding of the screw channel. This channel is limited at the top by the cylinder wall, at the bottom by the root of the screw and at the sides by the screw flanks. This simplification allows the use of rectangular coordinates (x, y, z) in the development of the mathematical models that regulate the process, which, as will be verified, simplifies the deduction of analytical models [TAD 70, TAD 06]. The second simplification considers that the screw is stopped and it is the cylinder that rotates. The validity of this simplification is based on the fact that in most screws the ratio between the depth of the channel (H) and the diameter of the screw (D_s) is very small, that is, $H/D_s <<< 1$ [TAD 70, RAU 86, TAD 06].

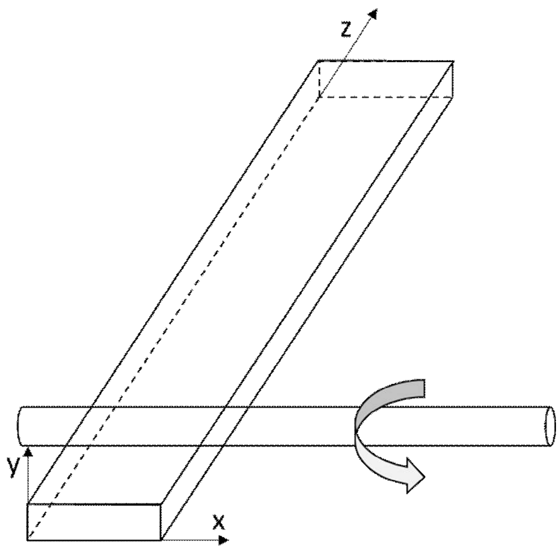

Figure 5- Unrolling of the screw channel

As a consequence, the angular velocity, N, corresponds to a linear velocity near the inner wall of the barrel (cylinder), V_c, which makes an angle, θ_c, with the z direction of the channel. Thus, the barrel velocity and its components in the axle system considered (Figure 6), are given by:

$$V_c = \pi N D_c \quad \textbf{(1)}$$

$$V_{cz} = V_c \cos\theta_c \quad \textbf{(2)}$$

$$V_{cx} = V_c \sin\theta_c \quad \textbf{(3)}$$

The effectiveness of the solids transport depends on the relative magnitude of the friction coefficients between the polymer particles and the cylinder and screw walls. Figure 7 illustrates, in a simplified way, what happens when a solid polymer plug is placed between two parallel plates in the following conditions: the top plate, representing the cylinder, moves at a constant speed, V_c, and the bottom, representing the screw, is stopped; the block of solids is subjected to a pressure, P, constant and uniform; this pressure being applied on the area, A, equal on the upper and lower surfaces, and the friction coefficient on the two plates is different, f_b on the upper and f_s on the lower.

It is easily possible to calculate the normal force, F_N, exerted due to the pressure on the upper and lower surfaces (equal on both) as being $F_N=P/A$.

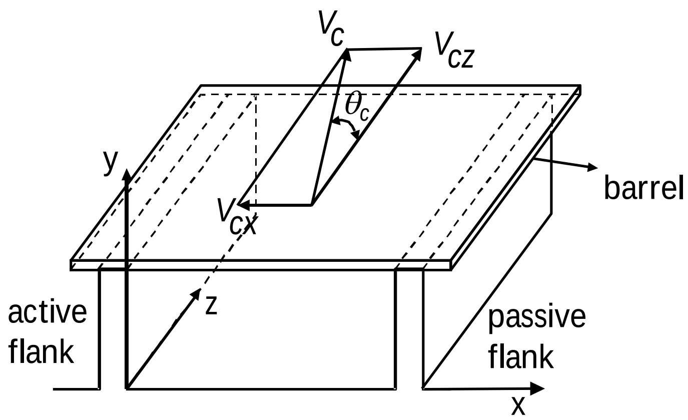

Figure 6- Velocity components in the barrel

Due to the movement imposed on the upper plate, there will be two frictional forces opposite and perpendicular to the normal force, one on the upper plate, F_c, and another on the lower plate, F_p. These forces result from:

$$F_c = F_N \; f_c \quad \textbf{(4)}$$

$$F_p = F_N \; f_p \quad \textbf{(5)}$$

Obviously, for the block of solids to move (ignoring the inertia of the system), *i.e.*, for the solids block velocity, V_{bs}, to be greater than 0, it is necessary that $F_c > F_p$, that is, taking into account the equations 4 and 5: $f_c > f_p$.

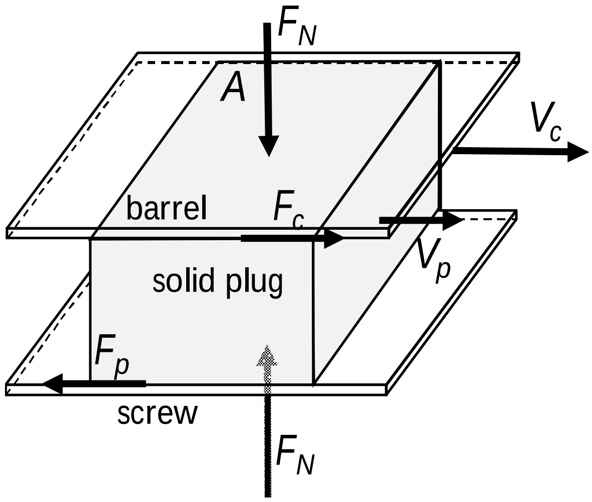

Figure 7- Movement of the solid plug due to friction

In summary, in practice, if we consider the upper plate as the cylinder and the lower plate as the screw, we can conclude the following:

1) If $f_c<f_p$, the polymer adheres to the screw sliding on the cylinder. The material does not advance in the channel, *i.e.*, the flow is null.
2) If $f_c>f_p$, the material slides on the screw, advancing axially due to the action of the cylinder movement. The flow rate will be greater than the difference between the friction coefficients.
3) When $f_c>>>f_p$, the flow rate can increase significantly, but the torque required to turn the screw as well as the pressure generated also increases considerably; factors that must be taken into account when designing the machine.

Due to the existence of friction between the polymer and the cylinder walls, the relative movement between the polymer and steel surfaces (cylinder and screw walls) causes the temperature to rise due to the dissipation of mechanical energy into thermal energy. For this reason, the polymer, on the surface next to the cylinder, reaches the melting temperature (in the case of semi-crystalline polymers) earlier than it would reach if only the increase in the temperature of the polymer was considered due to the heat conduction of the heated cylinder. It is the balance between the heat conduction of the cylinder and the frictional heat dissipation that defines the dynamics of the fusion process, as will be seen.

Figure 8 seeks to illustrate the phenomena that develop in the screw channel when the material begins to melt: (a) initially, a thin melt film is formed which, due to the fact that the granules are not yet sufficiently compacted, may infiltrate up in the space between those same solid polymer granules; (b) then, as it progresses in the screw channel, this film increases in dimensions, being thicker than the gap between the top of the screw flank and the cylinder; (c) since there is also friction on the surface of the screw (although the friction coefficient on that surface is lower), melt films can be formed at the root and flanks of the screw. This zone corresponds to the existence of a delay mechanism in relation to the normal melting mechanism. It starts when the material at the interface melts (by conduction of heat and/or by the dissipation of mechanical energy) and extends to the beginning of the formation of a melt pool next to the active flank, characterized by having a width similar to the depth of the channel (Figure 8-d).

Figure 9 shows, schematically, the way these functional zones develop along the screw channel. It should be noted the progressive increase in the width of the melt pool following a non-linear melting profile. This figure does not consider the decrease in the height of the channel in the intermediate zone of the screw (see Figure 2), which also contributes to this non-linearity as well as to the acceleration of the melting.

Another important aspect is related to the path of the polymer in the screw channel. Figure 10 illustrates the path taken by an elementary polymer particle. In the solids transport zone, the particle moves in the *z* direction of the channel, taking into account that we are in the presence of a block of solids with some cohesion. When it reaches the delay zone, and due to the fact that there is some material melting, the particle can move slightly upwards in the channel. It is from the moment it merges that its path undergoes more variations. When it reaches the melt pool, it makes a helical movement, which depends on its position in the channel. This has a major implication, particles positioned at different locations at the beginning of the channel do not have the same residence time inside the extruder. It is this fact that is responsible for mixing and homogenizing the melt, as will be seen next.

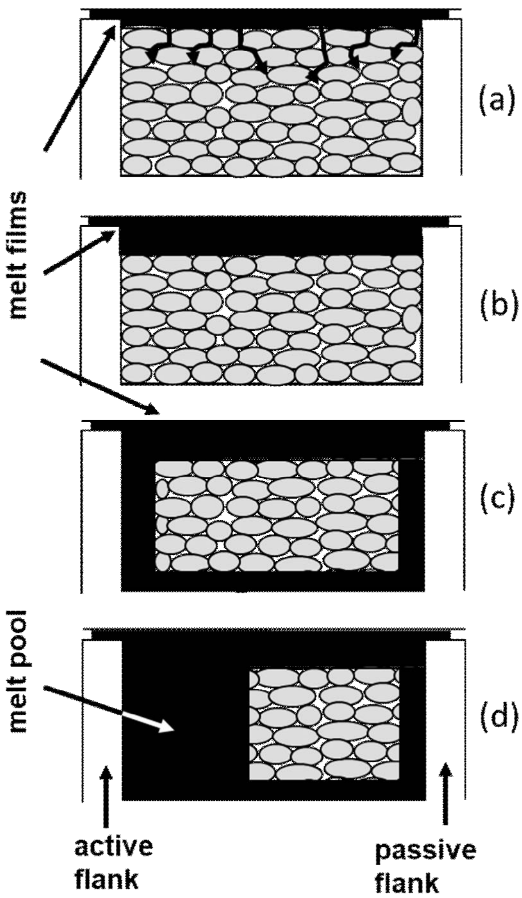

Figure 8- Beginning of melting

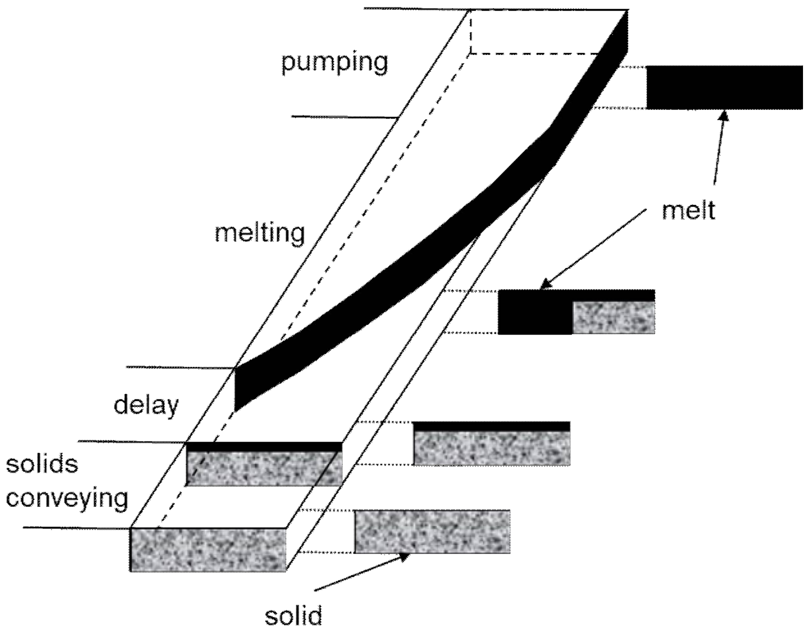

Figure 9- Functional zones along the screw channel

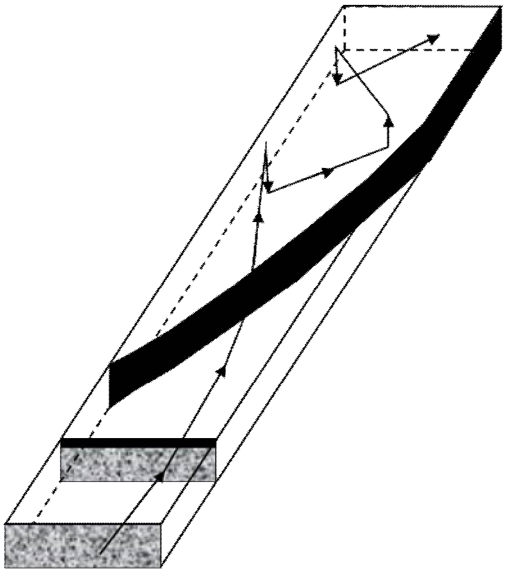

Figure 10- Flow path of a particle in the screw channel

2.3. Polymer properties

The characterization of the polymer concerning its thermal, rheological and physical properties is essential when it is intended to use software in the design of polymer processing equipment, either in the optimization of its operation or in the understanding and subsequent solution of problems that may occur during the process.

There are some properties that can be found easily in the literature, such as: glass transition temperatures (mainly for amorphous polymers) and melting temperatures and specific heat. However, some important properties are not easy to find, such as: thermal conductivity, specific mass and friction coefficients.

In the latter case, it will be necessary to determine it, having to bear in mind that it will always be necessary to determine the influence of process parameters, such as temperature and pressure, on its final value. As will be seen, this fact implies that it is necessary to define mathematical models that allow these variations to be taken into account.

For a typical case of modeling the extrusion process, the following properties are required:

- Specific mass of solid and melt;
- Coefficients of friction polymer granules/hopper walls and coefficient of internal friction (between the granules).
- Friction coefficients at the polymer/cylinder and screw walls interface;
- Thermal conductivity of solid and melt;
- Melting temperature;
- Enthalpy of melting;
- Glass transition temperature in the case of amorphous polymers;
- Specific heat of solid and melt;
- Rheological properties.

Physical properties

The specific mass of the solid polymer must take into account the fact that in the extrusion process there is a flow of solid particles that are progressively compacted and that, at the same time, are subject to temperature changes. That is, it is necessary to quantify an apparent specific density, where in the space between the granules there is air that decreases the effective specific density of the solid polymer. Hyun and Spalding [HYN 90] developed a model with the aim of quantifying this variation with pressure and temperature:

$$\rho_s = \rho_\infty + (\rho_0 - \rho_\infty)^{F\,P} \qquad \textbf{(6)}$$

$$F = b_0 + b_1\,T + b_2\,T^2 + \frac{b_3}{T_g - T} \qquad \textbf{(7)}$$

where P is the pressure, T is the temperature, ρ_s is the density at the pressure and temperature considered, ρ_∞ is the density of the solid (compacted) polymer, ρ_0 is the density of the granules at atmospheric pressure, T_g is the glass transition temperature and b_0, b_1, b_2 and b_3 are empirical coefficients determined from experimental data (adjusting these data to the model considered).

Table 1 shows the values of these parameters for a high density polyethylene. Figure 11 shows the variation in specific gravity with pressure for various temperatures. The complexity of this variation is clear, which leads to the conclusion that ignoring the effect of temperature and pressure on the density of solids can lead to erroneous results.

Likewise, the density of the melt varies with pressure and temperature. For its determination, a capillary rheometer is generally used in which a plug is placed on the side of the polymer outlet. Thus, when the piston is moved, at a certain temperature, the polymer is compressed, determining the density by varying the volume of the chamber and the pressure variation with the pressure sensor of the rheometer itself. Performing the test at various temperatures, a graph is obtained, which is called a PVT diagram.

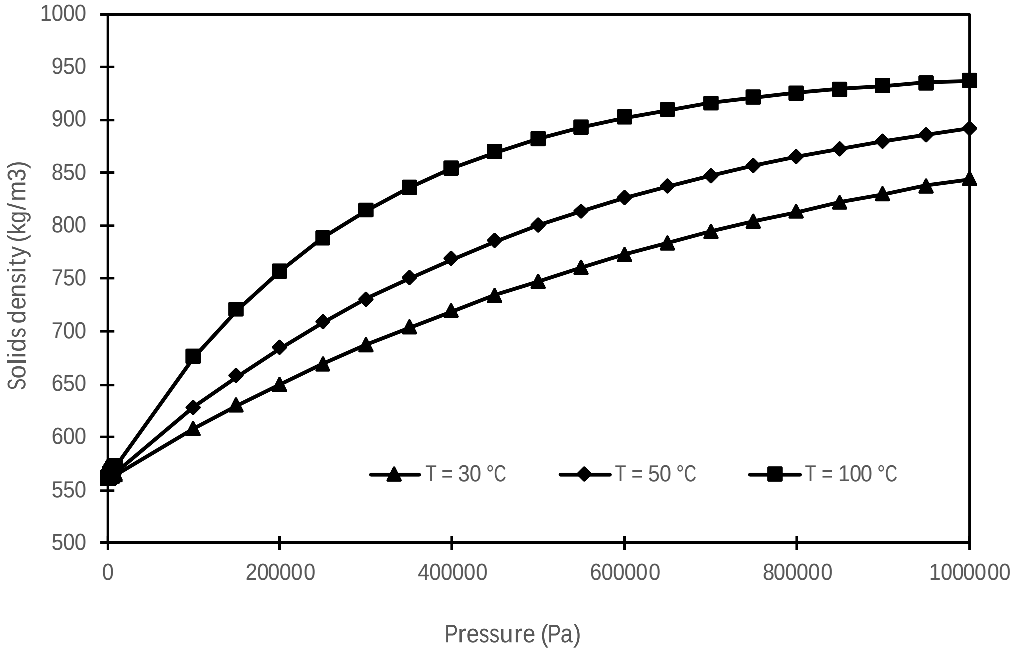

Figure 11- Solids density as a function of temperature and pressure (NCPE 0928, Table 1)

The following equation describes the change in melt density, ρ_m, as a function of temperature, *T*, and pressure, *P*:

$$\rho_m = g_0 + g_1\,T + g_2\,P + g_3\,T\,P \qquad \textbf{(8)}$$

Being: g_0, g_1, g_2 and g_3 empirical constants determined by adjusting the equation to the values obtained experimentally. Figure 12 shows the evolution of the melt density with the pressure for typical values of processing temperatures. As can be seen, the variation is linear with pressure and temperature. However, due to the great variations that exist, it is very important to take this model into account in the calculations to be carried out.

As identified above, the friction coefficients are important in two different situations: a) in the flow of the polymer in the hopper and b) in the transport of solids in the screw. Due to the local pressure and temperature conditions, the behavior of the solids with respect to friction is very different in these two conditions.

In the hopper there is a flow of loose solids, at a fixed room temperature and at relatively low pressures. In this case it is necessary to quantify the external friction coefficients, granules/hopper walls, and internal, between the polymer granules. The external friction coefficient corresponds to the flow angle of the granules when a plate is slowly tilted from the horizontal position, the angle of friction being obtained when most granules start to flow (see Figure 13-c). The external friction coefficient, $f_p^{'}$, can be calculated from this angle, β_w, by:

$$f_p^{'} = tg(\beta_w) \qquad \textbf{(9)}$$

Figure 13-b shows how the internal friction coefficient (β_e) is obtained, which corresponds to the initial flow of the polymer granules together.

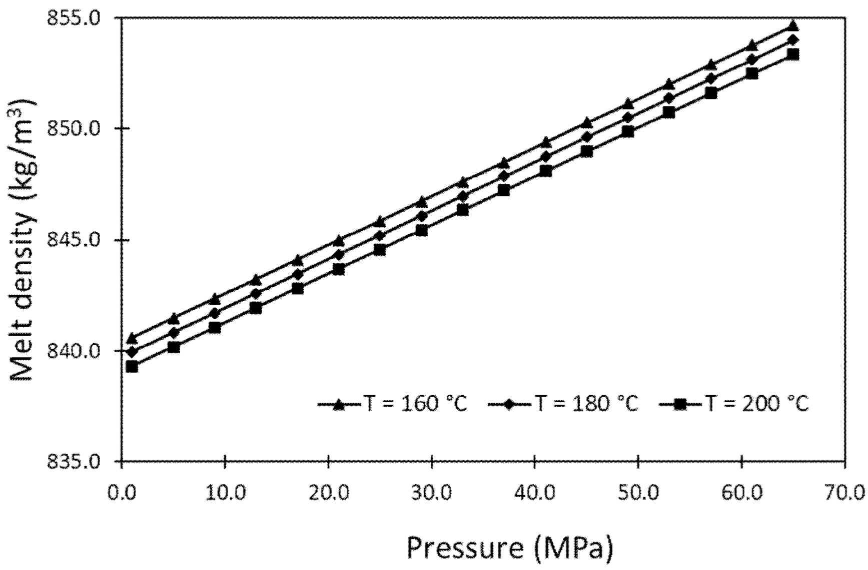

Figure 12- Melt density as a function of temperature and pressure (NCPE 0928, Table 1)

Second, the external friction coefficients, between the polymer and the inner walls of the cylinder and the walls of the screw, are decisive factors in the transport of solids in single-screw extruders. However, in the conditions of pressure and temperature that develop in areas where there are solids (*i.e.*, solids transport, delay and melting), the values of the referred friction coefficients do not remain constant, being very difficult to determine. Gamache *et al.* [GAM 99] developed a device capable of making this determination. In this work, different polymers, metallic surfaces and granule shapes were tested experimentally, in addition to studying the effect of temperature and pressure on the respective friction coefficients. As can be seen in this work, the value of the friction coefficients varies widely, however serving as a good starting point to be used in the calculations (the values shown in Table 1 were taken from the literature or provided by the manufacturer).

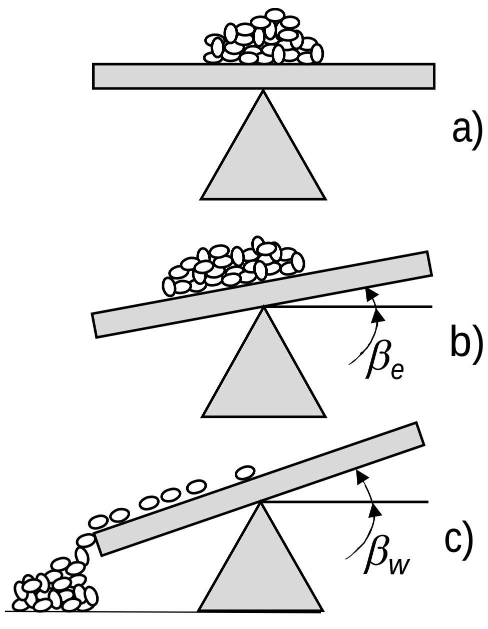

Figure 13- Experimental determination of the internal and external friction coefficients

Thermal properties

The thermal properties required to model the plasticization process, except for thermal conductivity, can be obtained using a Differential Scanning Calorimeter (DSC). With the DSC it is possible to easily obtain the glass, T_g, and melting, T_m, transition temperatures, the latent heat of fusion, *h*, and the specific heat of the solid, C_s, and of the melt, C_m. The specific heat of the solid and of the melt varies with the temperature following a law of the type:

$$C_{s,m} = C_0 + C_1\, T + C_2\, T^2 \qquad \textbf{(10)}$$

The constants C_0, C_1 and C_2 are obtained by adjusting the values obtained experimentally to the previous equation. Figure 14 shows the variation of the specific heat with the temperature for a high density polyethylene (HDPE). In this case, for temperatures below T_m the variation is quadratic, while for temperatures above T_m it is linear.

Thermal conductivity can be achieved through a miniaturized device consisting of a hot plate and using symmetric thermal flow [KAM 83]. With this device it is possible to obtain the values of the thermal conductivity of the solid and the melt, since it allows heating above the processing temperature (the values shown in Table 1 were taken from the literature or provided by the manufacturer).

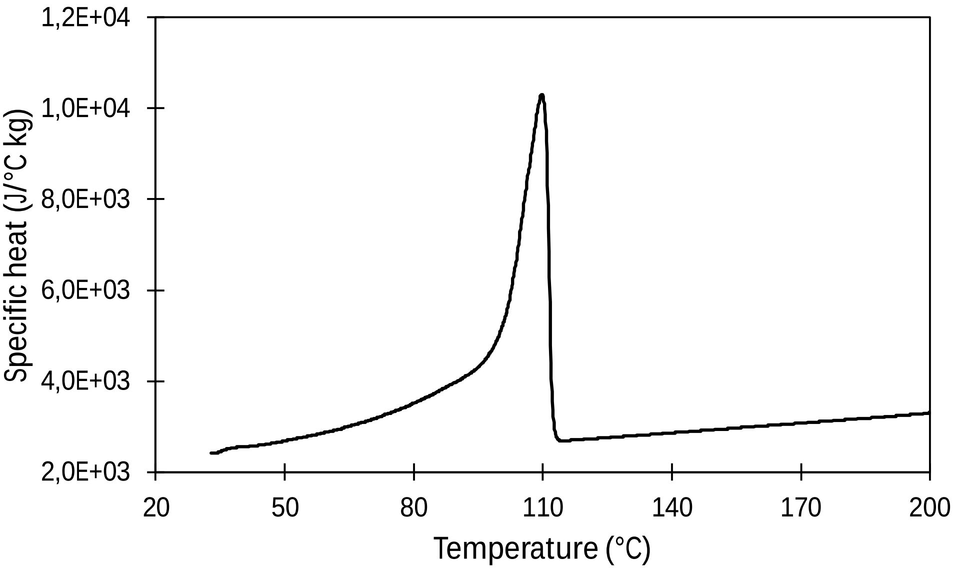

Figure 14- Specific heat as a function of temperature for an LDPE (LUPOLEN 33FM)

Rheological properties

The rheological properties for the temperature range and shear rates used in plasticization extrusion can be obtained from a capillary rheometer. For this purpose, tests are carried out at various temperatures, taking into account the effects of the die entry due to pressure, with the corrections of Bagley and Rabinowitsch being applied in order to obtain the real viscosity value.

The values hence obtained can be described by a law of the Power Law type:

$$\eta = \eta_0\, \dot{\gamma}^{(n-1)} e^{-a(T-T_0)} \qquad \textbf{(11)}$$

where η is the viscosity at temperature *T* and at shear rate $\dot{\gamma}$, η_0, *n* and *a* are material constants, which result from adjusting the equation to the experimental data, and T_0 is the reference temperature.

Another possibility is to use the Carreau-Yasuda law:

$$\eta = \eta_0 \, a_T \left(1 + (\lambda \, a_T \, \dot{\gamma})^a\right)^{\frac{n-1}{a}} \qquad \textbf{(12)}$$

where

$$a_T = \exp\left(\frac{E}{R}\left(\frac{1}{T} - \frac{1}{T_0}\right)\right) \qquad \textbf{(13)}$$

where η is the viscosity at temperature T and at shear rate $\dot{\gamma}$, η_0, n, λ, and a are material constants, which, as in the previous case, result from adjusting the equation to the experimental data, and T_0 is the reference temperature.

Figure 15 shows the viscosity curves for various temperature values of an HDPE (Table 2) using de Carreau-Yasuda law.

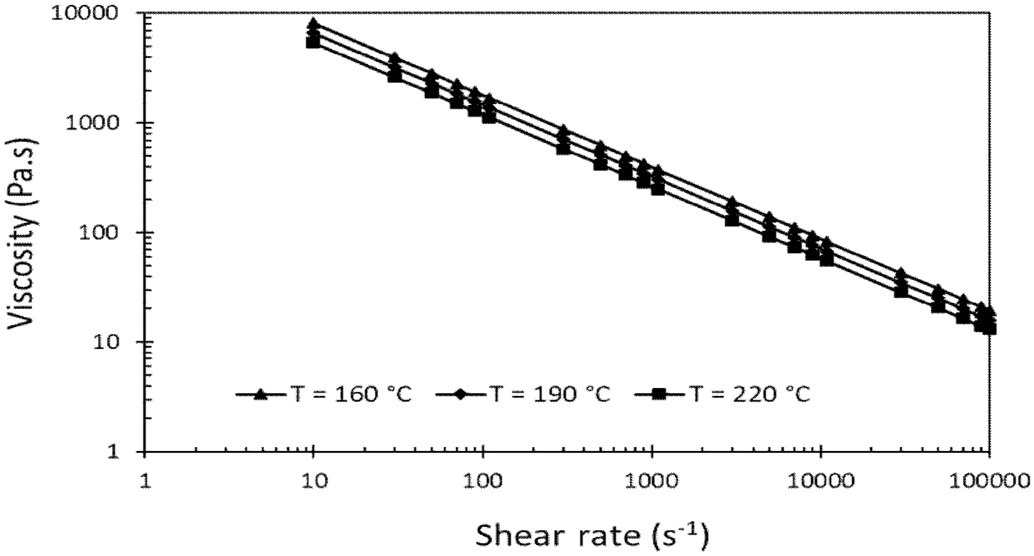

Figure 15- Viscosity at different temperatures for an HDPE (NCPE 0928, Table 2)

Table 1- Physical and thermal properties of polymers: HDPE –NCPE 0928, by Borealis; LDPE - LUPOLEN 33FM, by Basell; PP - ISPLEN 030G1E, by Repsol YPF (in the case where the coefficients of the polynomials are not shown it means that the property value is assumed to be constant, as is the case of the solid specific mass for LDPE which is 495.0 kg / m3).

Properties			HDPE	LDPE	PP	Unity
Density	*Solid* (ρ_s)	ρ_∞	948.0	495.0	691	Kg/m^3
		ρ_0	560.0	---	---	kg/m^3
		Tg	-125.0	---	---	°C
		b_0	-1.276e-9	---	---	1/Pa
		b_1	8.668e-9	---	---	1/°C Pa
		b_2	-5.351e-11	---	---	1/°C^2 Pa
		b_3	-1.505e-4	---	---	°C/Pa
	Melt (ρ_m)	g_0	854.4	923	902	kg/m^3
		g_1	-0.03236	---	---	kg/m^3 °C
		g_2	2.182e-7	---	---	kg/m^3 Pa
		g_3	3.937e-12	---	---	kg/m^3 °C Pa
Friction coefficients	*Internal*		0.67	0.53	0.50	---
	Hopper		0.30	0.30	0.30	---
	Barrel		0.45	0.40	0.45	---
	Screw		0.25	0.20	0.25	---
Thermal conductivity	*Solid*	k_s	0.186	0.141	0.210	W/m ºC
	Melt	k_m	0.097	0.078	0.180	W/m.ºC
Specific Heat	*Solid* (C_s)	C_0	1317.0	2725.0	1882.0	J/kg
		C_1	---	---	---	J/kg °C
		C_2	---	---	---	J/kg Pa
	Melt (C_m)	C_0	-1289.0	2574.0	1975.0	J/kg
		C_1	86.01	---	---	J/kg °C
		C_2	-0.3208	---	---	J/kg Pa
Enthalpy of melting		h	196000.0	116100.0	120490.0	J/kg
Melting temperature		T_m	119.6	100.3	169.1	ºC

Table 2- Rheological properties of polymers: HDPE – NCPE 0928, by Borealis; LDPE - LUPOLEN 33FM, by Basell; PP - ISPLEN 030G1E, by Repsol YPF.

Properties		HDPE	LDPE	PP	Unitiy
Viscosity: Power law	n	0.345	---	---	---
	k_0	29940.0	---	---	Pa/s
	a	0.00681	---	---	1/°C
	T_0	190	---	---	°C
Viscosity: Carreau-Yasuda law	η_0	---	33000.0	3041.5	*Pa.s*
	E/R	---	5000.0	4023.3	*K*
	$\hat{\lambda}$	---	1.00	0.17	*S*
	a	---	1.80	1.82	---
	n	---	0.35	0.35	---
	T_0	---	423.15	533.15	*K*

2.4. System geometry

Conventional screw

The single-screw extruder consists of a heated cylinder where an Archimedes' type screw rotates. In a conventional single screw, three distinct geometric zones can be distinguished (see Figure 16):

1) Feed zone: where the channel depth is constant;
2) Compression zone: characterized by a progressive decrease in the depth of the channel;
3) Metering zone: with reduced and constant channel depth.

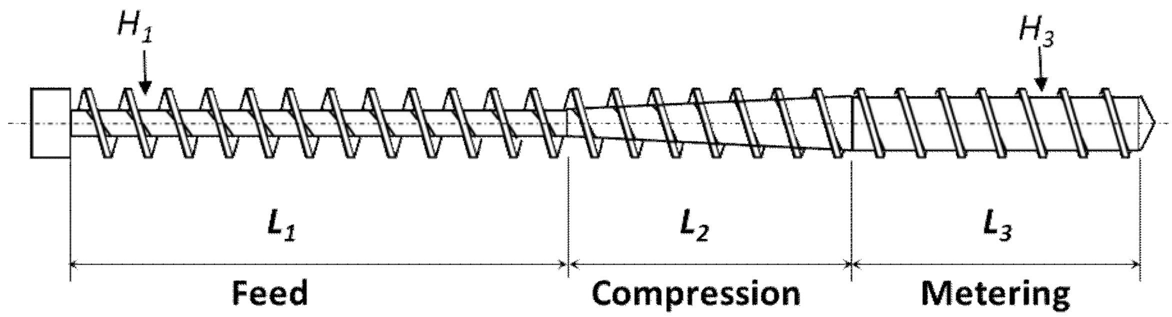

Figure 16- Geometric zones of a conventional single screw

The geometric parameters required for the study of plasticization in single-screw extruders are illustrated in Figure 17 and include: D_c, barrel inner diameter; D_i, inside diameter of the screw; D_p, outside diameter of the screw; S, screw pitch; H, channel depth; δ_f, clearance between the screw flight and the inside of the cylinder; θ, flight angle; e, fillet thickness and W, channel width. Being that:

$$D_p = D_i + 2H \quad \textbf{(14)}$$

$$D_c = D_p + 2\delta_f \quad \textbf{(15)}$$

However, as the clearance (δ_f) is very small, it can be neglected in some calculations, leaving $D_c \approx D_{sp}$.

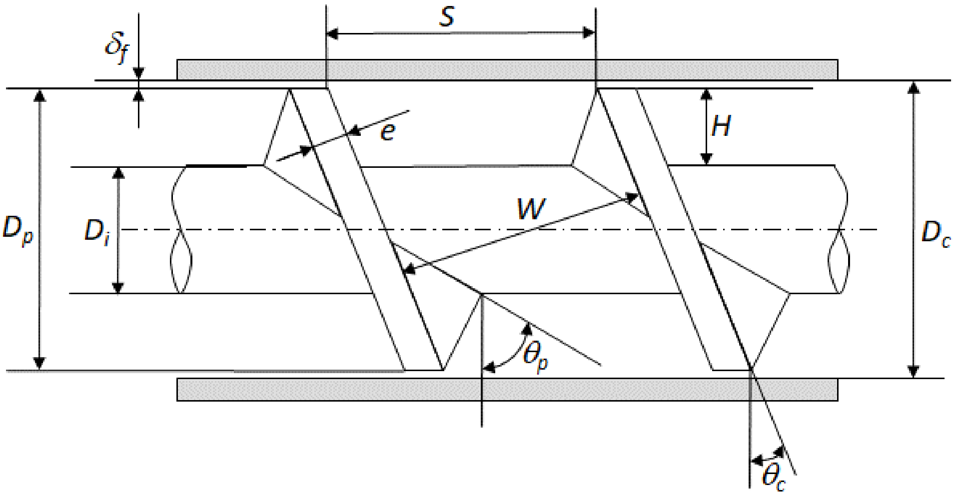

Figure 17- Geometric parameters of the screw

The flight angle (θ) varies with the distance from the screw axis (as shown in Figure 17), being its value, next to the screw root, given by the following equation:

$$\theta_p = arctg\left(\frac{S}{\pi D_i}\right) \quad \textbf{(16)}$$

and near the barrel walls by:

$$\theta_c = arctg\left(\frac{S}{\pi D_p}\right) \quad \textbf{(17)}$$

The width of the channel (W), such as θ, varies with the radial distance, being that next to the root of the screw can be calculated by:

$$W_p = S\cos\theta_p - e \quad \textbf{(18)}$$

and next to the cylinder by:

$$W_c = S\cos\theta_c - e \quad \textbf{(19)}$$

In the compression zone (Figure 16) the channel has a slope that can be calculated with the channel unrolled using the following equation (see Figure 18):

$$A = \frac{H_1 - H_3}{Z_2} \quad \textbf{(20)}$$

Z_2 being the unwound length of the compression zone channel obtained from:

$$Z_2 = \frac{L_2}{\sin\left(\bar{\theta}\right)} \quad \textbf{(21)}$$

where L_2 is the length of the compression zone along the channel, as shown in Figure 16, and $\overline{\theta}$ is the mean fillet angle (mean of θ_c and θ_p). The depth, H, of the channel at any location, z, along that same channel can be obtained from:

$$H = H_1 - A\,z \qquad \textbf{(22)}$$

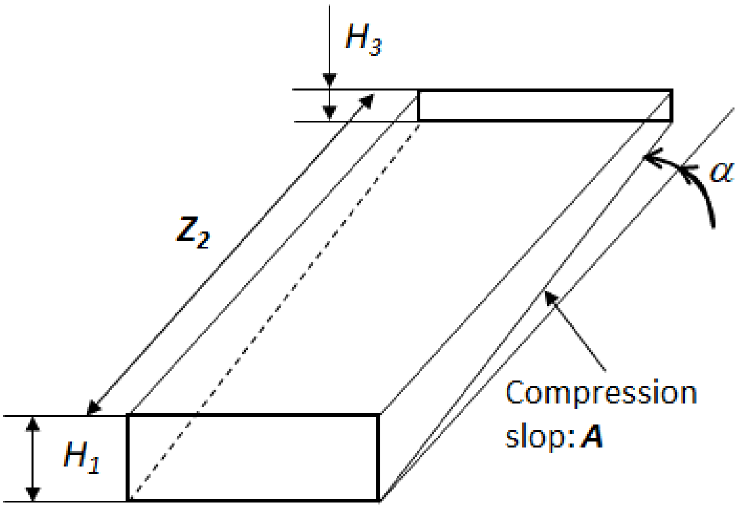

Figure 18- Screw compression zone: A - slope, α - compression angle

Finally, an important parameter in the characterization of a screw is its compression rate (TC), given y:

$$TC = \frac{H_1}{H_3} \qquad \textbf{(23)}$$

Complex geometries

The use of conventional extrusion screws has some limitations, namely with regard to mixing capacity, dynamic melting stability and the melting capacity. These limitations have been progressively resolved over several years. For this, different geometries were developed, capable of taking into account various aspects of the plasticization process and the functions that the extruder must perform, namely: barrel with grooves, mixing sections and barrier screws.

Grooves in the barrel

Taking into account the conditions previously defined, in terms of the relative values of the friction coefficients, to increase the flow capacity of the solids transport zone, the friction coefficient on the cylinder wall must be increased (maintaining the friction coefficient on the screw walls constant, which can be achieved by increasing its roughness. For this purpose, it is relatively common to machine longitudinal or helical grooves in the cylinder, as shown in Figure 19 for longitudinal grooves. The aim is to increase the flow rate considerably and reduce its sensitivity to pressure variations.

Table 3 shows, depending on the diameter of the screw, typical dimensions of the grooves, width and depth, as well as the number of grooves.

There are several models in the literature capable of quantifying the effect of grooves geometry on the performance of the extruder, which will be presented in the chapter on technological developments.

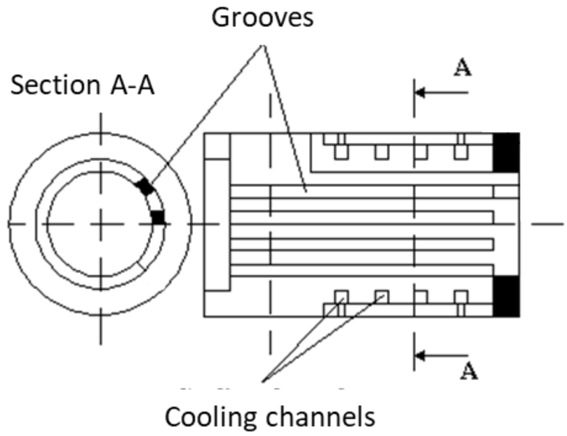

Figure 19- Longitudinal grooves

Table 3- Typical grooves dimensions.

Barrel diameter (mm)	Number of grooves	Width (mm)	Maximum depth (mm)
45	8	5.6	3.0
60	9	6.7	3.7
75	10	7.5	4.3
90	10	9.0	4.9
105	11	9.6	5.5
120	11	10.9	6.0

Barrier screws

The first barrier screw was patented by Maillefer (MBS) in 1959 [MAI 59]. It is characterized by having a second fillet in the compression zone with a helix angle different from the main fillet, and making the connection between the active and passive flanks of the main fillet (Figure 20). It has a double objective: a) to separate the block of solids from the melt pool, thus stabilizing the melting and eliminating the appearance of unmelted particles in the middle of the melt pool; b) increase the contact area between the block of solids and the walls of the channel in order to increase the melting rate. Later, other types of barrier screws were proposed: Dray and Lawrence (Dray and Lawrence Barrier Screw - DLBS) [DRA 70], Barr (BBS) [BAR 71], Kim (KBS) [KIM 72] and Ingen Housz (IHBS) [ING 80]. More recently, new solutions continue to be developed [ING 81, TAD 70, AME 88].

Schemes representing the various unwound barrier screws are illustrated in Figures 21 and 22, respectively for the screws, Maillefer, Dray and Lawrence, Barr and Kim.

Due to the sophistication of geometry, the modeling of the flow of the solid and molten polymer is also of some complexity, as can be seen in the work developed by the author in these two articles [GAS 14a, GAS 14b]. In this book no further details will be given on the modeling of this type of screws, the reader is referred to the works published by the author articles [GAS 14a, GAS 14b].

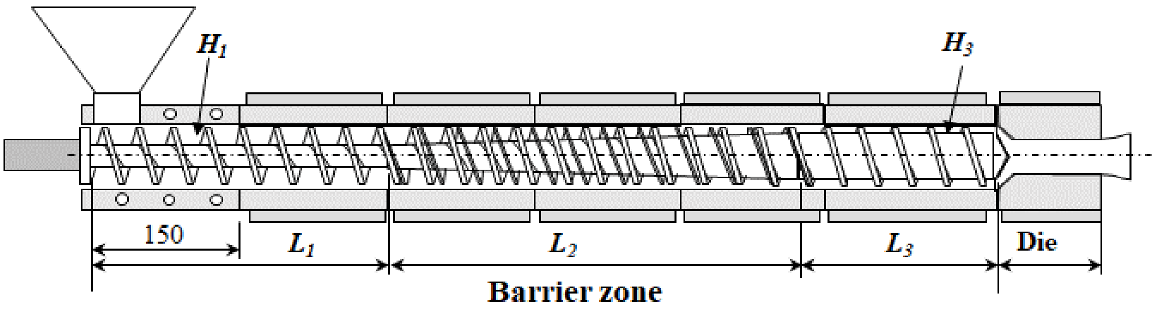

Figure 20- Barrier screw

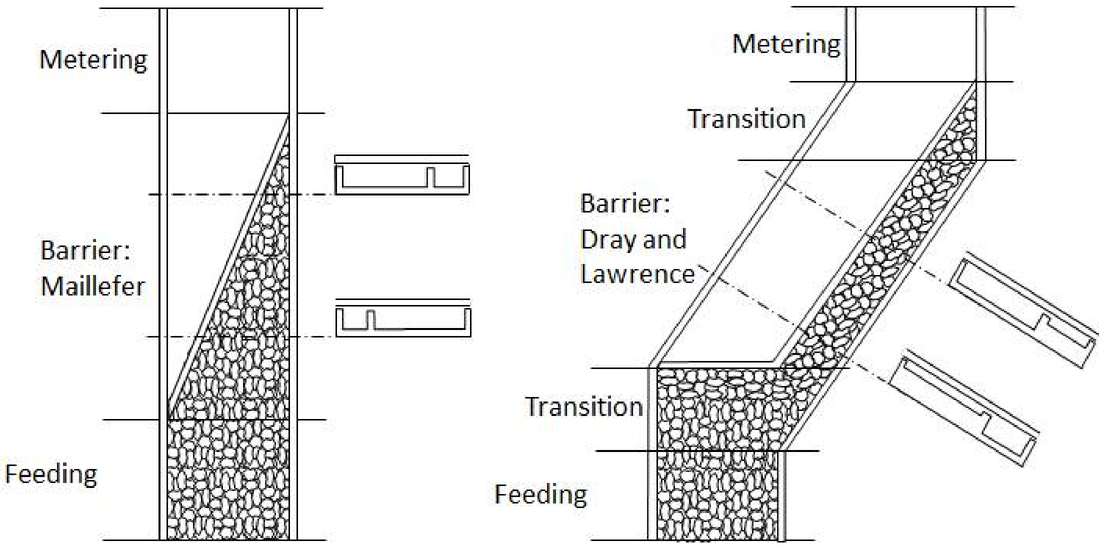

Figure 21- Barrier screws type: Maillefer and Dray and Lawrence

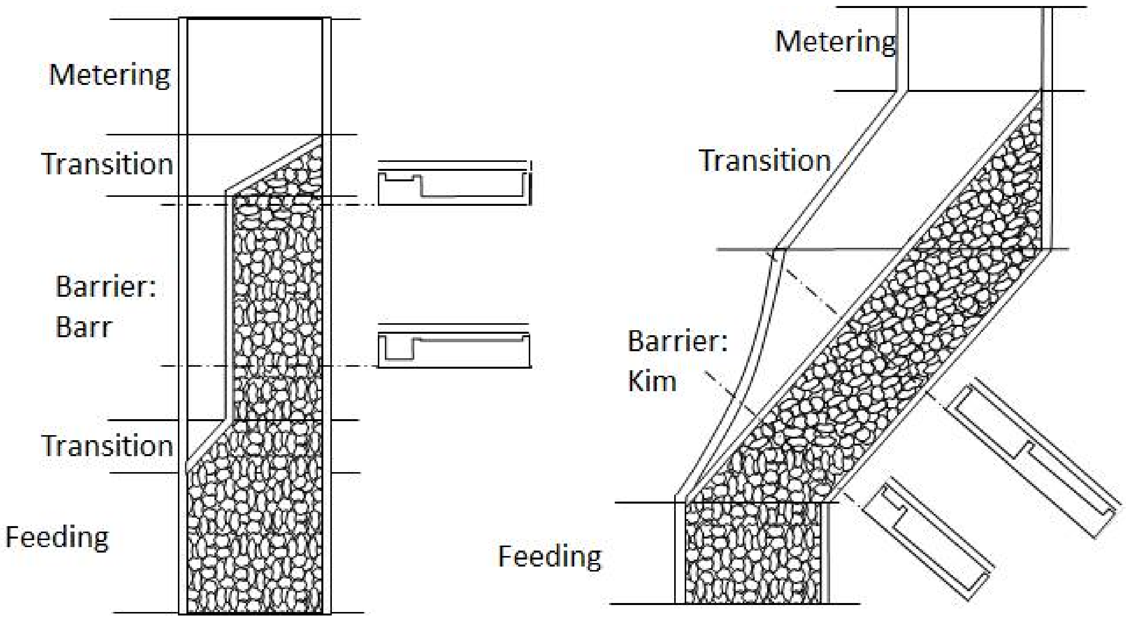

Figure 22- Barrier screws type: Barr and Kim

Mixing sections

Due to the simplicity of its geometry, in certain applications, the conventional screw may not promote adequate mixing. Thus, to obviate this problem, mixing sections can be incorporated in the screw body, which, depending on the type of construction, in addition to promoting the mixing and homogenization of the polymer can also prevent the eventual unmelted material from reaching the die. Generally, the mixing devices are inserted in the metering zone, and several devices of varying geometry and function can be used simultaneously [TAD 70, RAU 86, TAD 06].

The mixing can be distributive or dispersive. This concept is illustrated in Figure 23, simulating the use of two materials with different colors: a) when moving from left to right, the number of circles remains constant, however, the gray material was better distributed in space, that is, the two materials are better distributed; b) when moving from top to bottom, it is noted that the number of circles increases by breaking the larger circles, this means that the dispersion of the two materials has increased. Thus, the bottom circle on the right is the one with the best mix, both distributive and dispersive [TAD 70, RAU 86, TAD 06].

In view of the above, the mixing devices (or sections) are divided into two types, according to the type of mixture they promote: distributive mixing sections and dispersive mixing sections. In the first case, it is intended to increase the uniformity of the distribution of the different fluid elements, which is achieved through the division and recombination of material flows. In the case of dispersive sections, the objective is to reduce the unit size of one or more of the components, making it necessary to break the material agglomerates. This means that in the dispersive mixture it is necessary to apply high stresses, which can be shear, extensional or a combination of the two.

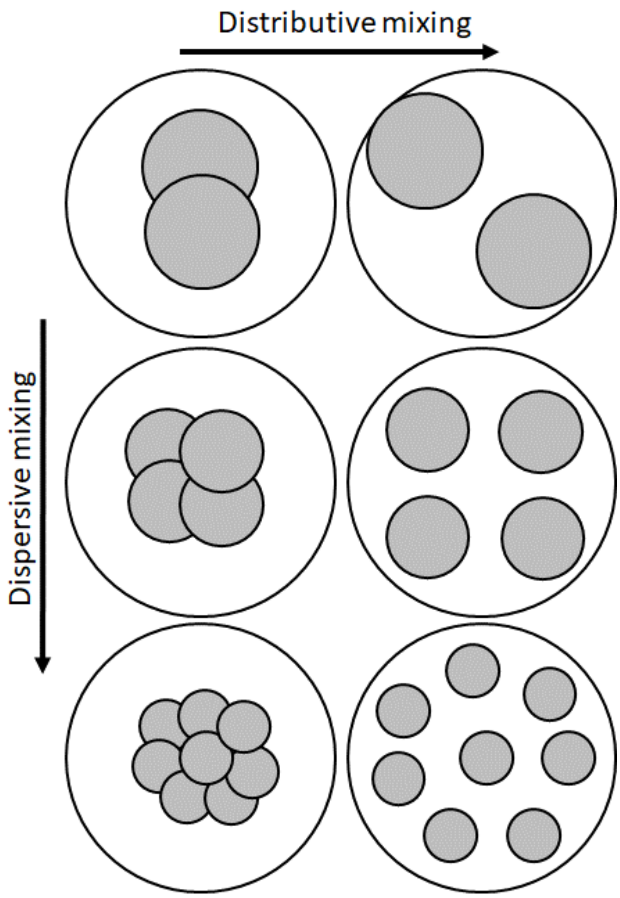

Figure 23- Distributive and dispersive mixing

Figure 24 shows two examples of distributive mixing sections: Pineapples and Pins. While in Figure 25 three examples of dispersive mixing sections are shown: Blister, Maddock and Union Carbide. This last mixing section is identical to Maddock, the only difference being the angle of the channels, since in Maddock section the channels are parallel to the axis of the screw.

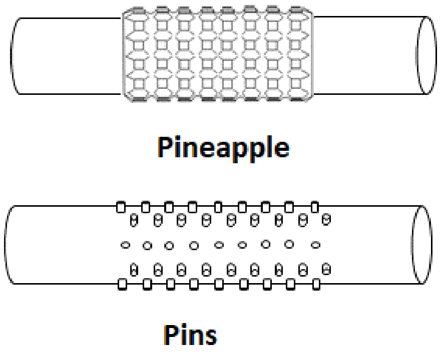

Figure 24- Examples of distributive mixing sections

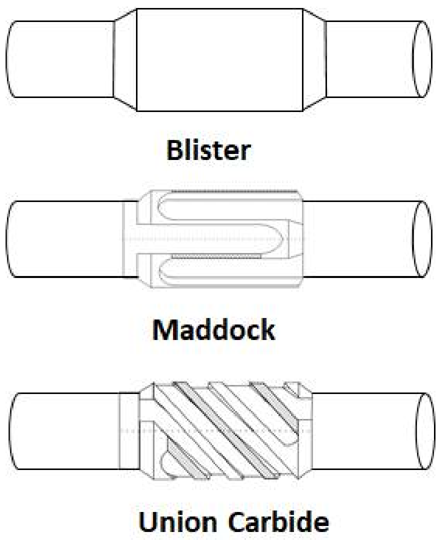

Figure 25- Examples of dispersive mixing sections

Application exercise

1. Determine the geometric constants of the extrusion screw illustrated in Figure 26.

Other data: square pitch screw; outer diameter of the screw: 60 mm; screw compression ratio: 2.5, cylinder inner diameter: 61 mm; fillet thickness: 5 mm.

Note: The constants must be determined for all geometric areas of the screw.

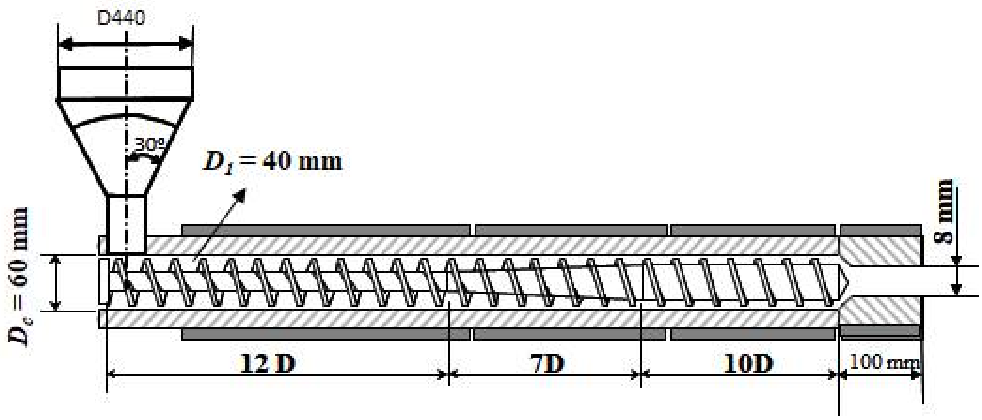

Figure 26 - Extruder geometry

3. Plasticizing in single screw extruders

3.1. Solids transport in the hopper

The hopper is the start of the transport of solids in the extruder. The transport of solids extends until the polymer begins to melt, which usually happens over a length of several diameters in the screw. Generally, as shown in Figure 27, hoppers are made up of: (1) a section of parallel walls above; (2) a section of converging walls in the middle; (3) a section of parallel walls at the bottom, which serves to fit the hopper overture to the barrel of the extruder. The cross section can be cylindrical, square or rectangular.

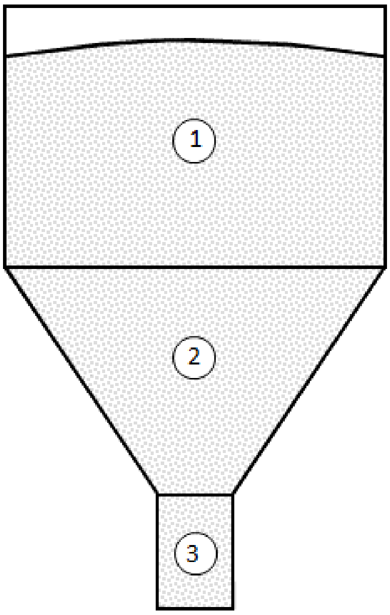

Figure 27- Geometry of a hopper

The hopper's main functions are: i) to ensure a uniform flow of solid polymer (granules or powder) to the extruder; ii) establish the conditions of the material in terms of pressure at the entrance of the extruder and iii) define the maximum possible flow of the system.

Due to the existence of friction between the solid material and the walls of the hopper, and contrary to what happens in liquids, when the hopper is filled with granules or power the pressure along the hopper does not increase linearly. In fact, as can be seen in Figure 28, the pressure increases to a maximum, remaining constant, or even decreasing, after this distance to the upper part of the hopper.

The existence of friction between the polymer particles and between them and the walls of the hopper can bring some problems to the flow of polymers in Hoppers, the consequence of which is the decrease in pressure along the hopper. In Figure 29 two of these problems are illustrated: i) the arching, due to the massive flow and ii) the tube effect, due to the funnel flow. In both cases, the absolute value of the output and its stability are affected. These issues, which occur mainly with more difficult-to-flow materials, can be minimized by adopting vibrating hoppers or with a screw incorporated into them, processes that significantly help the flow.

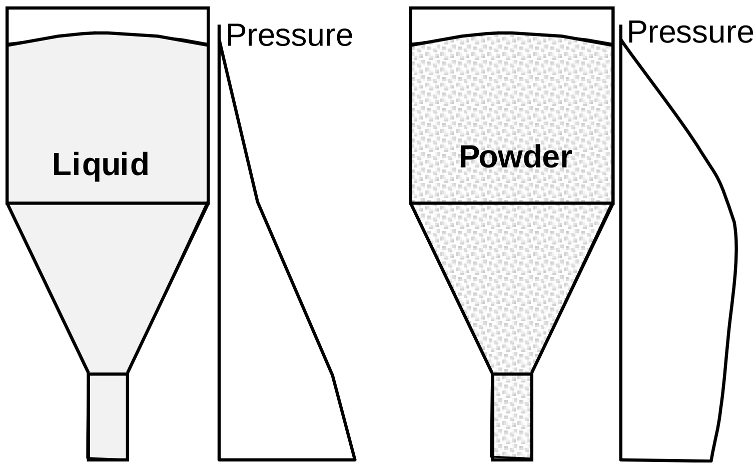

Figure 28- Variation of pressure with the height of a liquid and a powder

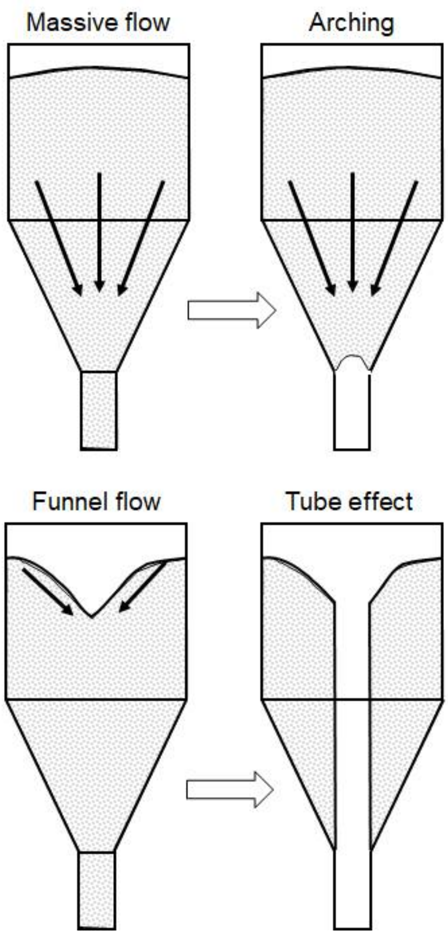

Figure 29- Problems with the flow of polymers in Hoppers

Additionally, the feed opening width and position also play a role in the process, manly in what concerns the output capacity of the hopper [SIK 13a, SIK 13b, SIK14]. In fact, the feed opening of the hopper depends directly from the internal barrel diameter, more specifically from the ratio between the sizes of the pellets and of the internal barrel diameter. Usually, in the link between the hopper and the barrel a feed pocket is machined on the side of the barrel toward the direction the screw rotates. The performance of the process depends on the screw speed, the width and position of the opening and of the pellets size [SIK 13a, SIK 13b, SIK14].

It is the geometry of the hopper that determines the type of flow that develops and, as a consequence, the stability of the process, the maximum possible flow rate and the pressure at the beginning of the extruder. A simple example seeks to demonstrate the flow capacity of a conical hopper with a 70 mm opening, granules with a diameter of 3 mm and material with an apparent density of 600 kg/m^3. In this case the output is given by:

$$Q = 0.58\rho_s \; g^{0.5}\left(D - K \; d_p\right)^{2.5} \tag{24}$$

where *D* is the diameter of the opening, ρ_s is the density of the material, d_p is the diameter of the material granules, *g* is the acceleration of gravity and *k* is a constant (≈1.4). The flow rate obtained, *Q*, is approximately 4300 kg/hr. It appears that this value is at least one order of magnitude higher than the real for the defined dimensions. This means that, when the hopper is completely opened, a dynamic pressure profile develops and that when the hopper is working together with the extruder, the pressure profile is quasi-static, since the actual flow rate is very smaller.

Janssen model

According to the model proposed by Janssen, in 1895, the vertical pressure profile (*P*) can be obtained by balancing forces acting on an element of material contained in a vertical column of solids, obtaining the following expression:

$$P = \frac{\rho_s \; g \; D\left\{1 - \exp\left[\left(\frac{K \; f_p^{'} \; D}{4}\right)\left(h - H\right)\right]\right\}}{4 \; f_p^{'} \; K} \tag{25}$$

where ρ_s is the density of the material, *g* is the acceleration of gravity, $f_p^{'}$ is the coefficient of external friction (close to the wall, see equation 9), *D* is the diameter of the hopper, *H* is the height of the column of solids, *h* is dimension considered from the base and *K* the ratio between normal and vertical stresses (being in this case the vertical stress is higher), given by:

$$K = \frac{1 - \sin\beta_w}{1 + \sin\beta_w} \tag{26}$$

β_w is the angle of external friction. With equation 25, the difference in the pressure profile that develops when using granules or a corresponding liquid can be determined in a simple way, as shown in Figure 30. It can be seen that at the top of the column, that is, when *h* is equal to *H*, the pressure, *P* is 0; and when *h* is 0, *P* tends to its maximum value, being obtained from:

$$P_{\max} = \frac{\rho \; g \; D}{4 f_p^{'}} \tag{27}$$

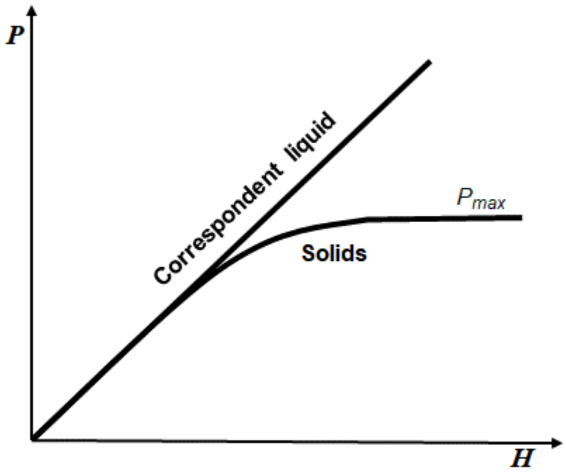

Figure 30- Pressure profile in hoppers

Walker model

As noted earlier, in a column of solid particles (granules or powder) there is no proportionality between the height of the material in the column and the pressure at the base, having as a consequence the development of a complex stress distribution in the system, which depends on its geometry and the particle properties (polymer/hopper friction coefficients and polymer/polymer friction).

The exact solution to this problem, in terms of determining the pressures developed and the material flow, is difficult to obtain; normally assuming that the flow is sufficiently slow, so that the particles are in permanent contact and the momentum transmitted by the collision between the particles is negligible (which is a reasonable assumption given the quasi-static pressure profile that develops, as previously seen) [RAU 86].

The cross section of the hopper can be circular or square, and for each type of section the walls can be vertical or convergent. The pressure and flow distribution equations are deduced according to the corresponding geometry.

Vertical hoppers

Walker [WAL 66] derived equations for vertical wall hoppers, having assumed a plastic equilibrium in an elementary volume of solid particles. Considering $h=H$ and $P=P_0$ (see Figure 31) the following equation is obtained:

$$P = P_o \exp\left[\frac{2\ B\ (h-H)}{R}\right] + \frac{\rho_s g\ R}{2\ B}\left\{1-\exp\left[\frac{2\ B\ (h-H)}{R}\right]\right\} \qquad \textbf{(28)}$$

where ρ_S is the specific gravity of the granules, g is the acceleration of gravity, R is the radius of the hopper section (if the section is circular), h is the height of the solids element relative to the base, H is the total height of the solid column and B is the ratio between the shear stress and the normal stress close to the wall, given by:

$$B = \frac{\sin\beta_e \sin\beta^*}{1-\sin\beta_e \cos\beta^*} \qquad \textbf{(29)}$$

on what:

$$\beta^* = \beta_w + \arcsin\left(\frac{\sin \beta_w}{\sin \beta}\right), \qquad \arcsin > \frac{\pi}{2} \tag{30}$$

where β_e is the internal friction angle (polymer-polymer), β_W is the external friction angle (polymer-hopper) and f_P' is the polymer-hopper friction coefficient, this is (see also equation 9):

$$\beta_w = arctg\left(f_P'\right) \tag{31}$$

In the case of square W-section hoppers, equation 28 can be used by replacing R with $W/2$:

$$P = P_o \exp\left[\frac{4\ B\left(h-H\right)}{W}\right] + \frac{\rho_s\, g\ W}{4\ B}\left\{1-\exp\left[\frac{4\ B\left(h-H\right)}{W}\right]\right\} \tag{32}$$

For rectangular sections the same equation is used, replacing R with the hydraulic radius, R_H:

$$R_H = \frac{2 \quad \text{Section} \quad \text{area}}{\text{Perimeter}} \tag{33}$$

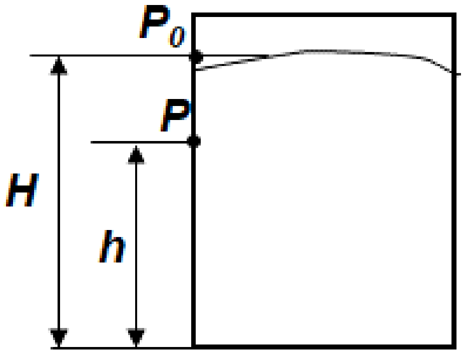

Figure 31- Hopper with vertical walls

Converging hoppers

As illustrated in Figure 32, Walker [WAL 66] also deduced equations for converging wall hoppers. The pressure distribution is in this case:

$$P = \left(\frac{h}{H}\right)^c P_o + \frac{\rho_s g h}{c-1}\left[1-\left(\frac{h}{H}\right)^{c-1}\right], \quad \text{for} \quad c \neq 1 \tag{34}$$

$$P = \frac{h}{H} P_o + \rho_s\, g\, h.\ln\left(\frac{h}{H}\right), \quad \text{for} \quad c = 1 \tag{35}$$

The constant c varies with the type of hopper cross section:

$$c = \frac{2B^`}{tg\alpha}, \quad \text{for circular sections} \qquad \textbf{(36)}$$

and

$$c = \frac{B^`}{tg\alpha}, \quad \text{for square sections} \qquad \textbf{(37)}$$

of which α is the angle of inclination of the hopper walls (Figure 32) and B' is the ratio between the shear stress and the normal stress close to the wall, given by:

$$B' = \frac{\sin\beta_e \sin\left(2\,\alpha + \beta^*\right)}{1 - \sin\beta_e \cos\left(2\,\alpha + \beta^*\right)} \qquad \textbf{(38)}$$

where:

$$\beta^* = \beta_w + \arcsin\left(\frac{\sin\beta_w}{\sin\beta_e}\right), \qquad \arcsin < \frac{\pi}{2} \qquad \textbf{(39)}$$

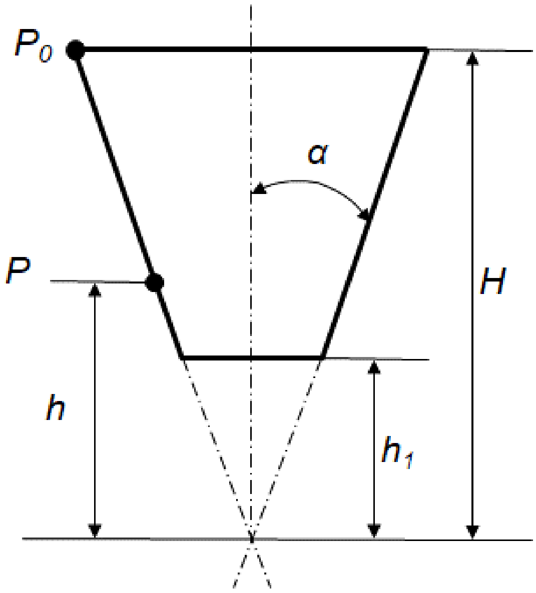

Figure 32- Hopper with converging walls

Figure 33 shows a typical hopper made up of three distinct geometric segments. Assuming that all cross sections are circular, the pressure at its base (P_3) will be calculated as follows: i) using equation 28, the pressure at the base of the first segment (P_1) is calculated, assuming that the pressure at the top is P_0=0; ii) the pressure P_2 is calculated using one of equations 34 or 35 (depending on the value of c), replacing in this equation P_0 with the value previously calculated (P_1); iii) finally, P_3 is calculated using, again, equation 28 and assuming (in this equation) that P_0 is the value calculated in the previous step (P_2).

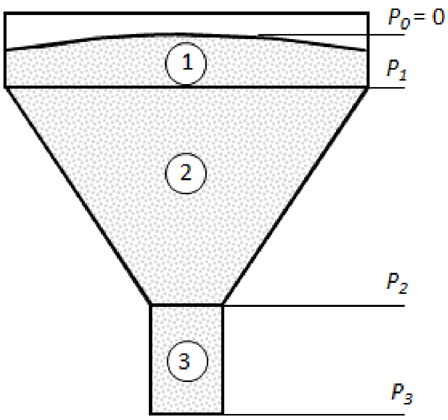

Figure 33- Process of calculating the pressure profile in a hopper with three geometric sections

Output calculation

The models in the literature for calculating hopper flow rate were the subject of a review by Shamlou [SHA 88]. The flow rate calculation depends on the geometry of the system and the particle dimensions, and the models proposed for vertical wall hoppers are based on dimensional or empirical analysis.

Brow and Richards [BRO 70] propose two different empirical equations for calculating the flow through hoppers with cylindrical and square openings. For cylindrical openings:

$$Q = \sqrt{\frac{2}{15}}\pi \; \rho_s \; g^{1/2} \left(D - k \; d_P\right)^{5/2} \Psi_c \qquad \textbf{(40)}$$

and for square openings:

$$Q = \sqrt{\frac{2}{3}}\rho_s \; g^{1/2} \; H \; \left(L - k \; d_P\right)^{3/2} \Psi_q \qquad \textbf{(41)}$$

where D is the diameter and L is the width of the hopper, k is a constant related to the shape of the granules (can be considered equal to 1, due to the great difficulty in determining it and the error is not significant), d_p is the average diameter of the particles, H is the height of the hopper and ψ_C and ψ_P are empirical constants, which in most of the practical cases can be considered equal to 1.

For converging wall hoppers, theoretical models were developed based on the resolution of the Bernouli equation [SHA 88]. Nedderman *et al.* [NED 82] developed equations for circular and square cross-section hoppers. The following equation was obtained for circular hoppers:

$$Q = \frac{\pi}{4} \frac{\rho_s \; g^{1/2} \; D^{1/2}}{\sin^{1/2} \alpha} \left[\frac{1 + K}{2(2k - 3)}\right]^{1/2} \qquad \textbf{(42)}$$

and for square openings:

$$Q = \frac{\rho_s \; g^{1/2} \; H \; L^{1/2}}{\sin^{1/2} \alpha} \left[\frac{1 + K}{2(k - 3)}\right]^{1/2} \qquad \textbf{(43)}$$

where α is the angle of inclination of the hopper walls and K is the ratio between major and minor stresses, the inverse of equation 26.

Application exercises

1. Consider the hopper shown in Figure 34. Determine the pressure at its base.

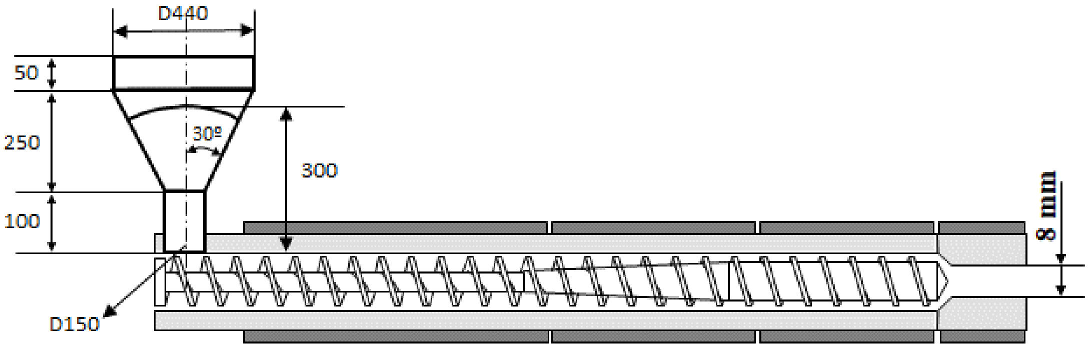

Figure 34- Hopper geometric data (exercise 1)

Material data:

- Density of material in the hopper = 630 kg / m3
- Material-hopper friction coefficient = 0.3
- Internal particle friction angle = 34 °
- Total material height = 300 mm.

2. Plot the pressure profile along the hopper in Figure 35. Consider the same properties as the previous exercise.

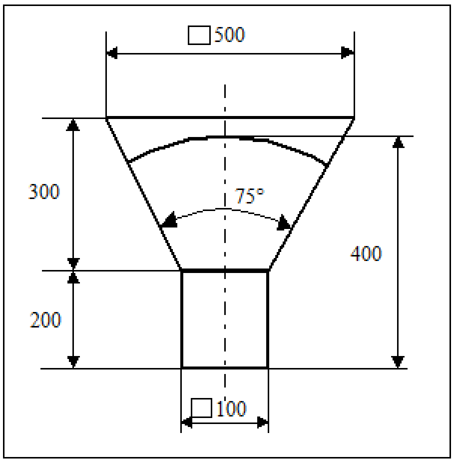

Figure 35- Hopper geometric data (exercise 2)

3.2. Solids transport in the screw

In the mathematical modeling of this zone, it is generally assumed that the polymer behaves from the beginning as a continuous elastic solid plug, acquiring the rectangular shape of the screw channel. It is also possible to consider that what happens in this zone is a granular flow of loose solids, that is, each granule has its own movement resulting from the collision with the other granules and with the channel walls [MIC 14]. This is in fact a more realistic situation, however due to its complexity it will not be considered here.

As previously noted, the efficiency of the transport of solids in the screw channel depends on the relative values between the coefficients of friction of polymer particles and the walls of the cylinder and the screw channel, and two extreme situations can happen:

1) The polymer sticks to the screw and slides over the cylinder: in this case, the flow rate is zero.
2) The polymer slides over the screw and sticks to the cylinder: in this case the flow rate of the extruder is high.

This means that in order to increase the flow rate of solids, the friction coefficient near to the screw must be decreased and increased near to the cylinder. For this reason, many cylinders are grooved internally, thus increasing the friction coefficient even further. In addition, the friction coefficient is an intrinsic property of the material that varies with temperature, pressure and velocity – that is, operating conditions – affecting process performance.

The effect of this zone on the performance of the extruder depends on its longitudinal length [BRO 72]. If the process is controlled by the capacity of the pumping zone, the solids transport zone may be limited to the first turns of the screw, and consequently the pressure generation will be negligible. When the extruders are intended to operate with a relatively long solids transport zone (efficiently cooling the cylinder in this zone, for example), the pressure generation will be higher and the flow capacity of the extruder will be increased. In these cases, where the generation of pressure in the solids transport zone contributes significantly to the total generation of pressures in the extruder, it is not valid to assume that the process is isothermal, as a considerable amount of heat is generated by friction, mainly on the cylinder surface.

The theoretical models presented below allow to predict for this zone: mechanical power consumption, flow rate, longitudinal pressure profile and longitudinal and transversal temperature profiles.

Isothermal model

The model proposed by Broyer and Tadmor [BRO 72] is adopted, which was developed from the initial work of Darnell and Mol [DAR 56]. In developing this model, it is considered that:

- The solid material behaves from the beginning as an elastic solid plug;
- The block of solids contacts the four walls of the channel;
- The depth of the channel is constant (however, variations in the depth of the channel can be considered by taking small increments of the channel with different depth);
- The effect of the mechanical gap between the screw flight and the inner surface of the cylinder is disregarded, that is: $D_p = D_c$;
- The pressure distribution is isotropic, that is, the pressure varies only in the direction of the channel length;
- The material temperature is constant and uniform (but the values can be updated considering small increments of channel);
- The block of solids moves with uniform speed in any axial section;
- The friction coefficients are constant (independent of pressure, temperature and time) but have different values on the surface of the cylinder and of the screw;
- The specific mass of the polymer is constant;
- Gravitational forces are neglected.

Variations with temperature and/or pressure in the specific mass, friction coefficients and other material properties can be taken into account, provided that calculations are made considering small axial increments and these properties are updated with the new values, temperature and/or pressure in the previous increment.

Thus, the volumetric flow rate of the solid block (Q) can be quantified by the product of the axial velocity of the solid block (V_{ba}) by the effective area of the cross section (see Figure 36):

$$Q = V_{ba}\left[\tfrac{\pi}{4}\left(D_c^2 - D_i^2\right) - \frac{e\,H}{\sin\bar{\theta}}\right] \qquad \textbf{(44)}$$

As shown in Figure 36, the solids conveying angle (φ) is a measure of the difference between the velocity of the cylinder (V_c) and that of the block of solids along the channel (V_{bz}); the angle φ being inversely proportional to that difference, that is, it corresponds to the angle of the movement of the solids if the side walls of the screw channel did not exist. In this case: when V_{bz} is equal to zero, both Q and φ are also zero; when V_c is equal to V_{bz}, φ assumes its maximum value which is equal to 90º-θ_c.

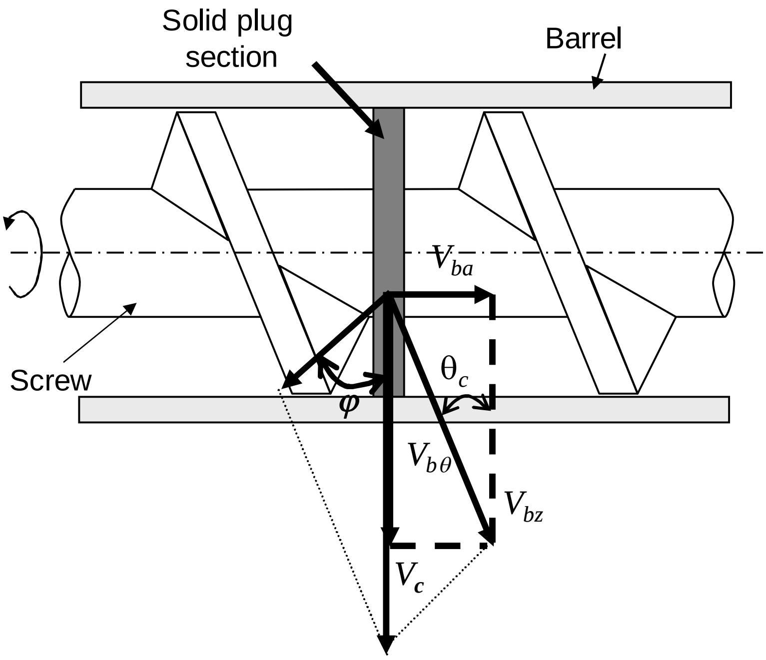

Figure 36- Components of the solid plug velocity in the directions of the channel, direction z (V_{bz}), axial (V_{ba}) and transversal ($V_{b\theta}$) and the solids conveying angle (φ)

From Figure 37 it is known that:

$$\tan\varphi = \frac{V_{ba}}{V_c - V_{b\theta}} \qquad \textbf{(45)}$$

and known that $\tan\theta_c = \dfrac{V_{ba}}{V_{b\theta}}$, from the previous equation we can obtain:

$$\tan\varphi = \frac{V_{ba}}{V_c - \dfrac{V_{ba}}{\tan\theta_c}} \quad \textbf{(46)}$$

this is, solving this equation as a function to V_{ba}:

$$V_{ba} = V_c \frac{\tan\varphi \tan\theta_c}{\tan\varphi + \tan\theta_c} \quad \textbf{(47)}$$

Since $V_c = \pi\ N\ D_c$ and $D_c^2 - D_i^2 = 4H\left(D_c - H\right)$, and replacing equation 47 in equation 44, the volumetric flow rate of the solid plug (Q) is expressed as a function of the solids conveying angle (φ), the rotation speed of the screw (N) and the geometry (e, H, D_c and θ):

$$Q = \pi^2 N\ H\ D_c (D_c - H) \frac{\tan\varphi \tan\theta_c}{\tan\varphi + \tan\theta_c} \left[1 - \frac{p\ e}{\pi (D_c - H) \sin\bar{\theta}} \right] \quad \textbf{(48)}$$

being p the number of flights, usually equal to 1.

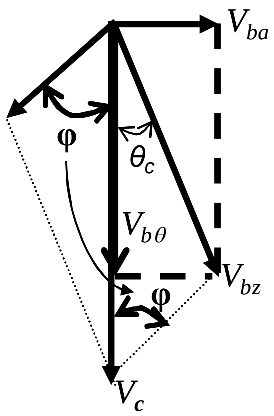

Figure 37- Vectors scheme for the determination of V_{ba}

To calculate the flow rate, it is necessary to determine the value of the angle φ. For this, it is essential to take into account the pressure variation along the channel, which can be obtained by a balance of forces and moments in a differential element of the solid plug, as shown in Figure 38 [BRO 72].

F_1 is the frictional force exerted on the outer surface of the block of solids, that is, the product of the friction coefficient in the cylinder (f_c) by the normal applied force, resulting in the product of the pressure (P) over the area where the pressure is applied ($W_c\ dz$):

$$F_1 = f_c P W_c dz \quad \textbf{(49)}$$

F_3, F_4 and F_5 are the frictional forces due to the contact between of the solid plug and the screw walls.

$$F_3 = F_7 f_p$$
$$F_4 = F_8 f_p \quad \textbf{(50)}$$
$$F_5 = f_p P W_p dz$$

In this case, F_7 and F_8 are the normal forces exerted by the screw flanks.

$$F_7 = PHdz + F^* \qquad F_8 = PHdz \tag{51}$$

An additional unknown force (F^*) has been added to the force F_7, exerted by the active flank, which must be determined by the simultaneous resolution of the equations resulting from the balance of forces and moments. Finally, F_2 and F_6 are the forces resulting from the pressure gradient in the direction of the channel length (direction z), whose difference between them (assuming the pressure increases in this direction) is calculated by the product of the average section area by the pressure difference (dp):

$$F_6 - F_2 = H\overline{W}dp \tag{52}$$

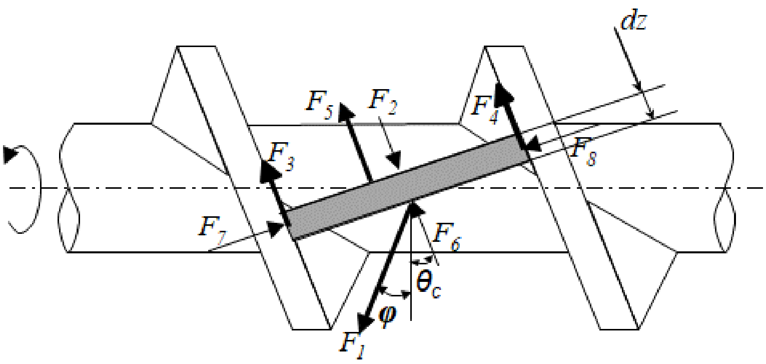

Figure 38- Balance of forces and moments in a differential element of the solid plug

As mentioned, through a balance of forces and moments:

$$\sum F_i = 0 \tag{53}$$

$$\sum M_i = 0 \tag{54}$$

and through the simultaneous resolution of the resulting equations, it is possible to eliminate the additional force F^*, obtaining the following relationship:

$$\cos\varphi = K_p \sin\varphi + M \tag{55}$$

where:

$$M = 2\frac{Hf_p}{W_c f_c}\sin\theta_c\left(K_p + \frac{\bar{D}}{D}\operatorname{cotg}\bar{\theta}\right) + \frac{W_p f_p}{W_c f_c}\sin\theta_c\left(K_p + \frac{D_i}{D}\operatorname{cotg}\theta_p\right) + \frac{\bar{W} H}{W_c\ z\ f_c}\sin\bar{\theta}\left(K_p + \frac{\bar{D}}{D}\operatorname{cotg}\bar{\theta}\right)\ln\left(P_2/P_1\right) \tag{56}$$

and

$$K_p = \frac{\overline{D}}{D_c}\left(\frac{\sin\overline{\theta} + f_p \cos\overline{\theta}}{\cos\overline{\theta} - f_p \sin\overline{\theta}}\right) \qquad \textbf{(57)}$$

In these equations: P_1 is the pressure at the beginning of the solids zone (z = 0), P_2 is the pressure at z. This equation can be rearranged in the form:

$$P_2 = P_1 \exp\left(\frac{B_1 - A_1 K_p}{A_2 K_p + B_2} z\right) \qquad \textbf{(58)}$$

where A_2, B_2 and K_P depend on geometry and A_1 and B_1 depend on geometry, friction coefficients and angle φ:

$$A_1 = f_c W_c \sin\varphi - \overline{W} \operatorname{tg}\alpha \sin\overline{\theta} + 2.H f_p \sin\theta_c + W_p f_p \sin\theta_c \left(\cos\alpha + \frac{\sin\alpha}{f_p}\right) \qquad \textbf{(59)}$$

$$A_2 = H\overline{W} \sin\overline{\theta} \qquad \textbf{(60)}$$

$$B_1 = f_c W_c \cos\varphi + \overline{W} \operatorname{tg}\alpha \cos\overline{\theta}\frac{\overline{D}}{D_c} - 2\, H\, f_p \sin\theta_c \operatorname{cotg}\overline{\theta}\frac{\overline{D}}{D_c} - W_p f_p \left(\cos\alpha + \frac{\sin\alpha}{f_p}\right) \sin\theta_c \operatorname{cotg}\theta_p \frac{D_p}{D_c} \qquad \textbf{(61)}$$

$$B_2 = H\overline{W} \cos\overline{\theta}\frac{\overline{D}}{D_c} \qquad \textbf{(62)}$$

where α is the slope angle of the channel (Figure 18) in the compression zone (generally, as the solids conveying occurs in the screw's geometric feed zone, this value is zero). As can be seen from equation 58, the pressure variation in the solids transport zone on the screw increases exponentially; this is illustrated in Figure 39 where the pressure evolution over 10 turns of a screw is shown.

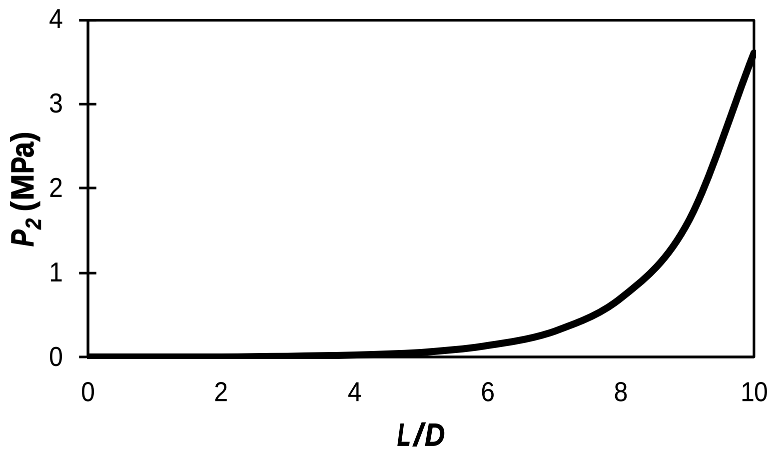

Figure 39- Exponential pressure variation over 10 turns of the screw to the solids zone

In solving problems for this zone, two different situations can arise: i) the flow rate is known and it is intended to determine the pressure variation and ii) the pressure variation is known and it is intended to calculate the flow rate. In the first case, the value of φ is determined from the flow equation (equation 48), finally calculating P_2 using equation 58. In the second case, it is necessary to solve equation 55 to determine φ, whose solution is given by:

$$\sin\varphi = \frac{\sqrt{1+K_P^2-M^2}-K_P\ M}{1+K_P^2} \qquad \textbf{(63)}$$

value that will be inserted in equation 48 to calculate the flow rate.

Figure 40, which shows the evolution of a dimensionless flow measurement, $(\mathrm{tg}\varphi.\mathrm{tg}\theta_c)/(\mathrm{tg}\varphi + \mathrm{tg}\theta_c)$, with the friction coefficients calculated with the model presented, clearly illustrates the operation of the solids conveying zone. This figure clearly shows that: i) the flow rate increases with f_c; ii) when $f_c \approx f_p$ the flow is small, but a small variation in f_c produces a significant variation in flow and iii) when fc»fp the flow is high and stable. This analysis allows us to conclude that, in order to have a stable solid area, the cylinder and the screw must be machined in such a way that the friction coefficient in the cylinder is two to three times greater than the friction coefficient on the surface of the screw.

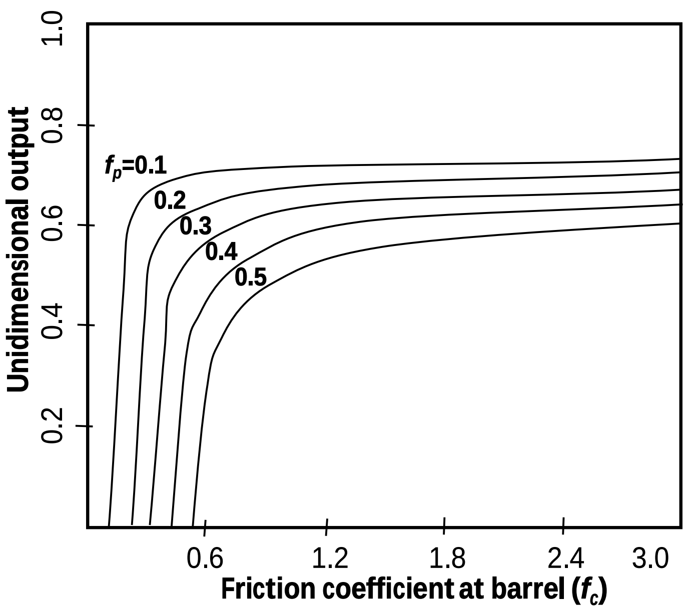

Figure 40- Unidimensional mass flow rate as a function of the friction coefficients

An analysis of equation 48 (flow equation) allows us to conclude that the flow has it maximum value when the expression $(\mathrm{tg}\varphi.\mathrm{tg}\theta_c)/(\mathrm{tg}\varphi + \mathrm{tg}\theta_c)$ is maximum, that is, the machine must operate with high φ values. For this to happen, from equation 55, K_p and M must be small.

For small M:

- Ratio f_p/f_c must be minimized, *i.e.*, the surface of the screw must be smooth than that of the cylinder;
- Ratio P_2/P_1 ratio must be minimized; this means that the transport mechanism depends on P_1 (pressure at the base of the hopper) and that the flow rate is maximum if P_2 is equal to P_1, *i.e.*, there is no pressure generation, and the transport capacity of the screw is affected by the need for generate pressure.

For small k_p:

• In this case, ratio D_i / D_c must be minimized.

It is also verified that the flow rate increases linearly with the rotation velocity of the screw (N).

Power consumption

An important aspect to take into account when designing extruders (or screws) is the energy required to turn the screw, that is, the total consumption of mechanical power required to turn the screw (e_w). For the solids conveying zone this power is calculated by the frictional force caused by the cylinder acting on the solid block multiplied by the velocity of the cylinder in the direction of the angle φ. This force is the product of the local pressure with the area of the interface that the block of solids does with the cylinder ($f_c W_c P_2 dZ_c$) [BRO 72]:

$$de_w = \pi N D_c \, f_c W_c P_2 Z_c \cos\varphi \; dz \qquad \textbf{(64)}$$

where P_2 is the pressure profile given by equation 58. The integration of this equation results in:

$$e_w = \pi N D_c \, f_c W_c P_m z \, \cos\varphi \qquad \textbf{(65)}$$

where P_m is obtained from:

$$P_m = \frac{P_2 - P_1}{\ln P_2 / P_1} \qquad \textbf{(66)}$$

The total power consumption in this zone is obtained by replacing z for the total length of the solids zone. In a more detailed analysis, it is known that the total power is the sum of the following components:

$$e_w = e_{wc} + e_{wp} + e_{wf} + e_{wpre} \qquad \textbf{(67)}$$

where, e_{wc} is the power dissipated at the cylinder surface, e_{wp} is the power dissipated at the root of the screw, e_{wf} is the power dissipated at the flanks of the screw and e_{wpre} is the power due to the pressure gradient along the axial increment. Each of these power terms can be calculated using the following equations:

$$e_{wc} = \pi N D_c \, f_c W_c P_m z \, \frac{\sin\theta_c}{\sin(\theta_c + \varphi)} \qquad \textbf{(68)}$$

$$e_{wp} = \pi N D_p \, f_p W_p P_m z \, \frac{\sin\theta_c}{\sin(\theta_c + \varphi)} \frac{\sin\theta_c}{\sin\theta_p} \frac{tg\theta_c}{tg\theta_p} r_1 \qquad \textbf{(69)}$$

$$e_{wf} = \pi N D_c f_p W_p P_m z \frac{\sin\theta_c}{\sin(\theta_c + \varphi)} \frac{\sin\theta_c}{\sin\overline{\theta}}$$

$$\left[2H \frac{\sin\theta_c}{\sin\overline{\theta}} + f_c W_c \left(\sin\varphi \cos\overline{\theta} + \frac{D_c}{\overline{D}} \cos\varphi \sin\overline{\theta} \right) + W_p f_p \sin\theta_c \cos\overline{\theta} \left(1 - \mathrm{cotg}\,\theta_p \, tg\overline{\theta} \frac{D_p}{\overline{D}} \right) \right] \quad \textbf{(70)}$$

$$e_{wpre} = \pi N D_c H \overline{W} \frac{\sin\theta_c}{\sin(\theta_c + \varphi)} \frac{\sin\theta_c}{\sin\overline{\theta}} P_m \ln\left(\frac{P_2}{P_1} \right) \quad \textbf{(71)}$$

where:

$$r_1 \frac{1 - \dfrac{e}{S \cos\theta_p}}{1 - \dfrac{e}{S \cos\theta_c}} \quad \textbf{(72)}$$

Non-isothermal model

Ignoring the effects of temperature variation, due to frictional heat generation between the polymer granules and the cylinder and screw surfaces, can be a major limitation of the previous model, since it is not possible to determine where the transport zone of solids ends. In the previous model, it is considered that solids conveying ends when the temperature in the cylinder reaches the melting temperature of the material (or about 50º C above the glass transition temperature for amorphous polymers), which, has been verified, may induce considerable errors in the calculations. This is because the pressure increase in this zone is exponential, and it does not matter whether the solids zone ends sooner. The non-isothermal model makes it possible to calculate the axial and cross-sectional temperature profiles in the solid plug and, consequently, locate the point from which the surface of the solid plug reaches the polymer melting temperature. This axial location occurs before that predicted by the isothermal model, which is reached when the temperature of the cylinder is equal to the melting temperature of the polymer.

Neglecting the heat flows at the root and flanks of the screw results in a one-dimensional transient heat transfer problem (heat flow perpendicular to the cylinder surface). The heat generated on the surface of the cylinder varies with time - t (or with the axial location on the screw - z) and with the distance in the solid block - y. A differential element of time - Δt - and another of distance - Δy - can be defined, so that:

$$\begin{cases} t = i\,\Delta t \\ y = j\,\Delta y \end{cases} \quad \textbf{(73)}$$

In other words, a mesh is defined where the temperature profile in the block of solids depends on two parameters, i and j, the calculations being made by finite differences. Figure 41 illustrates the mesh used in the calculations. The temperature at any point in this mesh is obtained from:

$$T_{bs}(i+1, j) = \frac{1}{2}\left[T_{bs}(i, j+1) + T_{bs}(i, j-1)\right], \quad Y - 1 \geq j \geq 0 \quad \textbf{(74)}$$

The solution's convergence occurs if the values of Δt and Δy follow the following relation:

$$\alpha_s \frac{\Delta t}{\Delta y^2} = \frac{1}{2} \quad \textbf{(75)}$$

where α_S is the thermal diffusivity of the solid polymer:

$$\alpha_s = \frac{k_s}{\rho_s\, C_s} \quad \textbf{(76)}$$

In these equations, T_{bs} is the temperature of the block of solids and Y is the number of increments in which the depth of the channel (H) is divided. The temperature value of the block of solids near the inner surface of the cylinder, $T_{bs}(i, Y)$, is given by:

$$T_{bs}(i,Y) = \frac{\dfrac{\Delta y}{k_s} q_c(i) + T_{bs}(i,Y-1) + \dfrac{k_b}{k_s}\dfrac{\Delta y}{b} T_c(i,b)}{1 + \dfrac{k_b}{k_s}\dfrac{\Delta y}{b}} \quad \textbf{(77)}$$

where k_s is the thermal conductivity of the solid polymer, k_b is the thermal conductivity of the cylinder material, b is the distance, in the cylinder, from the polymer-cylinder interface to the thermocouple position, $T_c(i, b)$ is the temperature of the cylinder at distance b and $q_c(i)$ is the heat generated per unit surface of the cylinder, value of which is given by equation 68 to be divided by the contact surface between the cylinder and the solid block ($\Delta z\, W_c$).

Although this is a transient problem, the extruder operates in a steady state, that is, the temperature profile is constant in each section considered. For this reason, it is important to obtain the temperature profile along the z direction. The following equation can be used to obtain the temperature values as a function of Δz.

$$\Delta z = \frac{G}{\rho_s\, A} \Delta t \quad \textbf{(78)}$$

where G is the mass flow rate and A is the cross-sectional area of the channel (equal to $W_c\, H$).

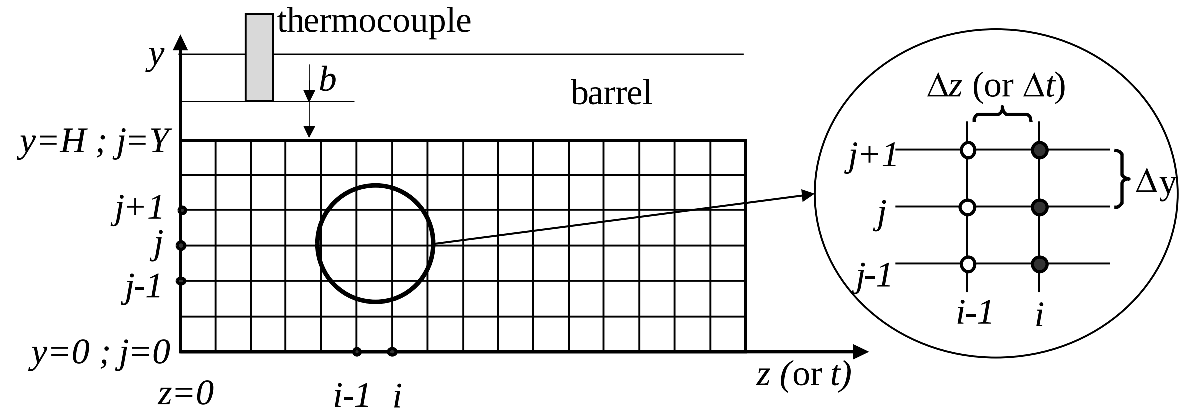

Figure 41- Finite difference mesh used in the calculations

The calculation is made taking into account the mesh defined in Figure 41, assuming that the following are known: i) the temperature for z=0 - $T_{bs}(0,j)$ and ii) the temperature in the cylinder at distance b from its inner surface, *i.e.*, $y = H + b$ - $T_c(i, b)$ - as given by equation 77. Thus, the calculation procedure is as follows:

1) Divide H into a fixed number of intervals, Y, giving Δy;
2) Δt is determined using equation 75;
3) $T_{bs}(i, Y)$ is determined using equation 77;
4) For each interval Δy, the temperature $T_{bs}(i + 1, j)$ is calculated using equation 74;
5) Time intervals, Δt, are transformed into Δz using equation 78.

Numerical Model

The temperature profile in the solid plug can be calculated by solving the energy equation, which depends on:

• Heat convection along the channel due to the movement of polymer in the z direction;

• Heat conduction, in the y direction, due to temperature gradients;

• Heat conduction in the transversal direction of the channel, direction x.

This last term can be neglected since it is much smaller when compared to the other two. Thus, the temperature profile along the screw channel can be described by the following equation, where the term on the left represents heat convection and the term on the right represents heat conduction.

$$V_{sz}\frac{\partial T(y)}{\partial z} = \alpha_s \frac{\partial^2 T(y)}{\partial y^2} \qquad \textbf{(79)}$$

V_{sz} is the velocity of the block of solids in the z direction, $T(y)$ is the profile of transversal temperatures (direction y) and α_s is the thermal diffusivity of the block of solids. Note that in this equation and in the following ones (in order to simplify writing) the temperature T represents the temperature in the solid block (T_{bs}), as previously designated.

Figure 42 shows the heat flows due to the friction existing on the different surfaces using a differential element of the channel. Heat flows through the flanks are generally neglected in the calculations [TAD 72]. However, the heat generation at the root of the screw will be taken into account in order to define the location of the channel where the polymer reaches the melting temperature, and where the second part of the delay zone begins (as will be seen in the next section).

Thus, the previous equation can be solved using finite differences and considering the heat fluxes (per unit area) defined by equations 68 and 69 to be divided by the surfaces where they act ($W_c\,\Delta z$ and $W_s\,\Delta z$, respectively). The heat generated on the surface of the barrel is dissipated through two flows simultaneously, one towards the solids and the other towards the cylinder [TAD 72]:

$$q_c = -k_s \left.\frac{\partial T(y)}{\partial y}\right|_{y=H} + k_b \left.\frac{\partial T(y)}{\partial y}\right|_{\text{cylinder}} \qquad \textbf{(80)}$$

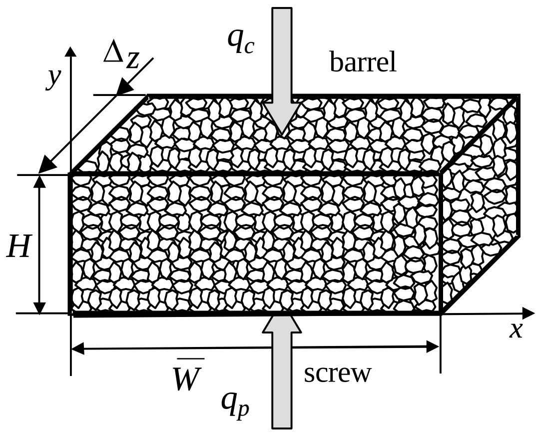

Figure 42- Flows of heat due to friction in a differential element of solids

The calculation of the heat flow by conduction in the cylinder is performed using the cylinder temperature value (T_c), which is obtained at a distance *b* through the interface and taking into account a linear temperature profile along the cylinder thickness (see Figure 41):

$$\left.\frac{\partial T(y)}{\partial y}\right|_{cylinder} = \frac{T_c - T}{b} \tag{81}$$

where *T* is the temperature of the cylinder's inner interface.

It is more difficult to calculate the heat flow in the screw, since the temperature of the screw is not known. It can also be considered that the temperature on the surface of the screw (T_p) is constant (for example, equal to the inlet temperature of the polymer - T_{s0}), or else, the existence of an adiabatic screw. In this case, the heat flow is given by:

$$q_p = k_p \left.\frac{\partial T(y)}{\partial y}\right|_{y=0} \tag{82}$$

where k_p is the thermal conductivity of the screw (metal).

Equation 79 can be solved using an implicit finite difference method such as the Crank-Nicolson method, along with the boundary conditions defined in the cylinder (equation 81) and at the root of the screw (equation 82). The differential element in the *y* (Δy) direction will be independent of the *z* (Δz) direction [TAD 72, MIT 80]. The screw channel is filled with a rectangular mesh with sides parallel to the *y* and *z* axes (Figure 41); Δy and Δz being the mesh (or differential elements) spacing in the *y* and *z* directions, respectively. The coordinates of the points in the mesh (*Y*, *Z*) are given by:

$$\begin{cases} Y = j\,\Delta y \\ Z = i\,\Delta z \end{cases} \tag{83}$$

with $i = 0, 1, \ldots M$ and $j = 0, 1, \ldots, N$.

The discretization of equation 79 is done using an approximation by central differences, obtaining for the first order derivatives:

$$\left.\frac{\partial T}{\partial z}\right|_{i,j} = \frac{T_{i,j} - T_{i-1,j}}{\Delta z} \tag{84}$$

$$\left.\frac{\partial T}{\partial y}\right|_{i,j} = \frac{T_{i,j+1} - T_{i,j-1}}{2\,\Delta y} \quad \textbf{(85)}$$

Using the Crank-Nicolson method for second order derivatives, we obtain:

$$\left.\frac{\partial^2 T}{\partial y^2}\right|_{i,j} = \frac{1}{2}\left[\frac{T_{i,j+1} - 2\,T_{i,j} + T_{i,j-1}}{\Delta y^2} + \frac{T_{i-1,j+1} - 2\,T_{i-1,j} + T_{i-1,j-1}}{\Delta y^2}\right] \quad \textbf{(86)}$$

Figure 41 shows the six points involved in these calculations for determining the temperature at point *T*(*i*,*j*). Replacing in equation 79 and rearranging:

$$\begin{gathered} -\frac{\alpha_s}{2\,\Delta y^2} T_{i,j-1} + \left(\frac{V_{sz}}{\Delta z} + \frac{\alpha_s}{\Delta y^2}\right) T_{i,j} - \frac{\alpha_s}{2\,\Delta y^2} T_{i,j+1} = \\ \frac{\alpha_s}{2\,\Delta y^2}\left(T_{i-1,j-1} - 2\,T_{i-1,j} + T_{i-1,j+2}\right) + \frac{V_{sz}}{\Delta z} T_{i-1,j} \end{gathered} \quad \textbf{(87)}$$

Since the temperatures on the left side of the equation are unknown and those on the right side were calculated in the previous step, or correspond to the initial temperature for $z = 0$ ($i = 0$).

Substituting j for 1, 2, ..., N-1 gives a system of equations that can be placed in matrix form, which can be solved using, for example, the Gaussian elimination method with partial pivot choice.

$$A\,T = B \quad \textbf{(88)}$$

$$A = \begin{bmatrix} -\frac{\alpha_s}{2\,\Delta y^2} & \frac{V_{sz}}{\Delta z} + \frac{\alpha_s}{\Delta y^2} & -\frac{\alpha_s}{2\,\Delta y^2} & 0 & 0 \\ 0 & -\frac{\alpha_s}{2\,\Delta y^2} & \frac{V_{sz}}{\Delta z} + \frac{\alpha_s}{\Delta y^2} & -\frac{\alpha_s}{2\,\Delta y^2} & 0 \\ \ldots & \ldots & \ldots & \ldots & \ldots \\ \ldots & \ldots & \ldots & \ldots & \ldots \\ 0 & 0 & -\frac{\alpha_s}{2\,\Delta y^2} & \frac{V_{sz}}{\Delta z} + \frac{\alpha_s}{\Delta y^2} & -\frac{\alpha_s}{2\,\Delta y^2} \end{bmatrix} \quad \textbf{(89)}$$

$$T^T = \begin{bmatrix} T_{i,0} & T_{i,1} & \ldots & T_{i,N-1} & T_{i,N} \end{bmatrix} \quad \textbf{(90)}$$

$$B = \begin{bmatrix} \frac{\alpha_s}{2\,\Delta y^2}\left(T_{i-1,0} - 2\,T_{i-1,1} + T_{i-1,2}\right) + \frac{V_{sz}}{\Delta z} T_{i-1,1} \\ \frac{\alpha_s}{2\,\Delta y^2}\left(T_{i-1,1} - 2\,T_{i-1,2} + T_{i-1,3}\right) + \frac{V_{sz}}{\Delta z} T_{i-1,2} \\ \ldots \\ \frac{\alpha_s}{2\,\Delta y^2}\left(T_{i-1,N-3} - 2\,T_{i-1,N-2} + T_{i-1,N-1}\right) + \frac{V_{sz}}{\Delta z} T_{i-1,N-2} \\ \frac{\alpha_s}{2\,\Delta y^2}\left(T_{i-1,N-2} - 2\,T_{i-1,N-1} + T_{i-1,N}\right) + \frac{V_{sz}}{\Delta z} T_{i-1,N-1} \end{bmatrix} \quad \textbf{(91)}$$

This system has N-2 equations and N unknowns, requiring two new equations that result from equations 80 and 82:

$$-\frac{k_s}{2\Delta y}T_{i,N-2}+\left(\frac{k_s}{2\Delta y}+\frac{k_b}{b}\right)T_{i,N}=-\frac{k_b}{b}T_c-q_c \quad \textbf{(92)}$$

$$\frac{k_s}{2\Delta y}T_{i,0}-\frac{k_s}{2\Delta y}T_{i,2}=q_p \quad \textbf{(93)}$$

The importance of being able to predict the temperature rise of the solid block at the interface with the cylinder surface is shown in Figures 43 and 44.

Figure 43 illustrates a situation where the initial temperature of the solid block is 27ºC and the cylinder temperature is 70ºC. It is verified that after an axial length of 0.09 m the temperature at the interface reaches the melting temperature of the material (110ºC), despite the average temperature being less than 50ºC. However, due to these conditions, the solids transport zone ends at this point, once the polymer at the interface begins to melt. Without the possibility of calculating this temperature at the interface, the end of this zone could not be predicted, where the pressure grows exponentially (reaching in this case about 35kPa).

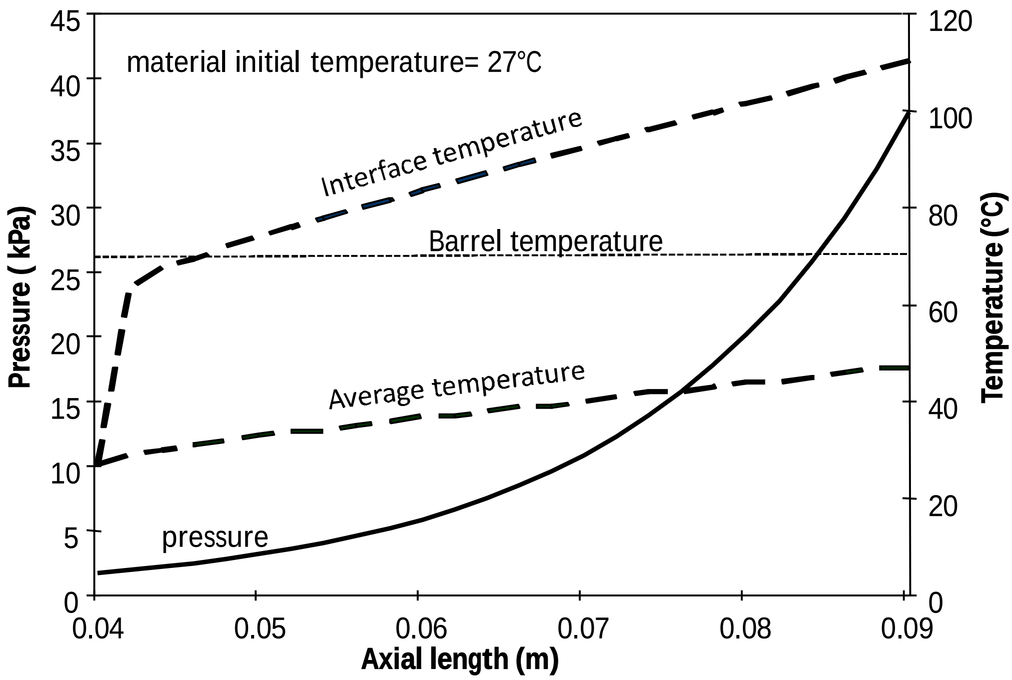

Figure 43- Evolution of temperature and pressure along the screw

Figure 44 shows the evolution of the temperature at the interface and the pressure for various values of the friction coefficient in the cylinder. It can be seen that when the friction coefficients on the surfaces of the screw and cylinder are equal (and low) the temperature at the interface never reaches the melting temperature and the pressure increases very little. In the opposite situation, keeping the friction coefficient on the surface of the screw constant and considerably increasing the friction coefficient on the surface of the cylinder, the pressure increases considerably and, at the same time, the length of the zone is very short, since the melting temperature is reached quickly at the interface of the solid block with the cylinder.

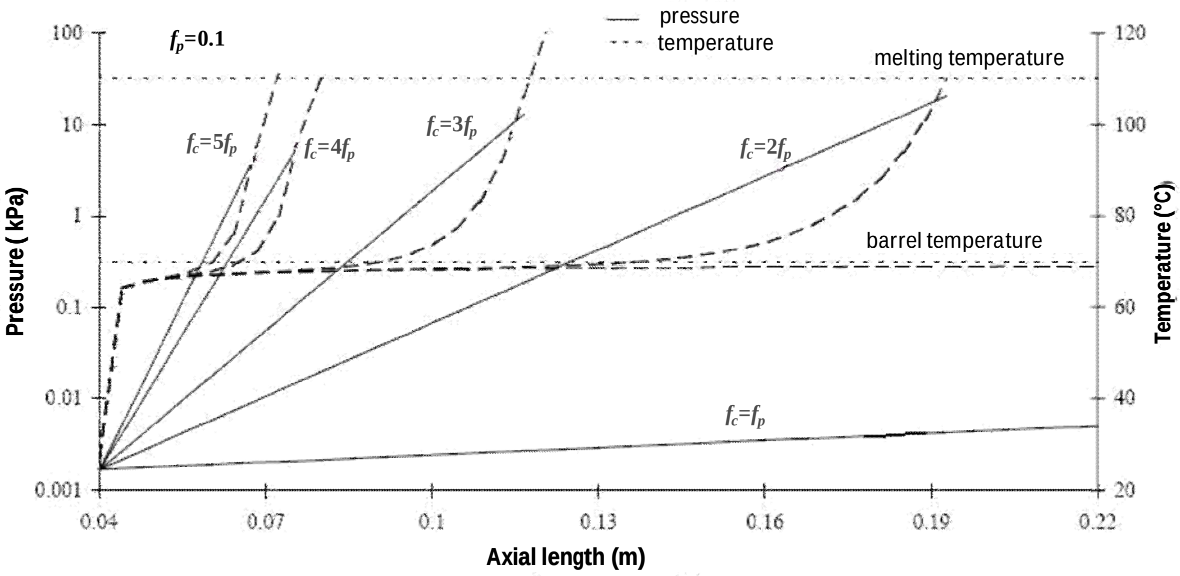

Figure 44- Evolution of temperature and pressure along the screw for various values of friction coefficients

Application exercise

1. The extruder/extrusion head set shown in Figure 45, produces HDPE rod (melting temperature 130°C) at a rate of 173 kg/hr and with a screw rotation speed of 60 rpm.

Determine the power consumption in the solids transport zone.

Notes: i) before starting the calculations, explain the methodology for solving the problem; ii) the hopper used is the same as in exercise 1 of the previous chapter.

Material data:

- Specific gravity of the material in the feed = 630 kg / m3;
- Specific gravity of the solid material = 940 kg / m3;
- Coefficient of material friction / hopper = 0.29;
- Material / screw friction coefficient = 0.24;
- Material / cylinder friction coefficient = 0.4;
- Internal particle friction angle = 34 °.

Screw:

- Square step;
- D = 60 mm;
- Compression rate = 2.8;
- Fillet width = 5mm.

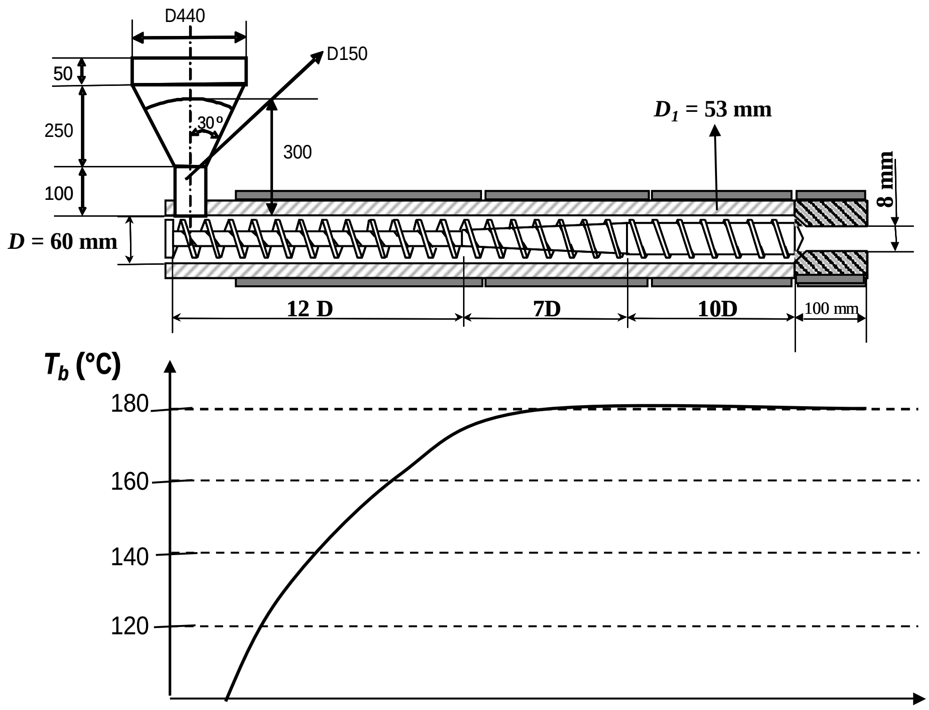

Figure 45- Extruder geometry and temperature profile in the barrel

3.3. Delay zone

Taking into account what was mentioned in chapter 3, that the melting of the polymer in the extruder is not instantaneous, it occurs gradually along the screw. As was observed experimentally by Maddock [MAD 59] and Tadmor *et al.* [TAD 67], the polymer melts in two steps (Figure 46):

1) The polymer that is in contact with the cylinder melts due to frictional heat generation and/or due the heat conducted from the cylinder, forming a melt film at the solid cylinder-polymer interface. Then, the melt film increases its thickness (Figure 46-a).

2) In this case, a melt pool is formed next to the active flank of the channel section. This melt pool progressively expands until the material is completely melted (Figure 46-b).

The first stage is generally known as the delay zone and is characterized by an increase in the thickness of the melt film formed between the cylinder and the solid block. There are at least two causes for this mechanism [AGA 96, TAD 67, KAC 72]. The melted material initially, instead of accumulating next to the flank, penetrates and fills the spaces between the granules, delaying the increase in film thickness. After the film is formed, the melting mechanism will only start when the thickness of the melt film exceeds the thickness of the clearance between the screw flight and the cylinder. Generally, the thickness of the film grows beyond the gap value (about five to seven times), until there is sufficient pressure in the channel capable of pushing and deforming the solid block against the passive flank [KAC 72, AGA 96].

However, taking into account that there is frictional heat dissipation close to the screw walls, there is also (at a certain location in the channel) the formation of melt films near the root and flanks of the screw, as shown in Figures 46-c and 46-d. Thus, this chapter will present three models that consider these differences. Initially, two analytical models will be presented. The first considers only the existence of a melt film at the solid block/cylinder interface, situation (a) of Figure 46, which evolves into a melt pool, situation (b). The second that considers the existence of melt films surrounding the block of solids, situation (c), which evolves to situation (d). Finally, a numerical model will be presented that considers a more realistic situation: i) the formation of a molten film next to the cylinder, situation (a), which will be called the Delay Zone I; ii) the formation of melt films close to the screw walls, situation (c), called the Delay Zone II; iii) the formation of a melt pool, situation (d). In all cases, the models that take into account the existence of the melt pool, situations (b) and (d), will only be considered in the next chapter - melting zone.

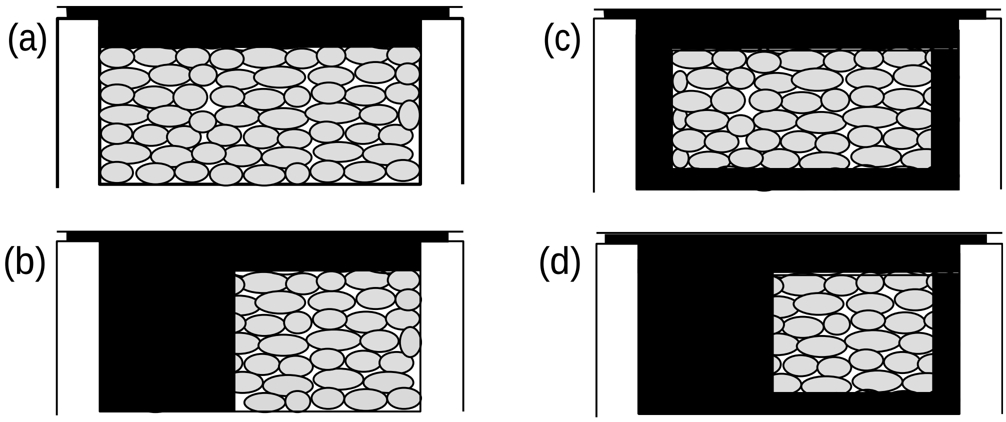

Figure 46- Formation of the films and the melt pool

Analytical models

Melt film next to the cylinder

Kacir and Tadmor [KAC 72] developed an analytical model that makes it possible to calculate the thickness profiles of the melt and pressure along the channel, taking into account the situation (a) identified in Figure 49. The thickness (δ) of the melt film of increases until it causes a pressure in the block of solids that deforms it and pushes it to the passive flank of the fillet, creating the melt pool. This means that the local pressure (ΔP) exceeds the "yield pressure" of the cohesive block of solid granules (P_c) [AGA 89].

$$\Delta P = \frac{6\,\eta\,V_c}{\sin\bar{\theta}}\,\frac{\delta - \delta_f}{\dfrac{\delta_f^3}{e} + \dfrac{\delta^3}{\overline{W}}} \qquad \textbf{(94)}$$

where, η_t is the apparent viscosity.

In order to calculate the film thickness and pressure profiles, it is first necessary to determine the length of the delay zone. For this purpose, it was verified experimentally for several thermoplastics [TAD 70] that the number of delay turns, n_{At}, is a function of parameter ψ (dimensionless melting parameter that will be presented in the next chapter):

$$n_{At} = E_0 + E_1\left(\frac{1}{\Psi}\right) + E_2\left(\frac{1}{\Psi}\right)^2 \qquad \textbf{(95)}$$

where E_0, E_1 and E_2 are empirical constants determined from experimental data resulting from these visualization studies. In practice, it can be seen that the length of the channel in the delay zone is that corresponding to that necessary for the thickness of the film to be five to seven times greater than that of the mechanical clearance, as shown in the graph in Figure 47.

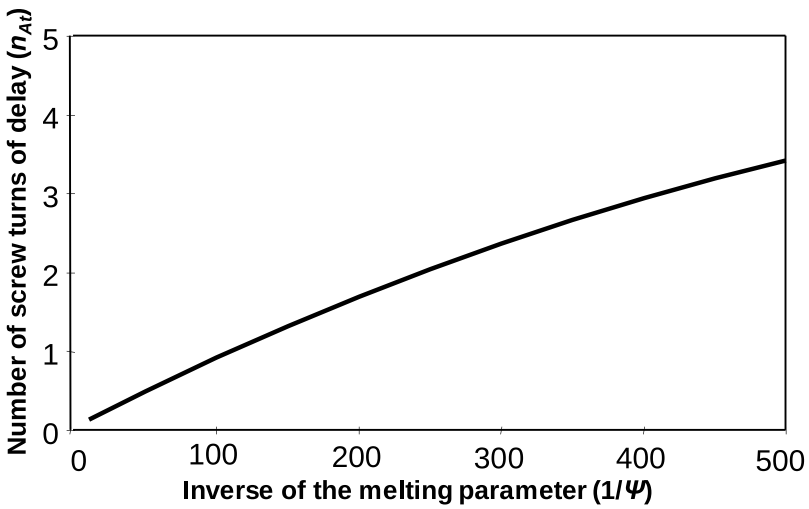

Figure 47- Formation of the films and the melt pool

The pressure profile in this zone is similar to that obtained for the solids conveying zone, where the frictional force F_1, which acts on the surface of the cylinder, is now replaced by a viscous force. The viscous force is given by $F_1 = \tau A$, being $\tau = \eta\dot{\gamma}$ and $\dot{\gamma} = V/\delta$, replacing it results that $F_1 = (\eta VA)/\delta$; finally the area of application of the force is $A = W_c\ dz$, this is:

$$F_1 = \frac{\eta}{\delta} W_c\ V_c\ dz \qquad \textbf{(96)}$$

A balance of forces and moments, as performed in the solids conveying zone, produces the following equation:

$$\begin{aligned} P_2 = P_1 \exp\left(\frac{B_1^{'} - A_1^{'}\ K_p}{A_2\ K_p + B_2} z \right) + \\ \frac{\tau\, W_c \left(\cos\overline{\theta}\right) - K_p \sin\overline{\theta}}{B_1^{'} - A_1^{'}\ K_p} \left\{ \exp\left(\frac{B_1^{'} - A_1^{'}\ K_p}{A_2\ K_p + B_2} z \right) - 1 \right\} \end{aligned} \qquad \textbf{(97)}$$

where:

$$A_1^{'} = \overline{W} tg\alpha\ \sin\overline{\theta} + 2.H\ f_p \sin\theta_c + W_p\ f_p \sin\theta_c \left(\cos\alpha + \frac{\sin\alpha}{f_p} \right) \qquad \textbf{(98)}$$

$$\begin{aligned} B_1 = \overline{W} tg\alpha\ \cos\overline{\theta} \frac{\overline{D}}{D_c} - 2\ H\ f_p \sin\theta_c\ \mathrm{cotg}\,\overline{\theta} \frac{\overline{D}}{D_c} \\ - W_p\ f_p \left(\cos\alpha + \frac{\sin\alpha}{f_p} \right) \sin\theta_c\ \mathrm{cotg}\theta_p \frac{D_p}{D_c} \end{aligned} \qquad \textbf{(99)}$$

where A_2, B_2 and K_p, are given by equations 60, 62 and 57, respectively (see previous chapter), and τ is the shear stress, calculated at an average temperature and at shear rate $\overline{\dot{\gamma}}$:

$$\bar{\dot{\gamma}} = \frac{V_c \sin\theta_c}{\delta \sin(\theta_c + \varphi)} \tag{100}$$

When calculating the power consumption for this zone, the equations of the solids conveying zone are used, except for the interface between the solid plug and the cylinder, with the total power consumption ($e_w^{'}$) and the power dissipated at the surface cylinder ($e_{wc}^{'}$), given, respectively, by (see also equations 67 and 68):

$$e_w^{'} = e_{wc}^{'} + e_{wp} + e_{wf} + e_{wp} \tag{101}$$

$$e_{wc} = \pi N D_c \tau \; W_c \, z \, \frac{\sin\theta_c}{\sin(\theta_c + \varphi)} \tag{102}$$

Block of solids surrounded by molten films

An alternative is to consider that the block of solids is surrounded by melt films (Figure 46-c). This model was proposed by Chung [CHU 71, CHU 75], in which he considered that the movement of the block of solids is controlled by shear forces in the melt films (instead of the frictional forces during the first turns of the screw, when there are only solids). F_1 being obtained from equation 96 and F_3, F_4 and F_5 from:

$$F_3 = F_4 = \frac{\eta}{\delta} V_{cz} H dz \tag{103}$$

$$F_5 = \frac{\eta}{\delta} W_p dz \tag{104}$$

Through balance of forces and moments, the pressure profile is, in this case:

$$\begin{aligned} \frac{P_2 - P_1}{z} &= \frac{C_1 K_c}{H\delta^n}\left[\frac{\sin\theta_c}{\sin(\theta_c + \varphi)}\pi N D\right]^{n_c} \\ &(C_1 \cos\theta_c \cos\varphi - \sin\theta_c \sin\varphi) - \frac{K_p}{\delta^n}\left[\frac{\sin\varphi}{\sin(\theta + \varphi)}\pi N D\right]^{n_p} \\ &\left[\frac{C_2}{H}\left(\frac{C_2}{C_1}\right)^{n_p}\left(\sin^2\theta + C_2\cos^2\theta\right) + \frac{2}{\pi D \sin\theta}\left(\frac{1}{C_1}\right)^{n_p}\right] \end{aligned} \tag{105}$$

where:

$$C_1 = \frac{1}{1 - \dfrac{H}{D_c}} \tag{106}$$

$$C_2 = \frac{1 - 2\frac{H}{D_c}}{1 - \frac{H}{D_c}} \qquad \textbf{(107)}$$

and K_c, n_c, K_p and n_p are viscosity power law constants for the films next to the cylinder and next to the screw, respectively.

Numerical Model

Depending on the operating conditions, particularly the screw temperature, it is possible that the polymer next to the screw surfaces (walls and root) reaches the melting temperature during the delay zone. As shown in Figure 46, on the flanks and root of the screw there is also friction dissipation, with a consequent gradual increase in the temperature of the solid polymer. Therefore, the delay zone can have two phases (Figures 46-a and 46-c), that is, from a specific location onwards, melt films are formed next to all surfaces of the screw. In the model proposed here, it is considered that these two phases occur sequentially. The first is called Delay Zone I (Figure 46-a) and the second Delay Zone II (Figure 46-c).

Delay Zone I

As shown in Figure 48, the solid block (section A) is in contact with the walls and the screw root, where the local temperature increases due to frictional heat dissipation. This mechanism ends when the polymer, locally, reaches the melting temperature. At the same time, the solid polymer continues to melt at the interface of the solids with the melt film (section C, in Figure 48), with the heated cylinder and the intense shear rates occurring in the C film contributing significantly to this process.

The analytical model proposed by Kacir and Tadmor [KAC 72], and presented in the previous section, allows the calculation of the film thickness profile, the mechanical power consumption, the length of the zone and the longitudinal pressure profile (*z* direction). In the model presented here, the following will be considered:

1) Heat convection towards the channel,
2) Conduction of heat in the radial direction,
3) Heat convection in the radial direction.

Thus, it will be possible to calculate the temperature profiles in the film and in the solid block in the *y* direction. For this, the following simplifications are considered:

- The block of solids is a continuous and isotropic medium;
- The melt flow over the clearance is neglected;
- The molten polymer is treated as a viscous inelastic liquid;
- The flow reaches a steady state;
- The solid-melt interface is smooth;
- The flow of the molten film is fully developed in the directions of the channel and transversal to the channel (*i.e.*, $\partial V_x/\partial x = 0$ and $\partial V_z/\partial z = 0$);
- Gravitational and inertial forces are neglected.

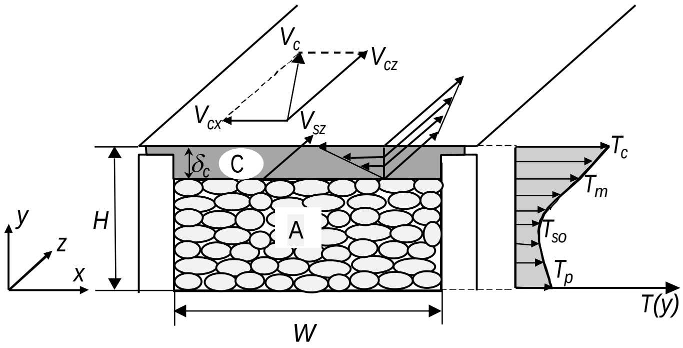

Figure 48- Cross section for the Delay Zone I, where the velocity profiles are shown in the film and in the cylinder, the average speed of the solid block and the temperature profile in the y direction

Melt Film

The momentum and energy equations are as follows [ELB 84, LEE 90, HUA 93, HAN 96]:

$$\frac{\partial P}{\partial x} = \frac{\partial}{\partial y}\left(\eta \frac{\partial V_x}{\partial y}\right) \quad \textbf{(108)}$$

$$\frac{\partial P}{\partial y} = 0 \quad \textbf{(109)}$$

$$\frac{\partial P}{\partial z} = \frac{\partial}{\partial y}\left(\eta \frac{\partial V_z}{\partial y}\right) \quad \textbf{(110)}$$

$$\rho_m \, C_m \, V_z(y)\frac{\partial T}{\partial z} = k_m \frac{\partial^2 T}{\partial y^2} + \eta \, \dot{\gamma}^2 \quad \textbf{(111)}$$

where ρ_m, C_m and k_m are the specific mass, specific heat and thermal conductivity of the melt, respectively, and η is the viscosity that can be calculated using one of the models presented above with the shear rate calculated as follows:

$$\dot{\gamma} = \left[\left(\frac{\partial V_x}{\partial y}\right)^2 + \left(\frac{\partial V_z}{\partial y}\right)^2\right]^{1/2} \quad \textbf{(112)}$$

Once the flow in the gap is neglected, the melt suffers recirculation in the *x* direction, implying that:

$$\int_0^{\delta_C} V_x(y)\, dy = 0 \quad \textbf{(113)}$$

δ_C being the thickness of the melt film. Thus, the boundary conditions to consider are:

$$\begin{cases} V_x(y=0) = 0 \\ V_x(y=\delta_C) = -V_{cx} \end{cases} \quad \begin{cases} V_z(y=0) = V_{sz} \\ V_z(y=\delta_C) = V_{cz} \end{cases} \quad \begin{cases} T(y=0) = T_m \\ T(y=\delta_C) = T_c \end{cases} \quad \textbf{(114)}$$

The resolution of equations 108, 110, 111 and 113, together with the boundary conditions, equation 114, allows to calculate the velocity and temperature profiles in the melt film. The mesh to be used is similar to that shown in Figure 41 of the previous section, where the *y* coordinate varies between y = 0 (at the solid-melt interface) and $y = \delta_c$ (the thickness of the film). The equations are non-linear, since the viscosity depends on the temperature and the velocity profile, being necessary to use a specific discretization by finite differences [MIT 80, ZIE 83]. The solution to equations 108 and 110 can be obtained using the Crank-Nicholson implicit scheme.

$$\frac{\partial P}{\partial x} = \frac{1}{2}\left[\frac{\eta_{i-1,j+\frac{1}{2}} Vx_{i-1,j+1} - \left(\eta_{i-1,j+\frac{1}{2}} + \eta_{i-1,j-\frac{1}{2}}\right) Vx_{i-1,j} + \eta_{i-1,j-\frac{1}{2}} Vx_{i-1,j-1}}{\Delta y^2} + \frac{\eta_{i,j+\frac{1}{2}} Vx_{i,j+1} - \left(\eta_{i,j+\frac{1}{2}} + \eta_{i,j-\frac{1}{2}}\right) Vx_{i,j} + \eta_{i,j-\frac{1}{2}} Vx_{i,j-1}}{\Delta y^2}\right] \tag{115}$$

$$\frac{P_{i,j} - P_{i-1,j}}{\Delta z} = \frac{1}{2}\left[\frac{\eta_{i-1,j+\frac{1}{2}} Vz_{i-1,j+1} - \left(\eta_{i-1,j+\frac{1}{2}} + \eta_{i-1,j-\frac{1}{2}}\right) Vz_{i-1,j} + \eta_{i-1,j-\frac{1}{2}} Vz_{i-1,j-1}}{\Delta y^2} + \frac{\eta_{i,j+\frac{1}{2}} Vz_{i,j+1} - \left(\eta_{i,j+\frac{1}{2}} + \eta_{i,j-\frac{1}{2}}\right) Vz_{i,j} + \eta_{i,j-\frac{1}{2}} Vz_{i,j-1}}{\Delta y^2}\right] \tag{116}$$

where $\eta_{i-1,j+\frac{1}{2}}$ is the viscosity calculated using the average shear rate and temperature given by:

$$\dot{\gamma} = \left[\left(\frac{Vx_{i-1,j+1} - Vx_{i-1,j}}{\Delta y}\right)^2 + \left(\frac{Vz_{i-1,j+1} - Vz_{i-1,j}}{\Delta y}\right)^2\right]^{1/2} \tag{117}$$

$$T = \frac{T_{i-1,j+1} + T_{i-1,j}}{2} \tag{118}$$

$\eta_{i-1,j-\frac{1}{2}}$, $\eta_{i,j+\frac{1}{2}}$ e $\eta_{i,j-\frac{1}{2}}$ are calculated using a similar rule.

The different terms of the energy equation (equation 111) must be replaced by equations 84 and 86 (from the previous chapter), respectively:

$$\rho_m C_m Vz_{i,j} \frac{T_{i,j} - T_{i-1,j}}{\Delta z} = k_m \frac{1}{2}\left[\frac{T_{i,j+1} - 2T_{i,j} + T_{i,j-1}}{\Delta y^2} + \frac{T_{i-1,j+1} - 2T_{i-1,j} + T_{i-1,j-1}}{\Delta y^2}\right] + \left(\eta\, \dot{\gamma}^2\right)\Big|_{i,j} \tag{119}$$

Replacing *j* for 1, 2, …, N-1, we obtain a system of equations that can be placed in matrix form (as in the previous chapter). The system must be complete with equation 113 and an equation that quantifies the mass flow of the film, obtained through a mass balance.

The resolution of this problem implies the use of an iterative process where $V_x(y)$, $V_z(y)$, $\frac{\partial P}{\partial x}$, P and $T(y)$, are determined for each section *i*; the numerical resolution process is similar to that carried out in the previous chapter.

Solid block (Section A)

In this section, the solids flow in the direction of the melt film, as they are melting [TAD 70, ELB 84]. Thus, it is necessary to include an additional term in the energy equation (when comparing the phenomena that occur in this zone with those that occur in the previous zone, equation 79), that is, the convection of heat in the radial direction:

$$V_{sy}\frac{\partial T(y)}{\partial y}+V_{sz}\frac{\partial T(y)}{\partial z}=\alpha_s\frac{\partial^2 T(y)}{\partial y^2} \quad \textbf{(120)}$$

V_{sy} being the speed at which the solids move towards the interface with the melt (*y* direction). At the root of the screw the heat generated by friction has two components, one towards the solids and the other towards the root of the screw:

$$q_s = k_s\left.\frac{\partial T(y)}{\partial y}\right|_{y=0} - k_p\left.\frac{\partial T(y)}{\partial y}\right|_{y=0} \quad \textbf{(121)}$$

In solving this problem, it is necessary to know the temperature of the screw, however, just as in the solid conveying zone, the screw is considered to be adiabatic, being possible to apply equation 82. The energy equation can be discretized as same way as in the previous chapter.

Mass and heat balances through the solid-melt interface

The system is only complete after the introduction of equations that take into account the mass and heat balances through the solid-melt interface. The mass flow in the melt film ($\dot{m}_{C|z+\Delta z}$) is determined by the melting rate through the interface (R_C): as shown in Figure 49, which represents an element of the interface section between film C and solids block A.

$$\dot{m}_{c|z+\Delta z} = \dot{m}_{c|z} + R_C \quad \textbf{(122)}$$

where:

$$\dot{m}_{c|z} = W_c\ \rho_m\int_0^{\delta_c} V_z(y)\,dy \quad \textbf{(123)}$$

$$R_C = \rho_s\ V_{sy}\ \Delta z\ W_c \quad \textbf{(124)}$$

Since ρ_s is the specific mass of the solid block and the indices C|*z* and C|*z*+Δ*z* refer to the increments along the channel *z* and *z*+Δ*z*,, respectively, in zone C.

The mass flow in the solid ($\dot{m}_{A|z+\Delta z}$) is given by:

$$\dot{m}_{A|z+\Delta z} = \dot{m}_{A|z} - R_C \qquad \textbf{(125)}$$

where:

$$\dot{m}_{A|z} = \rho_s \, V_{sz} \left(H_{s|z} \, W_s \right) \qquad \textbf{(126)}$$

And $H_{s|z}$ is the height of the block of solids. The total mass flow ($\dot{m}_T$) is calculated from:

$$\dot{m}_T = \dot{m}_{A|z+\Delta z} + \dot{m}_{c|z+\Delta z} \qquad \textbf{(127)}$$

Finally, the heat balance through the interface is:

$$k_m \left(\frac{\partial T}{\partial y} \right)\bigg|_{y=H-\delta_c} - k_s \left(\frac{\partial T}{\partial y} \right)\bigg|_{y=H-\delta_c} = \rho_s \, h \, V_{sy} \qquad \textbf{(128)}$$

The pressure gradient is calculated using the analytical equations presented previously [KAC 72].

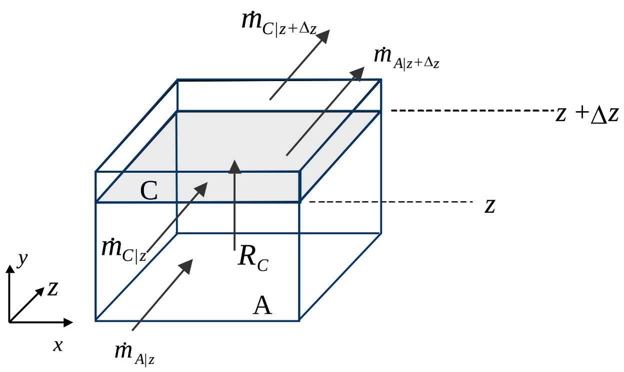

Figure 49- Mass balances through the solid-melt interface

Delay Zone II

As seen above, in this area the block of solids is surrounded by melt films on the surfaces of the cylinder and screw. For modeling purposes, this zone (Figure 50) will be considered a particular case of the melting zone to be presented in the next chapter.

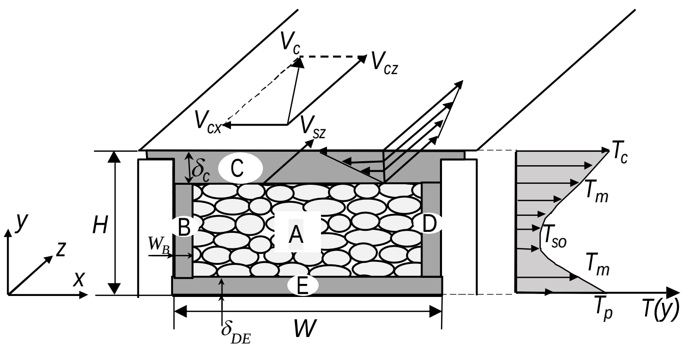

Figure 50- Cross section of the channel for the Delay Zone II

In the Delay Zone II the block of solids (A) is surrounded by melt films adjacent to the cylinder wall (C), the root of the screw (E) and the flank of the active (B) and passive (D) screw. This zone differs from the melting zone only in terms of melt pool B. The transition from Delay Zone II to the Melting Zone is a function of the thickness of B, and occurs when this thickness is equal to the depth of the channel [ELB 84]. The model for these zones will be presented in the next chapter.

Application exercise

1. It is intended to produce a rod in HDPE with the extruder-extrusion head set shown in Figure 45 (see exercise in the previous section). The rotation speed is 60rpm, the temperature profile is as shown in the figure, with the set flow rate being 40kg/hr.

Compare the values obtained by the models presented for the pressure evolution in the delay zone, knowing that its length is 2 turns and the initial pressure is 2.5MPa. Make a critical analysis of the results obtained.

Notes: i) consider the material properties, the system geometry and the processing conditions indicated in the exercise at the end of the previous section; ii) before starting the calculations, explain the methodology for solving the problem.

3.4. Melting

One of the basic functions of an extruder is, as mentioned earlier, to fully melt the polymer some distance from the end of the screw. For this reason, a model for this zone must predict the amount of polymer melted at any point in the channel of the extruder, the length of the screw required for melting and the dependence of these two variables on the properties of the polymer, the geometry of the screw and the operative conditions.

Only after experimental observation of the process was it possible to conclude that there may be three distinct fusion mechanisms in practice, which are generally designated by the name of the researchers who described them:

- Maddock mechanism [MAD 59]/Tadmor [TAD 70] - the melt pool develops close to the active flank of the screw.
- Dekker mechanism [DEK 76] - where no melt pool is formed, but the melt surrounds the bed of solids.
- Menges and Klenk's mechanism [MEN 67] - the melt pool develops next to the passive flank.

In practice, it is verified that mechanism A is the most frequent, being therefore the one that will be the object of study in these book.

As in the previous zones, two analytical models and a numerical model based on finite differences will be presented. In the first case, two situations will be considered: i) the material is Newtonian and the isothermal regime, or ii) the material is non-Newtonian and the non-isothermal regime.

Newtonian and isothermal model

In this section, the Tadmor model will be adopted, as shown in Figure 51. The elementary volume of material perpendicular to the solid-melt interface, shown in Figure 52, will be analyzed in order to calculate the temperature profiles in the melt film and in the solid plug, the film thickness profile and the solids profile. The solid block has two velocity components, one in the direction of the channel (V_{sz}) and the other in the direction of the solid-melt interface (V_{sy}). Figures 51 and 52 also show the temperature profiles in the film and the block of solids.

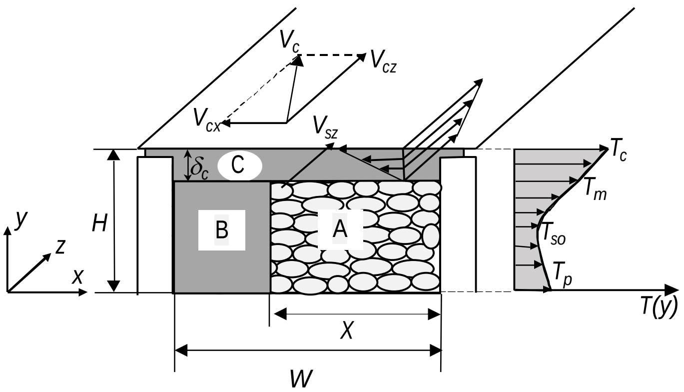

Figure 51- Channel cross section in the Tadmor model (X is the width of solids)

In developing these analytical models, the following simplifications will be taken into account:

- The channel is rectangular and full of material; the mechanical clearance does not influence the melting rate;
- The block of solids behaves as a cohesive solid: homogeneous and continuous;
- There is a stationary regime, that is, in each channel section the width of solids is *X* and the temperature of the cylinder T_c;
- The block of solids in the *y* direction has infinite depth in terms of heat transfer (*i.e.*, the contribution of the screw and the progressive heating of the material along the channel are ignored);
- The heat transfer from the melt pool to the solid block is negligible, considering only the melting of material at the solids/film interface next to the cylinder (one-dimensional heat transfer problem);
- The molten film moves between two parallel plates of infinite dimensions (when compared to the thickness of the film);
- The velocity of the block of solids in the direction of the length of the channel is constant;
- The melt is considered to be a Newtonian fluid (which implies a linear film velocity profile);
- The thermophysical properties of the material are constant (which variation with pressure, temperature and shear rate, can be taken into considering small channel increments in the *z* direction).

Simplification d) ignores the acceleration of the melting rate in the final part of the process caused by the increase in temperature of the screw and the melt. This simplification, like e), reinforces the conservative nature of the predictions of these models.

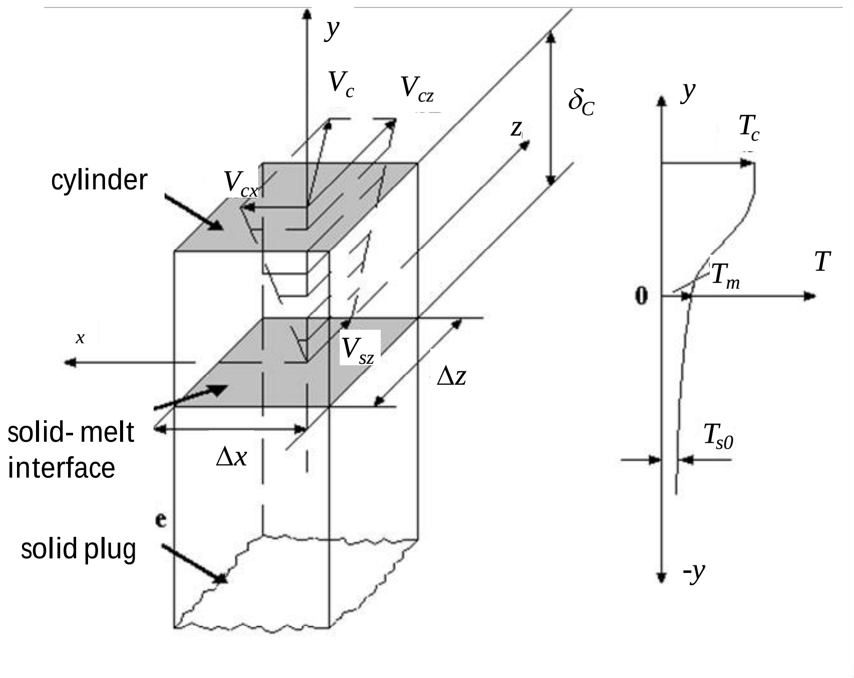

Figure 52- Elementary volume of the channel perpendicular to the interface: velocity and temperature profiles

As a result of simplification f), both "plates" are considered to move at velocities V_c and V_{sz}, making it possible, in this way, to assume that the lower one is stationary at temperature T_m, and the upper one moving at a speed V_j, in a direction j that makes an angle α_j with the direction z, at temperature T_c. The resulting velocity is obtained by vectorial subtraction of the initial velocities (see Figure 52):

$$\overrightarrow{V_j} = \overrightarrow{V_c} - \overrightarrow{V_{sz}} \tag{129}$$

resulting:

$$V_j = \left(|V_c|^2 + |V_{sz}|^2 - 2\,|V_c|\,|V_{sz}|\cos\theta_c\right)^{1/2} \tag{130}$$

$$\tan\alpha_j = \frac{V_{cx}}{V_{cz} - V_{sz}} = \frac{V_c \sin\theta_c}{V_c \cos\theta_c - V_{sz}} \tag{131}$$

One of the major objectives in this zone is the ability to predict the evolution of the solids width (X) along the channel (direction z), as shown in Figure 51. In this way, the sequence of calculations necessary to determine the profile X (z) is as follows:

1. Energy balances in the melt film and the solid plug;
2. Balance of heat flow at the solid/melt interface;
3. Mass balance in a film increment in the z direction;
4. Mass balance in the solids in the z direction;
5. Resolution of the differential equation obtained for the system geometry.

1- Energy balances in the melt film and the solid plug

Resolution of the energy equation in the film, where the convective term is neglected in the *z* direction (see equation 111 from the previous section):

$$k_m \frac{\partial^2 T}{\partial y^2} = \eta\, \dot{\gamma}^2 \qquad \textbf{(132)}$$

Integrating and taking into account boundary conditions (*i.e.*, for y=0, $T= T_m$ and for $y=\delta_C$, $T=T_c$), we can obtain-se:

$$\frac{T - T_m}{T_c - T_m} = \frac{\eta V_j^2 y}{2k_m \delta_C (T_c - T_m)}\left(1 - \frac{y}{\delta_C}\right) + \frac{y}{\delta_C} \qquad \textbf{(133)}$$

The average melt film temperature is:

$$T_{med} = \frac{2\,T_c + T_m}{3} + \frac{\eta V_j^2}{12\,k_m} \qquad \textbf{(134)}$$

From equation 133 it can be seen that the increase in temperature of the film is dependent on the ratio between the heat generated by viscous dissipation ($\eta\, V_j^2$) and the heat conducted from the heated cylinder ($k_m (T_c - T_m)$). This ratio is quantified by the *Brinkman* number:

$$Br = \frac{\eta\, V_j^2}{2k_m (T_c - T_m)} \qquad \textbf{(135)}$$

Figure 53 illustrates the effect of the value of this number on the temperature of the film, with two extreme cases: i) if *Br* <2, viscous dissipation is of little importance and the temperature of the film does not exceed T_c; ii) if *Br*> 2, the temperature of the film may exceed that of the cylinder due to the great importance of viscous dissipation. However, it is found that by increasing the temperature of the cylinder (*i.e.*, increasing the heat conduction), the viscosity decreases and, as a consequence, the viscous dissipation also decreases. This means that for a given temperature value in the cylinder it is possible to calculate the maximum rotation speed of the screw (quantified in this equation by V_j) which ensures that the temperature of the film does not exceed that of the cylinder, thus avoiding possible material degradation due to high temperatures.

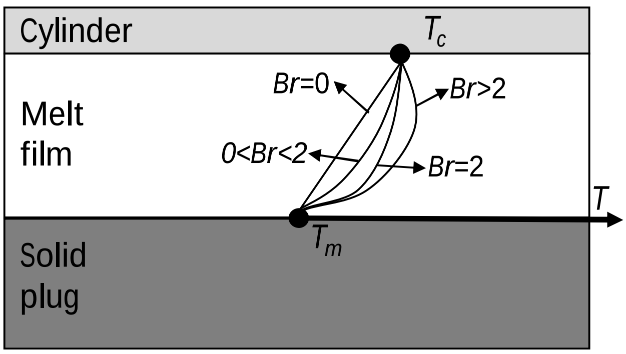

Figure 53- Balance between the heat generated by viscous dissipation and that conducted from the cylinder: temperature profiles in the melt film

As in the case of the film, the heat balance in the solid plug also does not include the convective term in the direction of the channel (see equation 120 in the previous section):

$$V_{sy} \frac{\partial T(y)}{\partial y} = \alpha_s \frac{\partial^2 T(y)}{\partial y^2} \tag{136}$$

The integration of this equation taking into account the boundary conditions (*i.e.*, for $y= -\infty$, $T=T_{s0}$, and for $y=0$, $T=T_m$) results in the following equation for the temperature profile in the solid plug:

$$\frac{T - T_{s0}}{T_m - T_{s0}} = \exp\left(\frac{V_{sy}}{\alpha_s} y\right) \tag{137}$$

2- Balance of heat flow at the solid/molten interface

The heat balance at the solid/melt film interface involves the transfer of heat from the film to the interface and from the interface to the solids, as defined in terms of the following equation, respectively. The heat transferred to the solids allows them to melt at V_{sy} velocity.

$$k_m \left.\frac{\partial T(y)}{\partial y}\right|_{y=0} - k_s \left.\frac{\partial T(y)}{\partial y}\right|_{y=0} = \rho_s \, h \, V_{sy} \tag{138}$$

3- Mass balance in the film in the z direction

Through the simultaneous realization of the heat balance at the interface and a mass balance in the film, it is possible to determine the evolution of the melt film thickness (δ_C) and the melting ratio (ω), that is, the melting rate per unit of channel length, which are given by the following equations

$$\delta_C = \left(\frac{\left[2 k_m (T_c - T_m) + \eta \, V_j^2\right] X}{V_{cx} \; \rho_m \left[C_s (T_m - T_{so}) + C_m (T_{med} - T_m) + h\right]} \right)^{1/2} \tag{139}$$

$$\omega = V_{sy} \; \rho_s \; X = \frac{V_{cx} \; \rho_m \; \delta_C}{2} = \Phi \sqrt{X} \tag{140}$$

where Φ is:

$$\Phi = \left(\left\{ \frac{V_{cx} \rho_m \left[k_m (T_c - T_m) + \frac{\eta}{2} V_j^2 \right]}{2\left[C_s (T_m - T_{s0}) + C_m (T_{med} - T_m) + h\right]} \right\} \right)^{1/2} \tag{141}$$

This quantity (Φ) quantifies the ratio between the heat supplied to the melt (the heat conducted plus the heat generated by viscous dissipation) and the heat needed to melt the polymer (the heat needed to increase the temperature plus the heat required by changing the state).

4- Mass balance in solids in the z direction

To obtain the solids profile and the length required for melting, Z_T, it is necessary to perform a mass balance in a solid element in the direction of the interface (*y* direction, see Figure 54), which will depend on the geometry of the channel (as see later). In this balance: the amount of solid entering the solid plug in *z* is equal to the amount of solid leaving the solid plug in $z+\Delta z$ plus the amount of solid leaving the plug through the solid/melt interface, as given by the following equation:

$$\rho_s V_{sz} H X |_z = \rho_s V_{sz} H X |_{z+\Delta z} + V_{sy} \rho_s \overline{X} \Delta z \quad \textbf{(142)}$$

By manipulating this equation and using equation 140, the variation in the area of solids ($H X$) with z is given by:

$$-\frac{d(HX)}{dz} = \frac{\omega}{\rho_s V_{sz}} \quad \textbf{(143)}$$

5- Resolution of the differential equation obtained for the system geometry

The resolution of the previous differential equation depends on the geometry of the channel. For a channel of constant depth, the solution obtained is as follows:

$$\frac{X}{W} = \frac{X_1}{W}\left[1 - \frac{\Psi}{2H}(z - z_1)\right]^2 \quad \textbf{(144)}$$

$$z_T = \frac{2H}{\Psi} \quad \textbf{(145)}$$

where ψ is:

$$\Psi = \frac{\Phi}{V_{sz}\, \rho_s \sqrt{X_1}} = \frac{\Phi\sqrt{W}}{G/H_0} \quad \textbf{(146)}$$

and for channels of variable depth, it results:

$$\frac{X}{W} = \frac{X_1}{W}\left[\frac{\Psi}{A} - \left(\frac{\Psi}{A} - 1\right)\sqrt{\left(\frac{H_1}{H_1 - A z}\right)}\right]^2 \quad \textbf{(147)}$$

$$z_T = \frac{H_1}{\Psi}\left(2 - \frac{A}{\Psi}\right) \quad \textbf{(148)}$$

where A is the slope of the compression zone as shown in Chapter 5.

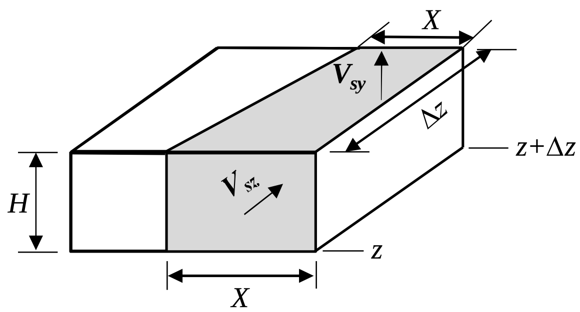

Figure 54- Mass balance in the solid block

Non-Newtonian and Non-Isothermal Model

In this case, it is assumed that the viscosity varies according to a linear temperature profile as given by the power law, where the temperature effect is quantified by an Arrehnius-type law, as represented by equation 11 in Chapter 4. In the same way as in the Newtonian and isothermal model, balances of mass and energy in an elementary volume are obtained:

Film temperature profile:

$$\frac{T-T_m}{T_c-T_m}=\xi+\frac{k_3}{A_4^2\,k_m\left(T_c-T_m\right)}\left[1-e^{-A_4\xi}-\xi\left(1-e^{-A_4}\right)\right] \qquad \textbf{(149)}$$

where:

$$\xi=\frac{y}{\delta_C} \qquad \textbf{(150)}$$

$$k_3=\eta_0\;\delta_C^2\;k_2^{n+1} \qquad \textbf{(151)}$$

$$k_2=\frac{A_4\,V_j}{\delta_C\left(1-e^{-A_4}\right)} \qquad \textbf{(152)}$$

$$A_4=\frac{a\left(T_c-T_m\right)}{n} \qquad \textbf{(153)}$$

Average film temperature:

$$T_{med}=\Theta\left(T_c-T_m\right)+T_m \qquad \textbf{(154)}$$

in which:

$$\Theta=\frac{\dfrac{A_4}{2}+e^{-A_4}\left(1+\dfrac{1}{A_4}\right)-\dfrac{1}{A_4}}{A_4+e^{-A_4}-1} \qquad \textbf{(155)}$$

Film thickness:

$$\delta_C = \left(\frac{\left[2\,k_m (T_c - T_m) + U_1\right] X}{U_2 V_{cx}\ \rho_m \left[C_s (T_m - T_{so}) + C_m\ \Theta\ (T_c - T_m) + h\right]} \right)^{1/2} \qquad \textbf{(156)}$$

where:

$$U_1 = \frac{2\,\eta_0\,V_c^{n+1}}{\delta_C^{n-1}} \left(\frac{A_4}{1 - e^{-A_4}} \right)^{n+1} \left(\frac{A_4 - 1 + e^{-A_4}}{A_4^2} \right) \qquad \textbf{(157)}$$

$$U_2 = 2\,\frac{1 - A_4 - e^{-A_4}}{A_4\left(e^{-A_4} - 1\right)} \qquad \textbf{(158)}$$

$$\Phi = \left(\left\{ \frac{V_{cx} \rho_m\, U_2 \left[k_m (T_c - T_m) + \frac{U_1}{2} \right] X}{2\left[C_s (T_m - T_{s0}) + C_m\ \Theta\ (T_c - T_m) + h\right]} \right\} \right)^{1/2} \qquad \textbf{(159)}$$

Solid profile:

The solid profile and the length required for the melting can be obtained using equations 144 to 148, depending on the geometry of the channel where the calculations are being performed.

Mechanical power

The mechanical power consumption for this zone, e_f, is the sum of the power consumed in the melt film, e_{mf}, the power consumed in the melt pool, e_{mp}, and the power consumed in the clearance between the screw flight and the cylinder, e_{cl} [RAU 86]:

$$e_f = e_{mf} + e_{mp} + e_{cl} \qquad \textbf{(160)}$$

where:

$$e_{mf} = \eta_0\ V_c\ \sin(\theta_c + \varphi) \frac{2\,V_j^n}{k_4 (2 - n)} \left(\delta_{\max}^{2-n} - \delta_C^{2-n} \right) z \qquad \textbf{(161)}$$

$$\delta_{\max} = \left(k_4\ W_c + \delta_C^2 \right)^{1/2} \qquad \textbf{(162)}$$

$$k_4 = \frac{4\,k_m (T_c - T_m) + 4\,B_3}{\rho_m\ V_j \left[C_s (T_m - T_{s0}) + h\right]} \qquad \textbf{(163)}$$

$$B_3 = \frac{k_m\ B_4\ \delta_C^2}{A_4^2}\left(A_4 - e^{k_2} - 1\right) \quad \textbf{(164)}$$

$$B_4 = \frac{\eta_0}{k_m}\left[\frac{V_j\ A_4}{\delta_C\ \left(e^{A_4} - 1\right)}\right]^{n+1} \quad \textbf{(165)}$$

$$e_{mp} = \left(1 + 3\ r_d\ + 4\ tg^2\theta_c\right)\frac{\eta_0\ X\ V_{cz}^2}{H}\ z \quad \textbf{(166)}$$

$$r_d\ = \frac{H^2}{6\ \eta_0\ V_{cz}}\ \frac{\Delta P}{z} \quad \textbf{(167)}$$

$$e_{cl} = \frac{V_c^{1+n}\ \eta_0\ e}{\delta_C^n}\ z \quad \textbf{(168)}$$

δ_{max} being the maximum film thickness. These equations, for the calculation of mechanical power consumption, can also be used in the case of the non-Newtonian model. To do this, simply replace the value of n with 1 and that of η_0 with viscosity (η).

Numerical model

Figure 55 schematically represents the melting mechanism that occurs in a cross section of the channel, which will be taken into account in the numerical model presented here. In this model, the moment and energy equations that describe each of the five individual regions will be considered, which will be complemented by the boundary conditions and the balances of force, heat and mass.

The main simplifications used in this model are [ELB 84, LIN 85]:

- The solid plug is continuous, homogeneous and isotropic;
- The melt flow over the gap is neglected;
- Molten polymer is considered to be a purely viscous liquid;
- The flow is stationary,
- The solid-melt interfaces are smooth;
- The flow of the molten films is fully developed in the transversal, x, and longitudinal, z, directions (*i.e.*, $\partial V_x/\partial x = 0$ e $\partial V_z/\partial z = 0$);
- The temperature profile of the melt films is fully developed in the transverse direction of the channel (*i.e.*, $\partial T/\partial x = 0$), but not in the longitudinal direction of the channel (*i.e.*, $\partial T/\partial z \neq 0$);
- The conduction of heat towards the channel is neglected (*i.e.*, $\partial^2 T/\partial z^2 << \partial^2 T/\partial y^2$);
- The forces of gravity and inertia are neglected;
- The velocity of the solid plug is constant.

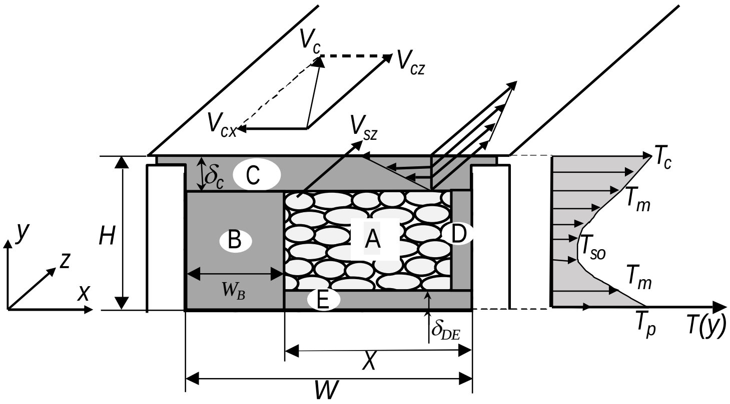

Figure 55- Melting model

Moment and energy equations

a) Melt films (C, D and E)

Taking into account the assumptions presented above and the existence of melt circulation around the block of solids, the moment and energy equations for the films, C, D and E are identical. Region D can be considered as an extension of region E, as suggested by the experimental work presented above [ELB 84]. The flow and thermal behavior in regions C and DE can be described by equations 108 to 112 with the following boundary conditions:

$$\begin{cases} V_x(y=0)=0 \\ V_x(y=\delta_C)=-V_{cx} \end{cases} \quad \begin{cases} V_z(y=0)=V_{sz} \\ V_z(y=\delta_C)=V_{cz} \end{cases} \quad \begin{cases} T(y=0)=T_m \\ T(y=\delta_C)=T_c \end{cases} \qquad \textbf{(169)}$$

for region C and

$$\begin{cases} V_x(y=0)=0 \\ V_x(y=\delta_{DE})=0 \end{cases} \quad \begin{cases} V_z(y=0)=0 \\ V_z(y=\delta_{DE})=V_{sz} \end{cases} \quad \begin{cases} T(y=0)=T_p \\ T(y=\delta_{DE})=T_m \end{cases} \qquad \textbf{(170)}$$

for region DE.

b) Melt pool (zone B)

When the width of the melt pool (W_B) becomes greater than or equal to the depth of the channel, recirculation begins to take place around the block of solids, that is, $\partial V_z/\partial y \neq 0$. Otherwise, it will be the Delay Zone II that will be considered in the calculations. During melting, the momentum equation in the *z* direction and the energy equation (equations 110 and 111, respectively) take the form:

$$\frac{\partial P}{\partial z}=\frac{\partial}{\partial y}\left(\eta\,\frac{\partial V_z}{\partial x}\right)+\frac{\partial}{\partial y}\left(\eta\,\frac{\partial V_z}{\partial y}\right) \qquad \textbf{(171)}$$

$$\rho_m\, C_m\, V_z(y)\frac{\partial T}{\partial z}=k_m\left(\frac{\partial^2 T}{\partial x^2}+\frac{\partial^2 T}{\partial y^2}\right)+\eta\,\dot{\gamma}^2 \qquad \textbf{(172)}$$

where the shear rate is:

$$\dot{\gamma} = \left[\left(\frac{\partial V_x}{\partial y} \right)^2 + \left(\frac{\partial V_z}{\partial x} \right)^2 + \left(\frac{\partial V_z}{\partial y} \right)^2 \right]^{1/2} \quad \textbf{(173)}$$

and the boundary conditions are:

$$\begin{cases} V_x(y=0)=0 \\ V_x(y=H)=-V_{cx} \end{cases} \quad \begin{cases} V_z(x=0)=0 \\ V_z(x=W_B)=V_{sz} \\ V_z(y=0)=0 \\ V_z(y=H)=V_{cz} \end{cases} \quad \begin{cases} T(x=0)=T_p \\ T(x=W_B)=T_m \\ T(y=0)=T_p \\ T(y=H)=T_c \end{cases} \quad \textbf{(174)}$$

c) Solid plug (zone A)

The solid plug is considered to move in the longitudinal direction of the channel at a constant speed:

$$V_{sz} = \frac{\dot{m}_T \; H \; W}{\rho_s} \quad \textbf{(175)}$$

where $\dot{m}_T$ is the mass flow.

Different rates of conduction and heat dissipation occur on the two opposite sides of the solid plug, causing an asymmetric temperature distribution. As a consequence, region A can be subdivided into two, as illustrated in Figure 56.

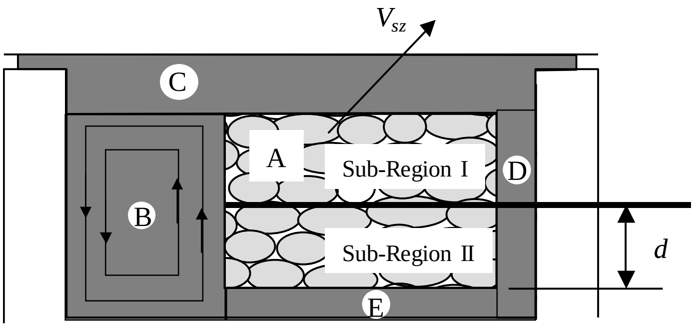

Figure 56- Sub-regions in the solid plug

$$-\frac{V_{sy1}}{\alpha_s}\frac{\partial T_{s1}}{\partial y} + \frac{V_{sz}}{\alpha_s}\frac{\partial T_{s1}}{\partial z} = \frac{\partial^2 T_{s1}}{\partial y^2} \qquad (d \leq y \leq H_{s|z}) \quad \textbf{(176)}$$

$$\frac{V_{sy2}}{\alpha_s}\frac{\partial T_{s2}}{\partial y} + \frac{V_{sz}}{\alpha_s}\frac{\partial T_{s2}}{\partial z} = \frac{\partial^2 T_{s2}}{\partial y^2} \qquad (0 \leq y \leq d) \quad \textbf{(177)}$$

where V_{sy1} and V_{sy2} are the velocities of solid polymer in the direction of the melt films, C and E, respectively, T_{s1} and T_{s2} are the temperature profiles for sub-regions 1 and 2, respectively, and d is the distance in the y direction of so that that $T_{s1}(y=d)=T_{s2}(y=d)$. The boundary conditions for these regions are as follows:

Sub-region I Sub-region II

$$\begin{cases} T_{s1}(y=H_s,z)=T_m \\ \dfrac{\partial T_{s1}(y=d,z)}{\partial y}=0 \end{cases} \quad \begin{cases} T_{s2}(y=0,z)=T_m \\ \dfrac{\partial T_{s2}(y=d,z)}{\partial y}=0 \end{cases} \tag{178}$$

Distance d is calculated iteratively, starting this process with an initial value (for example, $H_s|z/2$) until the temperature at a distance d (that is, at the interface of these regions) is the same for both regions.

Mass and heat balances

Taking into account the melt recirculation around the solid plug, the mass balance for region C (see Figure 57, which represents an element of the melt film interface, C, with the solid plug, A; see also Figure 55):

$$\dot{m}_{C|z+\Delta z} = \dot{m}_{C|z} - \dot{m}_{Cx|z} + \dot{m}_{DEx|z} + R_C \tag{179}$$

$$\dot{m}_{C|z} = W_{s|z}\ \rho_m \int_0^{\delta_{C|z}} V_z^{(C)}(y)\, dy \tag{180}$$

$$\dot{m}_{Cx|z} = \Delta z\ \rho_m \int_0^{\delta_{C|z}} V_x^{(C)}(y)\, dy \tag{181}$$

$$\dot{m}_{DEx|z} = \Delta z\ \rho_m \int_0^{\delta_{DE|z}} V_x^{(DE)}(y)\, dy \tag{182}$$

$$R_C = \rho_s\, V_{sy1|z}\ \Delta z\, W_{s|z} \tag{183}$$

where, $\dot{m}_{C|z}$ is the mass flow from region C in the direction of the channel, $\dot{m}_{Cx|z}$ is the flow from C to the melt well in the direction x and, $\dot{m}_{DEx|z}$ is the transversal flow to C from DE and $\delta_{DE|Z}$ is the thickness of the DE film.

The mass balance for the DE zone is given by the following equation (see Figure 57):

$$\dot{m}_{DE|z+\Delta z} = \dot{m}_{DE|z} - \dot{m}_{DEx|z} + \dot{m}_{By|z} + R_D + R_E \tag{184}$$

where, $\dot{m}_{By|z}$ is the melt recirculation rate through the melt well in the x-y plane, R_D is the melt rate through the AD interface for a Δz increment, R_D is the melting rate through the AE interface for an Δz increment and $\dot{m}_{DE|z}$ the mass flow along the channel. Being that $\dot{m}_{DE|z}$ and R_D are obtained from:

$$\dot{m}_{DE|z} = (W_s + H_s)_{|z}\ \rho_m \int_0^{\delta_{DE|z}} V_z^{(DE)}(y)\, dy \tag{185}$$

$$R_D + R_E = \rho_s \, V_{sy2|z} \, \Delta z \left(W_s + H_s\right) \quad \textbf{(186)}$$

The mass balance in solid plug A is (see Figure 57):

$$\dot{m}_{A|z+\Delta z} = \dot{m}_{A|z} - \left(R_C + R_B + R_D + R_E\right) \quad \textbf{(187)}$$

with:

$$\dot{m}_{A|z} = \rho_s \, V_{sz} \left(H_s \, W_s\right)_{|z} \quad \textbf{(188)}$$

Finally, the mass balance in the melt pool B (Figure 57) produces the following two equations, allowing the calculation of $\dot{m}_{By|z}$.

$$\dot{m}_{B|z+\Delta z} = \dot{m}_{B|z} - \dot{m}_{By|z} + \dot{m}_{Cx|z} + R_B \quad \textbf{(189)}$$

$$\dot{m}_{B|z+\Delta z} = \dot{m}_T - \left(\dot{m}_{A|z+\Delta z} + \dot{m}_{C|z+\Delta z} + \dot{m}_{DE|z+\Delta z}\right) \quad \textbf{(190)}$$

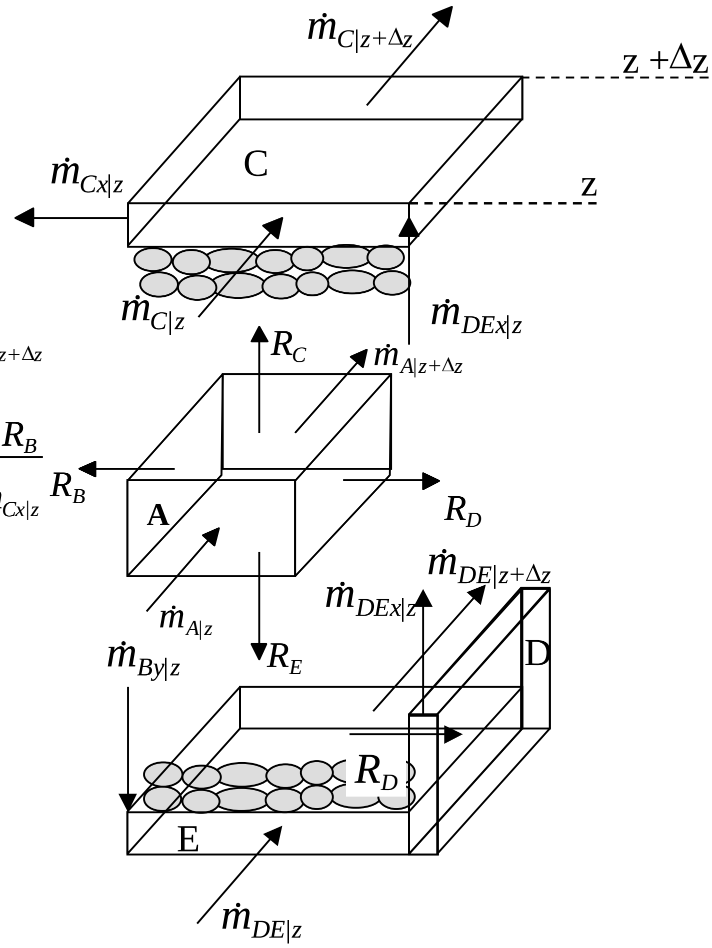

Figure 57- Mass balances

The velocities of the solid polymer in the direction of C (V_{sy1}) and DE (V_{sy2}) melt films can be determined by heat balances on the A-C and A-DE interfaces. The corresponding equations are respectively:

$$k\frac{\partial T}{\partial y}|_{A-C,melt} - k_s\frac{\partial T}{\partial y}|_{A-C,solid} = \rho_s\ h\ V_{sy1} \qquad \textbf{(191)}$$

$$k_s\frac{\partial T}{\partial y}|_{A-DE,solid} - k\frac{\partial T}{\partial y}|_{A-DE,melt} = \rho_s\ h\ V_{sy2} \qquad \textbf{(192)}$$

Balance of forces

This analysis is concluded by making a balance of forces acting on the melt pool in the *x* and *y* directions:

$$\frac{\partial P^{(C)}}{\partial x} + \frac{\partial P^{(DE)}}{\partial x} = \frac{2\left(\tau_{yx|DE} + \tau_{yx|C}\right)}{H_s} \qquad \textbf{(193)}$$

$$\frac{\partial P^{(C)}}{\partial z} + \frac{\partial P^{(DE)}}{\partial z} = \frac{\partial P}{\partial z}\left(= \frac{\partial P^{(B)}}{\partial z}\right) \qquad \textbf{(194)}$$

and including a condition of continuity of pressure along the solid plug:

$$\frac{\partial P^{(C)}}{\partial x}W_s = +\frac{\partial P^{(DE)}}{\partial x}\left(W_s + H_s\right) \qquad \textbf{(195)}$$

where $\tau_{yx|DE}$ e $\tau_{yx|C}$ are the shear stresses that act on the interfaces A-DE and A-C, respectively. Finally, the resulting system of equations must obey the following two geometric constraints and be solved by finite differences, using a scheme similar to that presented previously for the other differential equations.

$$\delta_C + H_s + \delta_{DE} = H \qquad \textbf{(196)}$$

$$W_B + W_s + \delta_{DE} = W \qquad \textbf{(197)}$$

Influence of parameters on the process

Taking into account the models presented, it will be important to validate how some of the process parameters influence its performance. In this analysis, operational parameters will be considered, such as the rotation speed of the screw and the cylinder temperature profile, and geometric parameters, such as the channel depth (*H*) and/or the compression slope (*A*). It would also be possible to study the influence of other parameters, the temperature of the solids, the width of the channel and the slope of the compression, are some examples, which will not be addressed in this text.

Figure 58 illustrates the influence of the rotation speed of the screw on the evolution of the melting rate (or solids profile), quantified by the *X*/*W* ratio. An increase in the rotation speed of the screw from 10 to 90 rpm increases the flow rate from 8.0 to 65.3 kg/hr. This increase in throughput has two consequences with regard to the heat transfer mechanisms used to melt the material (see equation 141). Firstly, there is greater viscous dissipation due to the greater speed, that is, V_j increases considerably. Simultaneously, due to the increase in temperature, the viscosity (η) decreases. However, this last effect does not cancel out the increase in viscous dissipation due to the shear rates generated by the increase in speed. On the other hand, the heat conduction decreases, given that the higher the speed, the less the residence time inside the extruder, that is, less time for the heat transfer by conduction. Finally, by analyzing the graph it appears that the polymer melts much earlier at lower rotation speeds. This means that the prevailing effect is the conduction of heat. However, it is important to note that, due to the pseudoplastic nature of the polymers, more and more speed increases cause progressively smaller temperature increases.

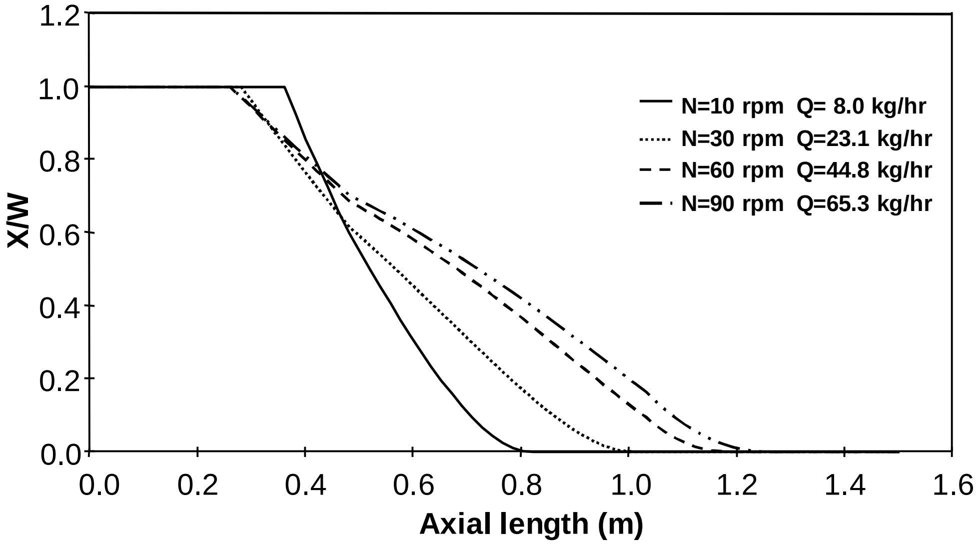

Figure 58- Influence of the rotation speed of the screw on the melting rate

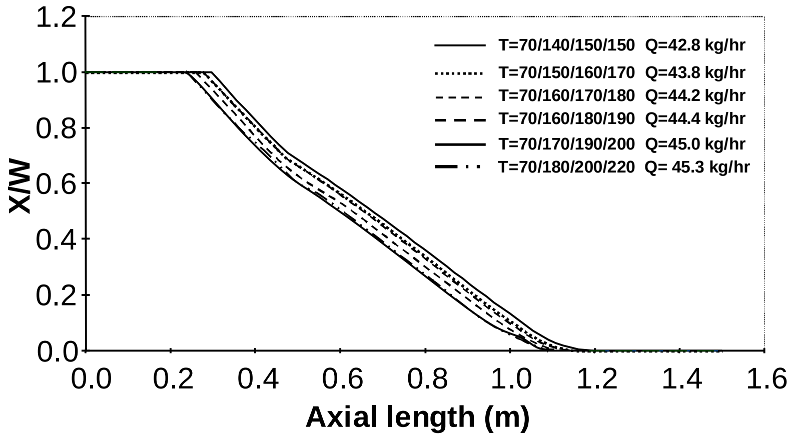

Figure 59- Influence of the temperature profile on the cylinder on the melting rate

With the variation of the temperature profile in the cylinder, the flow rate of the extruder increases slightly due to the decrease in the viscosity of the polymer, as shown in Figure 59. An increase in the temperature of the cylinder (in this case from 150 to 220 ºC, considering only the value of the last heating band) implies greater heat conduction, due to the greater difference between the average temperature of the film and that of the solid plug. However, despite the lower viscous dissipation (as the viscosity decreases with increasing temperature), it appears that the length required to melt the material is shorter when the temperature is increased, that is, it is the heat conduction that prevails. It is also verified that, considering the remaining variables, there is a cylinder temperature that maximizes the combined effect of conduction and viscous dissipation, since between the last two temperature profiles there is no variation in the length necessary to melt the material.

Figure 60 illustrates the influence of the compression zone geometry on the evolution of the solids profile. It can be seen that for a screw of constant depth (A=0) the length for melting (Z_T - equation 148) is maximum and that X/W decreases along the length of the channel following the shape of a parabola. By increasing the value of A, the value of Z_T is reduced and the shape of the X/W curve becomes less concave and then convex. On the other hand, if $A/\Psi=1$, Z_T remains at its minimum value, that is, the channel remains full of solids for a certain helical distance, reducing its width (X) to zero in a small increment. It is important to note that the variation in the compression slope can be achieved either by varying the length of this zone or the depth of the channel (in the feed or metering zones). It is also verified that when A is high, the melting rate may not follow the compression rate, with an increase in the width of solids along the channel. Eventually, in this case, the solids can block the channel, causing instabilities in the process. To avoid this problem, the length of the compression zone (L_2) must be greater than a minimum value, given by:

$$L_{\min} \geq \frac{V_{cz}\,\sqrt{X_1}\,H_1\,\rho_s\left(\dfrac{H_1}{H_3}-1\right)\sin\theta_c}{\Phi\left(\dfrac{H_1}{H_3}\right)} \qquad \textbf{(198)}$$

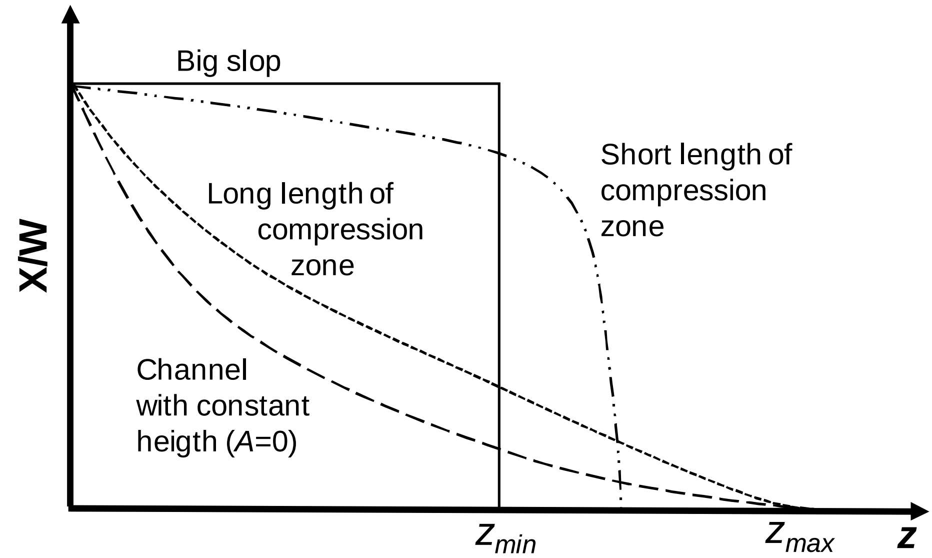

Figure 60- Influence of the compression zone geometry on the melting rate

Application exercise

1. It is intended to produce HDPE rod with the extruder-extrusion head set shown in Figure 61. The rotation speed of the screw is 60 rpm, the temperature profile is as shown in the figure, the flow rate being 40 kg/hr. Indicate the screw turn on which you expect to find only molten material.

Screw:
- Square pitch - D_p = 59.8 mm
- Compression ratio=3
- Flight thickness =5 mm
- Flight clearance (δ_f) = 0.1 mm

Material data:

Physical properties:

Specific mass at feeding = 630 kg/m³

Specific mass of solid= 950 kg/m³

Friction coefficient material/hopper = 0.30

Friction coefficient material/screw = 0.25

Friction coefficient material/cylinder = 0.4

Friction angle of the particles = 33,7º

Melt specific mass at different temperatures (kg/m³):

T=25ºC – 950

T=150ºC – 800

T=179ºC – 760

T=180ºC – 750

T=200ºC – 750

Thermal properties:

Solid thermal conductivity = 0.51 J/m.s.K

Melt thermal conductivity = 2300 J/kg/.K

Solids specific heat = 1317 J/kg/K

Melting heat = 230 kJ/kg

Melting temperature = 130 ºC

Viscosity: Power law	N	0.345	--
	k_0	29.94	kPa s⁻¹
	a	0.00681	ºC⁻¹
	T_0	190	ºC

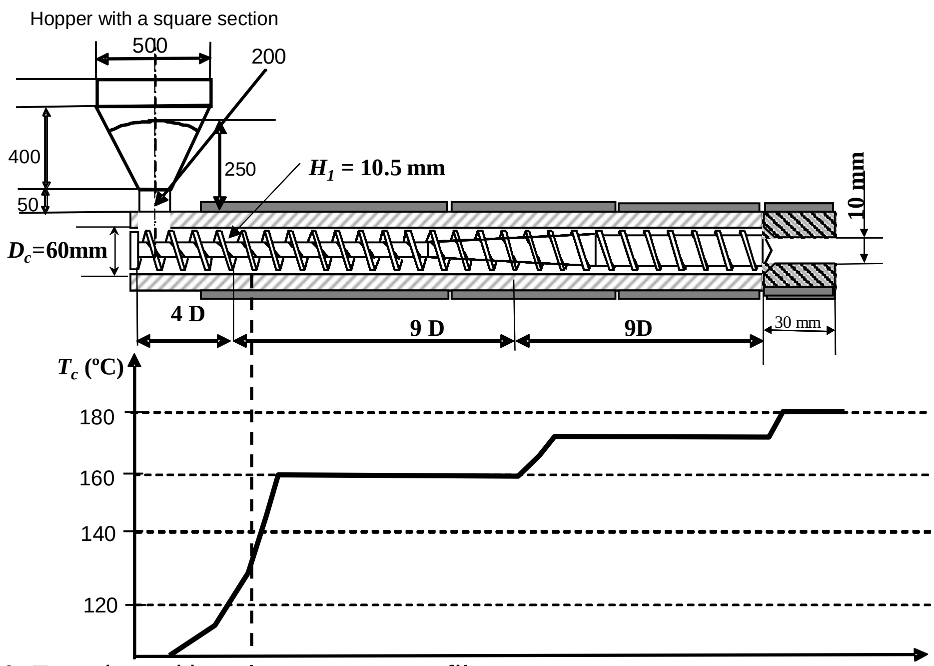

Figure 61- Extruder and barrel temperature profile

3.5. Pumping and operating point

The pumping zone occurs after the melting is completed, being fundamental in the accomplishment of three of the basic functions of the extruder: ensuring that the necessary pressure is created so that the melted polymer crosses the die with the desired flow rate and promotes mixing and homogeneity of the melt temperature [TAD 70, RAU 86].

With the modeling of the pumping zone it will be possible to obtain equations for calculating the flow rate, pressure, temperature profiles, mechanical power consumption and residence time distribution (a measure of the mixture), from the physical properties of the material, extruder geometry and operating conditions [TAD 70].

As before, due to the complexity of the system, namely with regard to the number of variables involved, the geometry of the screw and the non-Newtonian nature of the polymers, the derivation of the equations will be conveniently simplified. Since the depth of the channel is small in this geometric zone, it can once again be assumed that the channel is unrolled and that the polymer flow occurs between two parallel plates of infinite dimensions [CAR 53].

In this chapter, two models are presented: analytical and numerical.

Analytical model

In developing this model, the following simplifications were used [RAU 86, CAR 53, McK 62]:

- The regime is stationary;
- There is no slip on the channel walls;
- The fluid is incompressible and the gravity and inertia effects are neglected
- Newtonian fluid;
- The depth of the channel is much lower than the width and the diameter of the screw (flow between infinite parallel surfaces);
- There is no material flow through the mechanical clearance;
- Isothermal flow (no viscous dissipation).

Figure 62 shows the velocity profiles in the *x* and *z* directions. The velocity profile in the *z* direction is linear since the fluid has been considered Newtonian. In the *x* direction there is a curvature due to the fact that there is a circulatory flow across the channel, as will be seen below. Regarding the temperature, due to the lack of viscous dissipation, its variation is linear (between the cylinder temperature and the screw temperature).

The determination of the velocity and pressure profiles results from the resolution of the moment equations in the x and z directions:

$$\frac{\partial P}{\partial x} = \eta \frac{\partial^2 v_x}{\partial y^2} \qquad \textbf{(199)}$$

$$\frac{\partial P}{\partial y} = 0 \qquad \textbf{(200)}$$

$$\frac{\partial P}{\partial z} = \eta \frac{\partial^2 v_z}{\partial y^2} \quad \textbf{(201)}$$

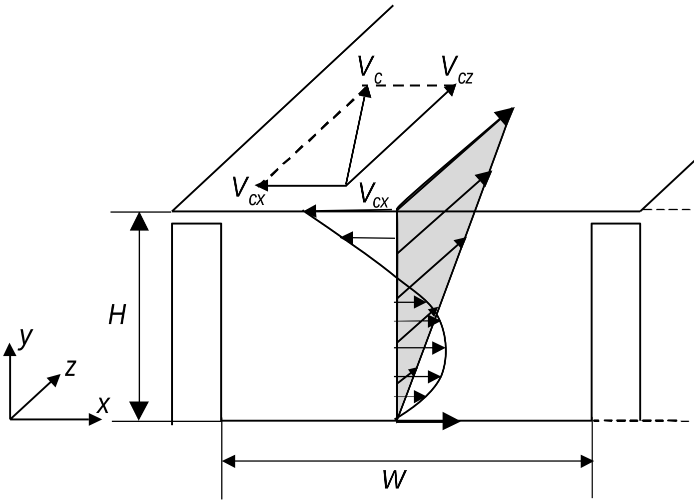

Figure 62- Velocity profiles in the pumping zone: Newtonian model

The integration in the *x* direction takes into account that the flow in that direction is zero (there is no flow in the flight clearance), that is, Q_x=0, and the following boundary conditions: $V_x(0)=0$ and $V_x(H)=-V_{cx}$. Thus, the following equations are obtained for the pressure variation and the velocity profile, respectively:

$$\frac{\partial P}{\partial x} = -\frac{6\pi\ N\ D_c \sin\theta_c\ \eta}{H^2} \quad \textbf{(202)}$$

$$V_x = V_{cx}\frac{y}{H}\left(2 - 3\frac{y}{H}\right) \quad \textbf{(203)}$$

It can be concluded from the previous equation that V_x is independent of pressure and viscosity. As can be seen in Figure 63, since the flow in the *x* direction (Q_x) is nil, the velocity is canceled for $y = 2/3H$. It appears that this circulatory flow is the main mechanism for mixing and homogenizing the melt. Finally, the pressure increases towards the active flank up to a maximum value.

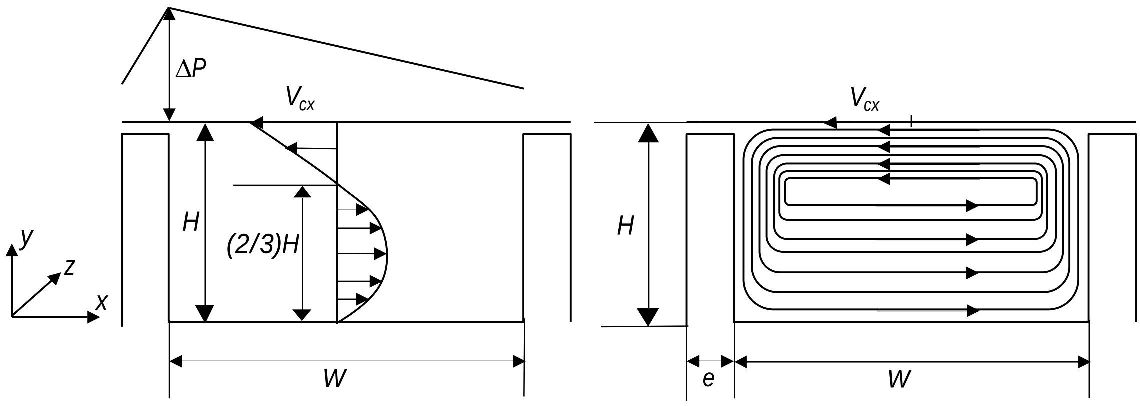

Figure 63- Velocity and pressure profiles and circulatory flow in the x direction

For the integration of equation 201 in the *z* direction, the boundary conditions are $V_z(y=0)=0$ and $V_z(y=H)=V_{cz}$, it being necessary to take into account that the flow is not zero, being given by:

$$Q = \int_0^H V_{cz}\,\overline{W}\,dy \qquad \textbf{(204)}$$

Thus, obtaining the following equation for the flow in the pumping zone:

$$Q = \frac{V_{cz}\,\overline{W}\,H}{2} - \frac{\overline{W}\,H^3}{12\,\eta}\frac{\Delta P}{Z} \qquad \textbf{(205)}$$

Z being the total length of the pumping zone. Since $\partial P/\partial z$ is constant it can be replaced by $\Delta P/Z$.

The first term of this equation represents the drag flow (Q_D) generated by the relative movement of the two surfaces, while the second term is the pressure flow (Q_P) that results from the flow resistance offered by the die. Figure 64 shows the vectorial sum of the speed profiles due to the drag and back pressure of the die.

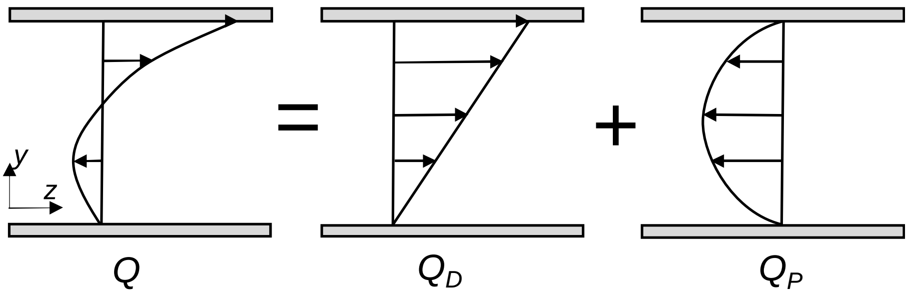

Figure 64- Velocity profiles due to drag (Q_D) and pressure (Q_P) and total flow (Q) in the z direction

As can be seen in Figure 64, the die creates a restriction on the flow of the material causing a pressure gradient in the direction of the channel, but in the opposite direction. Thus, the flow rate of the extruder in this zone (Q) is the sum of the flow rate due to the viscous drag (Q_D) with the flow rate caused by the pressure gradient (Q_P) [TAD 70, RAU 86]. It can be seen that the velocity component in the direction of the channel (V_{cz}), as illustrated in Figure 64, causes viscous drag flow, while the transverse component (V_{cx}), illustrated in Figure 63; induces mixing of the polymer additives and does not contribute to the flow rate [TAD 70].

The pressure gradient changes the velocity profile in the channel, decreasing the flow and increasing the degree of mixing. Figure 65 shows the velocity profiles in the *z* direction for various values of the Q_P/Q_D ratio. The maximum pressure is obtained when the total flow rate is zero, that is, by equalizing the flow (equation 204) to zero the result obtained is:

$$\Delta P_{máx} = \frac{6\,V_{cz}\,\eta\,Z}{H^2} \qquad \textbf{(206)}$$

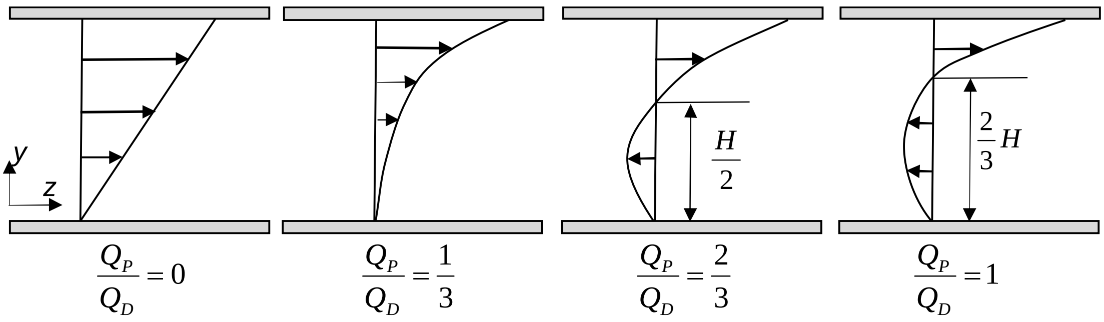

Figure 65- Velocity profiles for various values of the Q_P/Q_D ratio

In addition, for each value of rotation speed of the screw (N) there is a depth of the channel (H) and an angle of the screw helix (θ) that maximize the throughput. For this, it is necessary to calculate the derivative the flow equation in order of H and in order of θ (in the latter case considering $H=H_{Qmax}$), obtaining:

$$\begin{cases} \dfrac{dQ}{dH}=0 \Rightarrow H_{Q_{máx}}=\sqrt{\dfrac{2\eta\,\pi\,N\,D\cos\theta}{\Delta P/Z}} \\ \dfrac{dQ}{d\theta}=0 \Rightarrow \theta_{Q_{máx}} \approx 30^{o} \end{cases} \tag{207}$$

A joint analysis of the flow equation and of Figure 65 gives an idea of the sensitivity of the system to the back pressure exerted by the extrusion head. It appears that the higher the Q_P value, the greater the sensitivity of the extruder to pressure fluctuations in the die. For example, if Q_P represents only ten percent of the value of Q, a fifty percent change in pressure in the die causes five percent variation in Q. However, if Q_P is fifty percent of Q, the same change of fifty percent pressure in the die now causes twenty-five percent change in Q.

The model presented here allows to determine how to reduce the sensitivity to back pressure. Basically, there are two alternatives: i) to reduce the value of H, since Q_P varies with H_3; ii) promote a substantial increase in pressure in the solids zone, which will propagate through the melting zone causing the pressure at the beginning of the pumping zone to be high.

Effect of screw flanks

In the deduction of the flow equation, the effect of the screw flanks was ignored. This effect can be taken into account through the application of shape factors for the drag and pressure flow, respectively F_D and F_P, which take into account the presence of the screw's flanks by reducing the flow rates themselves. Thus, obtaining the following expression for the flow in the pumping zone:

$$Q=\frac{V_{cz}\,\overline{W}\,H}{2}F_D-\frac{\overline{W}\,H^3}{12\,\eta}\frac{\Delta P}{Z}F_P \tag{208}$$

This shape factors can be calculated by:

$$F_D=\frac{16\,\overline{W}}{\pi^3\,H}\sum_{g=1,3,\ldots}^{\infty}\left(\frac{1}{g^3}\right)tgh\left(\frac{g\,\pi\,H}{2\,\overline{W}}\right) \tag{209}$$

$$F_P = 1 - \frac{192\,H}{\pi^3\,\overline{W}} \sum_{g=1,3,\ldots}^{\infty} \left(\frac{1}{g^5}\right) tgh\left(\frac{g\,\pi\,H}{2\,\overline{W}}\right) \qquad \textbf{(210)}$$

Figure 66 shows the variation of these shape factors with the H/W ratio. Bearing in mind that the width (W) is much greater than the depth of the channel (H), that is H/W less than 0.5, it appears that the shape factors are close to 1 and that they are not very different from each other.

Clearance effect

The effect of the clearance between the cylinder and the screw flight can be taken into account using the following expression [TAD 70]:

$$Q = \frac{V_{cz}\,\overline{W}\left(H - \delta_f\right)}{2} - \frac{\overline{W}\,H^3}{12\,\eta}\frac{\Delta P}{Z}\left(1 + f_L\right) \qquad \textbf{(211)}$$

where f_L is a correction factor that takes into account the ratio between the viscosity in the channel (η) and the viscosity in the gap (η_f), this value being different from the viscosity in the screw channel, since the local value of shear rate is very different.

$$f_L = \left(\frac{\delta_f}{H}\right)^3 \frac{\eta\,e}{\eta_f\,\overline{W}} + \frac{\left(1+\frac{e}{W}\right)\left[-\frac{Q_D}{Q_P} + \frac{1+\frac{e}{W}}{tg^2\theta_c}\right]}{1 + \frac{\eta_f}{\eta}\left(\frac{H}{\delta_f}\right)^3 \frac{e}{\overline{W}}} \qquad \textbf{(212)}$$

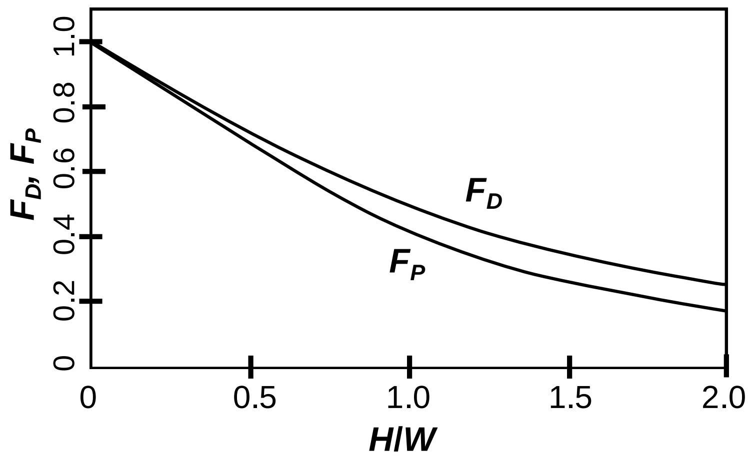

Figure 66- Shape factors as a function of H/W

Effect of non-Newtonian character

The non-Newtonian model is based on an analysis similar to the previous one, and the viscosity of the polymer is determined using the constants of the power law. The flow equation for this case is identical to equation 204, introducing correction factors that consider the effect of the non-Newtonian nature of the polymer [RAU 86].

$$Q = \frac{(4+n)V_{cz}\,\overline{W}\,H}{10} - \frac{\overline{W}\,H^3}{4(1+2n)\eta}\frac{\Delta P}{Z} \qquad \textbf{(213)}$$

Viscous dissipation effect

In the models presented above, the isothermal flow of the polymer was considered. However, especially in the melting and pumping zones, it is important to be able to calculate the temperature value of the polymer in order to predict the possible degradation of the material by excess temperature. Bearing in mind that the flow in this type of machines is essentially shearing and considering isothermal conditions in the cylinder and screw, the average temperature of a differential block of material between the cylinder and screw is given by [AGA 89]:

$$\overline{T} = T_0 + \eta\frac{V_{cz}^2}{12\,k_m}\left(1+\frac{12}{B_r}\right)\left[1-\exp\left(-12\,C_a\ z/L\right)\right] \qquad \textbf{(214)}$$

$$B_r = \frac{\eta\,V_{cz}^2}{k_m\ (T_c - T_{0)}} \qquad \textbf{(215)}$$

$$C_a = \frac{\alpha\ Z_B\,\overline{W}}{Q\,H} \qquad \textbf{(216)}$$

where, *Br* is the number of Brinkman, which represents a measure of the importance of the heat generated by viscous dissipation relative to the conducted heat, *Ca* is the number of Cameron, which translates the type of thermal conditions of the system, T_0 is the temperature of the polymer in the start of the pumping zone, Z_B is the helical length of the screw channel in the pumping zone and L is the axial length of the screw in the pumping zone.

Due to the difficulty in determining the screw temperature, isothermal conditions in the cylinder and adiabatic conditions in the screw are considered, obtaining:

$$\overline{T} = T_0 + \eta\frac{V_{cz}^2}{3k_m}\left(1+\frac{3}{B_r}\right)\left[1-\exp\left(-12C_a z/L\right)\right] \qquad \textbf{(217)}$$

This is the most realistic situation, allowing the calculation of the average temperature anywhere in the pumping zone at a distance z from its beginning.

Numerical model

The numerical model adopted here must be consistent with the numerical models presented for the previous zones, and must be able to predict the most relevant process variables (pressure gradient, energy consumption, temperature profile, residence time distribution and degree of mixture). For this, one must consider the non-isothermal and two-dimensional flow of a non-Newtonian fluid in the presence of convection. Figure 67 illustrates the velocity and temperature profiles for this zone. The main simplifications used in this model, as in the melt pool in the melting zone, are [FEN 77, FEN 79]:

- The melt flow over the flight clearance and slipping on the channel walls are disregarded;
- Molten polymer is considered to be a purely viscous liquid obeying the power law;
- The flow is stationary,

- The melt flow is fully developed in the transversal, x, and longitudinal, z, directions (*i.e.*, $\partial V_x/\partial x=0$ and $\partial V_z/\partial z=0$);
- The temperature field is fully developed in the transversal direction of the channel (*i.e.*, $\partial T/\partial x=0$), but not in the longitudinal direction of the channel (that is, $\partial T/\partial z\neq 0$);
- The conduction of heat towards the channel is neglected (*i.e.*, $\partial^2 T/\partial z^2 << \partial^2 T/\partial y^2$));
- The forces of gravity and inertia are neglected;
- The velocity of the solid plug is constant.

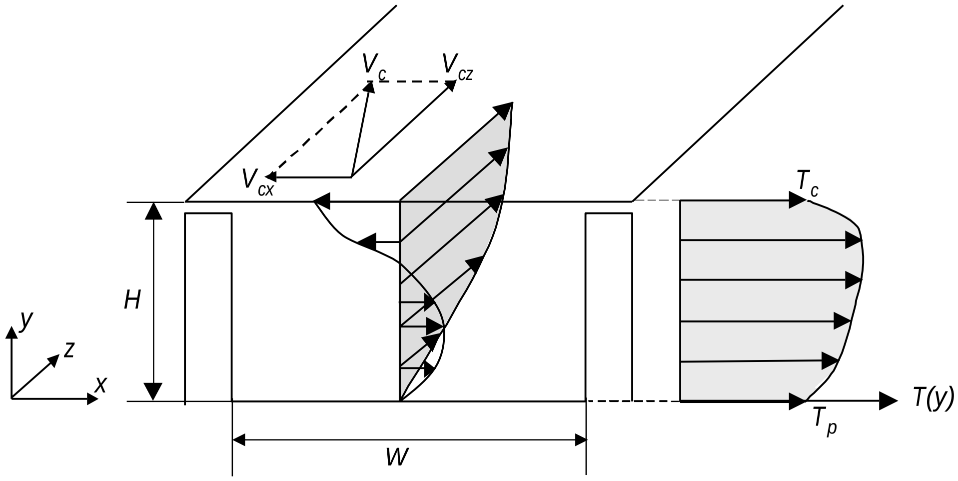

Figure 67- Cross section for the pumping zone

Under these conditions, the equations for moment and energy and the shear rate are the same as those used in the melt pool in the melting zone (equations 108, 109, 171 and 173), which are reproduced below due to their importance for this text.

$$\frac{\partial P}{\partial x}=\frac{\partial}{\partial y}\left(\eta\,\frac{\partial V_x}{\partial y}\right) \tag{218}$$

$$\frac{\partial P}{\partial y}=0 \tag{219}$$

$$\frac{\partial P}{\partial z}=\frac{\partial}{\partial y}\left(\eta\,\frac{\partial V_z}{\partial x}\right)+\frac{\partial}{\partial y}\left(\eta\,\frac{\partial V_z}{\partial y}\right) \tag{220}$$

$$\rho_m\, C_m\, V_z(y)\,\frac{\partial T}{\partial z}=k_m\left(\frac{\partial^2 T}{\partial x^2}+\frac{\partial^2 T}{\partial y^2}\right)+\eta\,\dot{\gamma}^2 \tag{221}$$

where the shear rate is:

$$\dot{\gamma}=\left[\left(\frac{\partial V_x}{\partial y}\right)^2+\left(\frac{\partial V_z}{\partial x}\right)^2+\left(\frac{\partial V_z}{\partial y}\right)^2\right]^{1/2} \tag{222}$$

and the boundary conditions are:

$$\begin{cases} V_x(y=0)=0 \\ V_x(y=H)=-V_{cx} \end{cases} \quad \begin{cases} V_z(x=0)=0 \\ V_z(x=W)=0 \\ V_z(y=0)=0 \\ V_z(y=H)=V_{cz} \end{cases} \quad \begin{cases} T(x=0)=T_p \\ T(x=W)=T_p \\ T(y=0)=T_p \\ T(y=H)=T_c \end{cases} \tag{223}$$

In solving these equations, the flow rate in the *x* direction is zero and in the *z* direction is:

$$Q=\int_0^H \overline{W}\ V_{cz}(y)\ dy \tag{224}$$

These two additional equations allow to obtain by finite differences a system of equations whose result will be the pressure profile in the direction of the channel and the transversal profiles of temperature and speed.

Power consumption

In this zone the total consumption of mechanical power (e_m) is the sum of the power dissipated in the screw channel (e_{cp}), the power dissipated in the clearance (e_{cl}) and the power due to the pressure gradient (e_P) [TAD 70, RAU 86].

$$e_m=e_{cp}+e_p+e_{cl} \tag{225}$$

$$e_{cp}=\frac{\eta\, V_c^2}{H}\left\{\cos^2\theta_c\left[1+3\left(\frac{Q_P}{Q_D}\right)^2\right]+4\sin^2\theta_c\right\}\overline{W}\ z \tag{226}$$

$$e_p=Q\,\Delta P \tag{227}$$

$$e_{cl}=\frac{\eta_f\, V_c^2\, e}{\delta_f}\, z \tag{228}$$

Distribution of residence times

The degree of mixing of a specific melt increases with the generation of interfacial area between its individual components and with the average residence time inside the extruder. The increase in the interfacial area is proportional to the increase in the shear stress of the molten polymer. The stress experienced by each polymer particle varies according to its position in the screw channel, as seen previously. Particles near the cylinder and the screw root suffer a higher level of stress than those that pass through the center of the channel. Therefore, the average stress can be used as a relatively simple, but satisfactory criterion to quantify the degree of mixing in an extruder [PIN 70, BIG 73, BIG 74].

Pinto and Tadmor [PIN 70] determined the Residence Time Distribution (RTD) and the "degree of mixing" (through a Weighted Average of the Total Strain - WATS, whose calculation details can be found in Gaspar-Cunha [GAS 09]), assuming the isothermal flow of a Newtonian fluid between parallel plates. The resulting equation for residence time is:

$$t_R = \left[\frac{L}{3 V_c \sin\bar{\theta} \cos\bar{\theta} \left(1 - \frac{Q_P}{Q_D}\right)} \right] \frac{3a - 1 + 3\sqrt{1 + 2a - 3a^2}}{a\left[1 - a + \sqrt{1 + 2a - 3a^2}\right]} \qquad \textbf{(229)}$$

of which: L is the longitudinal length of the screw in the pumping zone and a is the reduced depth of the channel ($a = y/H$). With this equation it is possible to calculate the residence time in the pumping zone of a particle at position a.

Thus, it can be concluded that the minimum residence time occurs when $a = 2/3$ and increases towards the surface of the cylinder ($a = 0$) and towards the root of the screw ($a = 1$). The average residence time is given by:

$$\bar{t} = \frac{2L}{V_c \sin\bar{\theta} \cos\bar{\theta} \left(1 + \frac{Q_P}{Q_D}\right)} \qquad \textbf{(230)}$$

The weighted average of the total deformation, WATS, is:

$$WATS = \bar{\gamma} = \int_0^{\infty} \gamma \; f(t) dt \qquad \textbf{(231)}$$

This value can be calculated in an efficient way using the following equation [TAD 06].

$$WATS = \bar{\gamma} = \frac{2L}{H\left(1 - \frac{Q_P}{Q_D}\right)}, \qquad -\frac{1}{3} \le \frac{Q_P}{Q_D} \le \frac{1}{3} \qquad \textbf{(232)}$$

Operating point

The flow equation for the pumping zone (equation 204) allows the graph of Figure 68 to be constructed, taking into account a Newtonian fluid. The flow rate is maximum when Q_P is zero (*i.e.*, $Q = Q_D$), and as the pressure increases, the flow decreases until $Q_P = Q_D$, which occurs when the pressure is maximum (as shown in the graph). When the rotation speed of the screw (N) changes, only the drag rate is affected. This effect is illustrated in Figure 68 with the two parallel dashed lines. As expected, an increase in the speed of rotation produces an almost linear increase in throughput. As previously mentioned, the extruder must generate the pressure necessary for the melted polymer to pass through the die at the desired rate. It is also obvious that the pressure is generated from the hopper, which means that at the beginning of the pumping zone the pressure is not zero.

Equation 233 relates the flow and pressure drop in the die to a Newtonian fluid, with G being a geometric constant that depends on the geometry of the die flow channel. For each specific geometry there will be a geometric constant and a shear rate that will allow calculating: the flow rate as a function of the pressure drop and vice versa and the viscosity for the defined shear rate. Figure 69 shows the flow as a function of the pressure necessary for the polymer to pass through a given die. The figure also shows the effect of viscosity and type of geometry on the slope of the line. An increase in viscosity causes a decrease in the slope, while the slope of the line decreases when the die is more restrictive to the flow, that is, for a die with a smaller section or with a longer length (value taken into account in the general constant G).

$$Q_{fieira} = G\frac{\Delta P_{fieira}}{\eta_{fieira}} \tag{233}$$

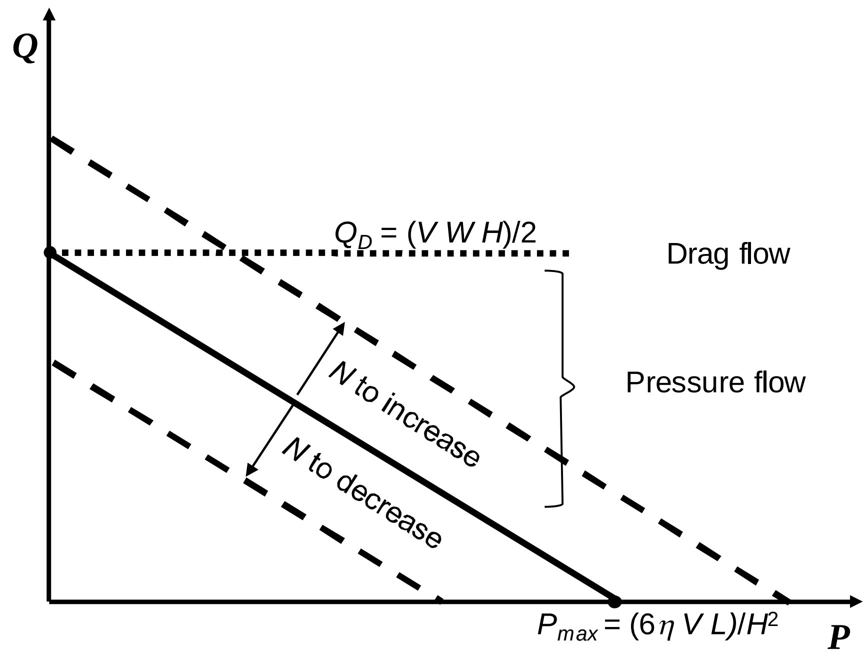

Figure 68- Flow rate according to the pressure generated in the pumping zone: effect of the rotation speed of the screw

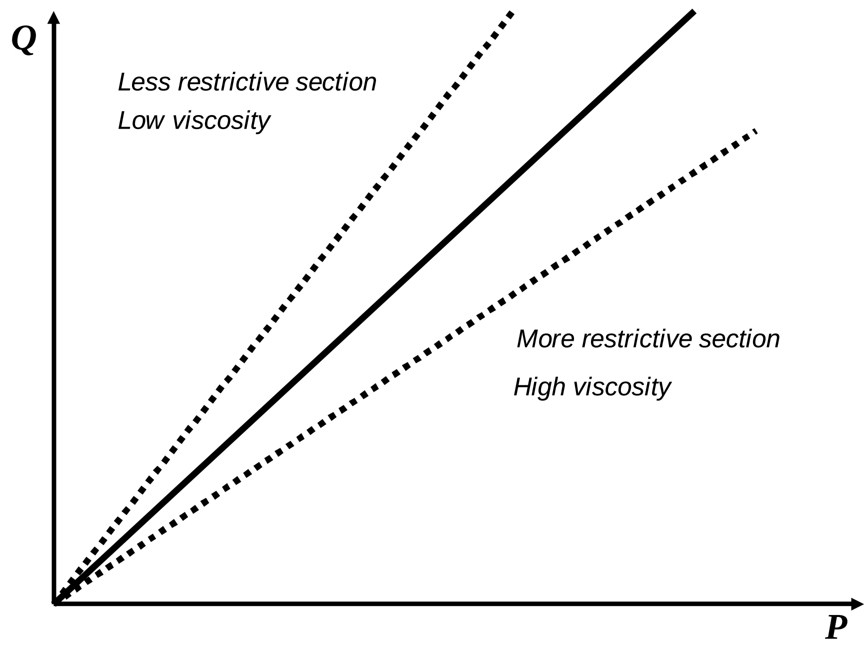

Figure 69- Flow rate as a function of a general die: effect of die viscosity and geometry

The junction of these two lines produces what is called the machine's operating point, that is, when an extruder is joined with a specific die, the flow through the two devices must be equal and the pressure generated in the extruder is totally consumed in the die. This concept is illustrated in Figure 70 by the crossing points of the defined extruder and die lines. Taking for example point 1, the specified extruder-die assembly operates at pressure P_1 and flow rate Q_1. The effect of the rotation speed of the screw is also illustrated, where the operative point may move between points 2 and 3 when varying N and between points 3 and 4 when varying the die geometry or when viscosity varies in the die (either by the effect of temperature or by the variation of the shear rate).

One of the most efficient ways of varying the operating point is through the channel geometry of the metering zone, which can be performed by changing the channel depth (H). Figures 71 and 72 illustrate this effect. As the value of H is part of the two terms of the output equation; it appears that increasing H the value of Q_D increases linearly while the value of Q_P increases by the cube. The effect of these changes at the operative point is shown in Figure 71. Three different situations can occur when increasing H: i) for a less restrictive die, the throughput increases (Die 1 in Figure 72); ii) the output remains constant in the case of Die 2; iii) the flow rate decreases for more restrictive dies (Die 3).

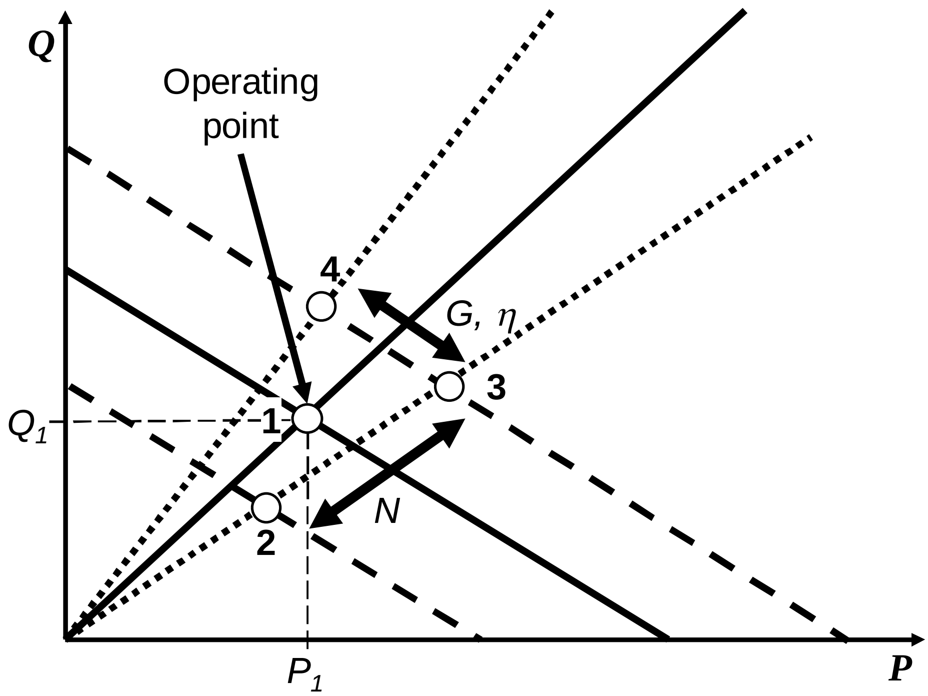

Figure 70- Operative point: effect of the rotation speed of the screw, the viscosity in the die and the geometry of the die

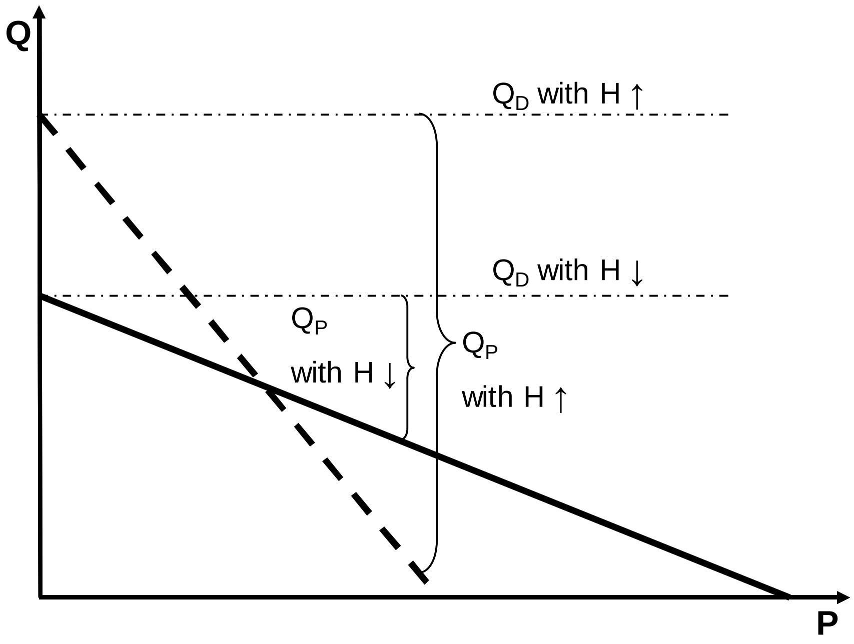

Figure 71- Effect of channel depth on the pressure curve of the extruder

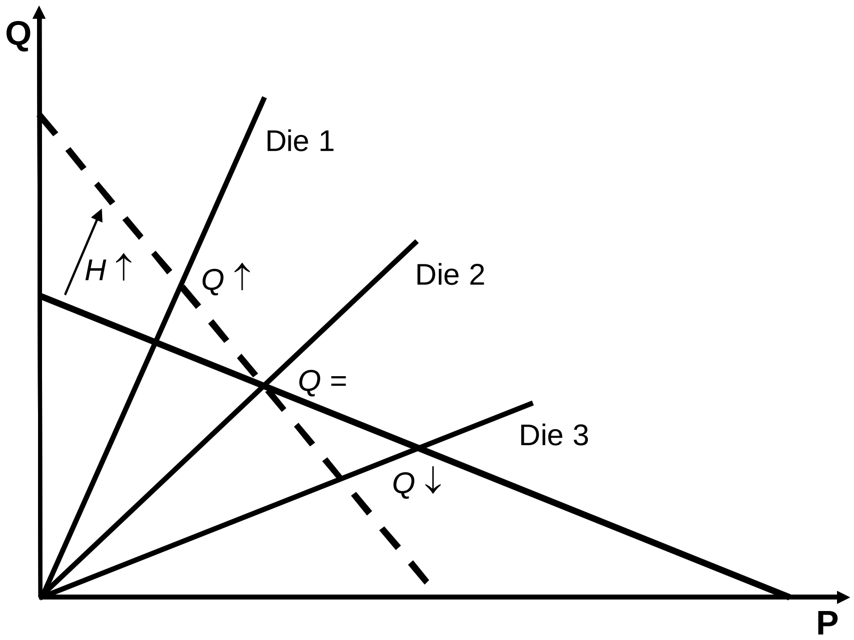

Figure 72- Operative point: effect of the depth of the channel in the measurement zone

Application exercise

1. Consider the extruder-die set outlined in the figure 73, and the pressure and temperature profiles indicated. Knowing that the screw rotates at 100 rpm and that the material is an HDPE and is all melted at the end of the compression zone and that the pressure at that point is given in the graph in Figure 73. Determine the back pressure in the extruder head and the output obtained.

Note: - Before starting the calculations, explain the methodology for solving the problem.

Screw:

- Square pitch - D_p = 59.8 mm
- Compression ratio=3
- Flight thickness =5 mm
- Flight clearance (δ_f) = 0.1 mm

Material data:

Physical properties:

Specific mass at feeding = 630 kg/m^3
Specific mass of solid= 950 kg/m^3

Friction coefficient material/hopper = 0.30
Friction coefficient material/screw = 0.25
Friction coefficient material/cylinder = 0.4
Friction angle of the particles = 33,7º

Melt specific mass at different temperatures (kg/m^3):

T=25ºC – 950
T=150ºC – 800
T=179ºC – 760
T=180ºC – 750
T=200ºC – 750

Thermal properties:

Solid thermal conductivity = 0.51 J/m.s.K
Melt thermal conductivity = 2300 J/kg/.K
Solids specific heat = 1317 J/kg/K
Melting heat = 230 kJ/kg
Melting temperature = 130 ºC

Viscosity: Power law	n	0.345	--
	k_0	29.94	kPa s^{-1}
	a	0.00681	ºC^{-1}
	T_0	190	ºC

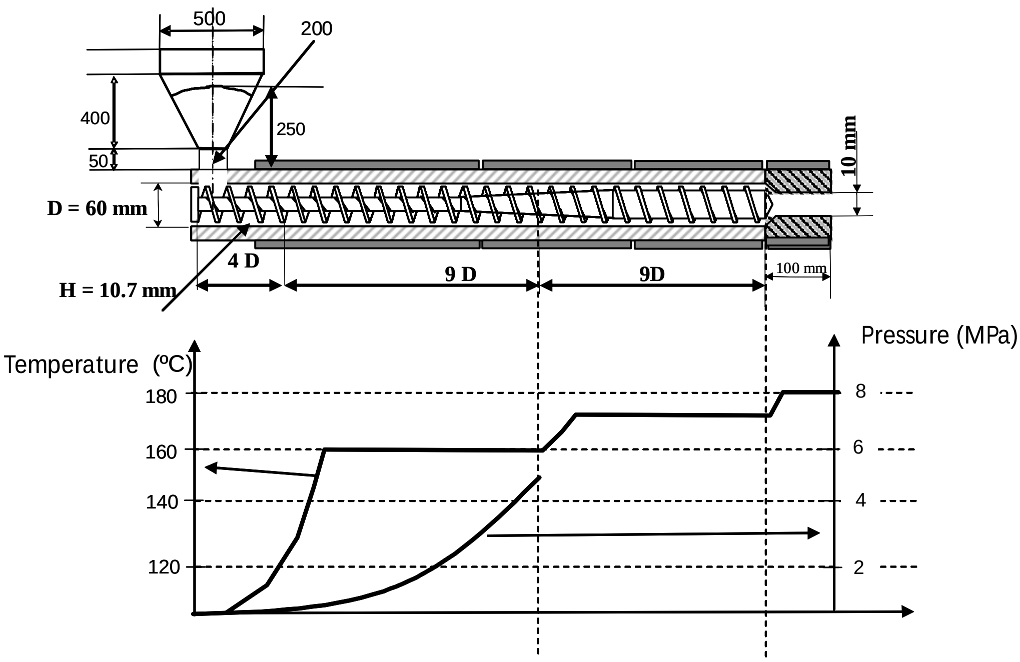

Figure 73- Extruder and die geometry and cylinder temperature profile

$$Q_{die} = \frac{\pi \ R^4}{8\,L} \frac{\Delta P_{die}}{\eta_{die}} \tag{234}$$

$$\dot{\gamma}_{die} = \frac{4\,Q_{die}}{\pi \ R^3} \tag{235}$$

4. Technological developments

4.1. Grooved extruders

Numerous theoretical and experimental studies have been carried out using extruders with grooves in the cylinder [BOE 90, POT 85, RAUT 82a, RAUT 82b, GRÜ 84, RAU 86, POT 88, POT 89, GOL 71]. From these studies it can be seen that there are two methods of approaching the problem, the first considers that the coefficient of friction polymer-cylinder with grooves can be replaced by an average effective friction coefficient, the second method considers the existence of flow of granules from the polymer along the grooves. For the calculation of the average friction coefficient, four models will be presented, for which some simulations were carried out with the aim of verifying their suitability and their sensitivity to the change in the geometry of the system, with the results obtained being presented and discussed. With regard to the second calculation method, due to its complexity, it will not be addressed in these notes.

The heat generated by friction on the surface of the cylinder is proportional to the value of the friction coefficient, and is therefore much higher in the case of grooves, which makes the rate of temperature increase also higher. In this way, it is necessary that this zone is thermally isolated from the following and that its temperature be controlled and maintained below the melting temperature or above the glass transition temperature, depending on whether the polymers are semi-crystalline or amorphous [POT 88]. This insulation prevents the polymer from starting to melt, starting the delay zone.

System geometry

The purpose of the grooves is to increase the coefficient of friction between the solid polymer granules and the inner walls of the cylinder which, as is known, increases the flow capacity of the extruder. The grooves can be longitudinal or helical, as shown in Figure 74.

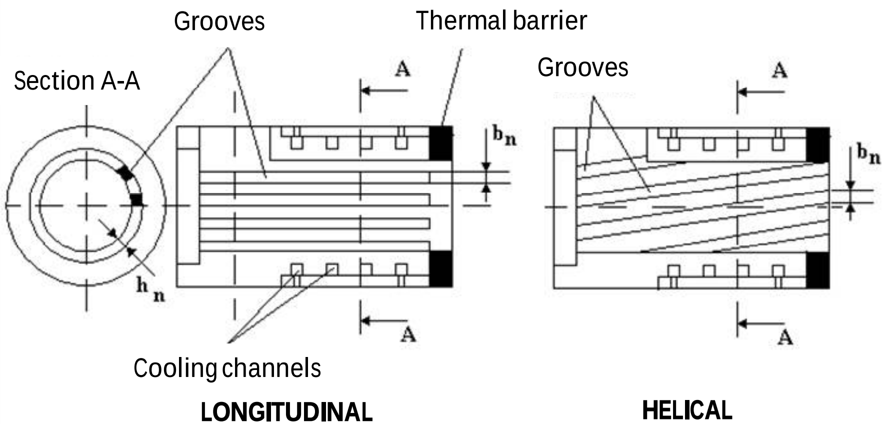

Figure 74- Longitudinal and helical grooves in the cylinder

Generally, the depth of the grooves (h_N) is not constant, but varies from a maximum value at the entrance of the grooves (h_{N0}) to being canceled at the exit, according to the equation:

$$h_N = h_{N0} - A_N \; Z_N \qquad \textbf{(236)}$$

of which: A_N is the slope and Z_N is the length of the grooves. The effect of feed section groove taper angle on the performance of a single-screw extruder was studied by Sikora [SIK 01]. For that purpose, an active grooved section was developed enabling the change of the size and the number of grooves during the process. Sasimowski *et. al* [SAS 14] used this device to study the effectiveness of the grooved section in single-screw extrusion and conclude that the process is very efficient with the presence of grooves in the solids conveying zone.

Average effective friction coefficient

This method considers that the increase in friction caused by the grooves can be quantified as long as the polymer-cylinder friction coefficient is replaced by the average effective friction coefficient [POT 85].

The average effective friction coefficient is due to the fact that when the block of solids moves along the screw channel, friction on the cylinder wall varies between polymer-cylinder friction and internal friction (polymer-polymer), Figure 75.

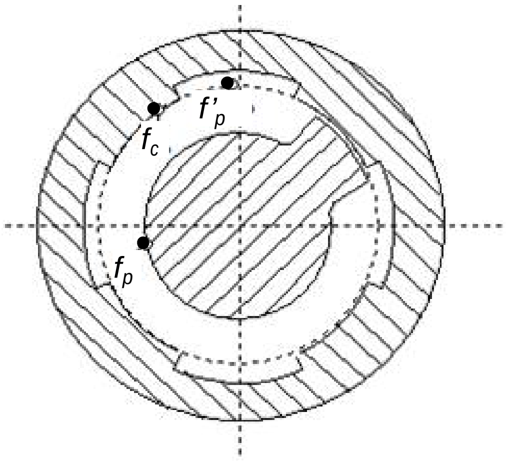

Figure 75- Friction coefficient with grooves

When implementing such a method, attention should be paid to the great simplification that is being made, since it is considered that the transport dynamics does not change. Several models have been proposed for the calculation of the average friction coefficient:

- Goldacker - 1971 [GOL 71],
- Potente - 1985 [POT 85],
- Rautenbach and Peiffer - 1982 [RAUT 82a, RAUT 82b] and
- Grünschloβ - 1984 [GRÜ 84].

Goldacker [GOL 71] considered that the average effective friction coefficient (f_{ef}) should take into account the polymer-cylinder friction coefficient (f_c), the internal friction coefficient (f_p') and the groove surface:

$$f_{ef} = f_c + \left(f_p^{'} - f_c\right)\frac{B}{\pi D_c} \qquad \textbf{(237)}$$

where D_c is the internal cylinder diameter and B the total with of the grooves, determined by:

$$B = b_N \; N_N \qquad \textbf{(238)}$$

This is an expeditious and simple method, but it does not take into account the number of grooves or their depth, parameters whose influence can be considerable, as verified by Rautenbach, Peiffer and Grünschloβ [RAUT 82a, RAUT 82b, GRÜ 84].

Thus, Potente [POT 85] considers that the equation for the average effective friction coefficient should take the following form:

$$f_{ef} = f_c + \left(f_p^{'} - f_c\right)\frac{B}{\pi D_c}\left\{1 - \exp\left[-\alpha\left(\frac{h_N}{B}N_N\right)^{\beta}\right]\right\} \qquad \textbf{(239)}$$

being α and β empirical constants, which must have a value of 5 and 0.9, respectively [POT 85].

Bearing in mind that the friction coefficients on the internal surface of the cylinder and at the base of the grooves (f_{Na}) may be different, the previous equation is replaced by:

$$f_{ef} = \left[f_c + \left(f_p^{'} - f_c\right)\frac{B}{\pi D_c}\right]\left\{1 - \exp\left[-0.65\left(\frac{f_{Na}}{f_c} - 1\right)^{1.2}\right]\right\} +$$
$$\left[f_c + \left(f_p^{'} - f_c\right)\frac{B}{\pi D_c}\left\{1 - \exp\left[-5\left(\frac{h_N}{B}N_N\right)^{9}\right]\right\}\right] \qquad \textbf{(240)}$$
$$\exp\left[-0.65\left(\frac{f_{Na}}{f_c} - 1\right)^{1.2}\right]$$

for: $f_{NA} \geq f_c$.

Rautenbach and Peiffer [RAUT 82a, RAUT 82b] developed a model for the average effective friction coefficient based on balance of forces for a channel volume element, using a material law (Hooke's Law). Considering that the polymer granules flow in the channel as a cohesive block, neglecting the forces of inertia and gravity and neglecting the distribution of stresses transversal to the direction of the channel, it is possible, with the coordinate system of Figure 76 and a balance of the forces of friction that act in the grooves to obtain the expression [RAUT 82a]:

$$f_{ef} = \frac{1}{e^{A^+\varphi_E} - 1}\sum_{n=1}^{M}\left\{f_c\left[e^{A^+\left(n\varphi_F + (n-1)\varphi_N\right)} - e^{A^+(n-1)(\varphi_N + \varphi F)}\right]\right.$$
$$\left. + f_p^{'}\left[e^{A^+ n(\varphi_N + \varphi F)} - e^{A^+\left(n\varphi_F + (n-1)\varphi_N\right)}\right]\right\} \qquad \textbf{(241)}$$

where:

$$M = \frac{\varphi_E}{\varphi_F + \varphi_N} \qquad \textbf{(242)}$$

φ_E is the length of the dimensionless screw channel:

$$\varphi_E = 2\,\pi\,E\cos\theta_C \qquad \textbf{(243)}$$

φ_N is the slot angle in the grooved zone:

$$\varphi_N = arctg\frac{b_N}{D_c} \qquad \textbf{(244)}$$

φ_F is the angle of the zone without grooves:

$$\varphi_F = \frac{2\,\pi - N_N\,\varphi_N}{N_N} \qquad \textbf{(245)}$$

A^+ can be considered a constant and equal to 0.5, as it does not significantly influence the final result, E is the number of turns with grooves and θ_c is the angle of inclination of the screw helix.

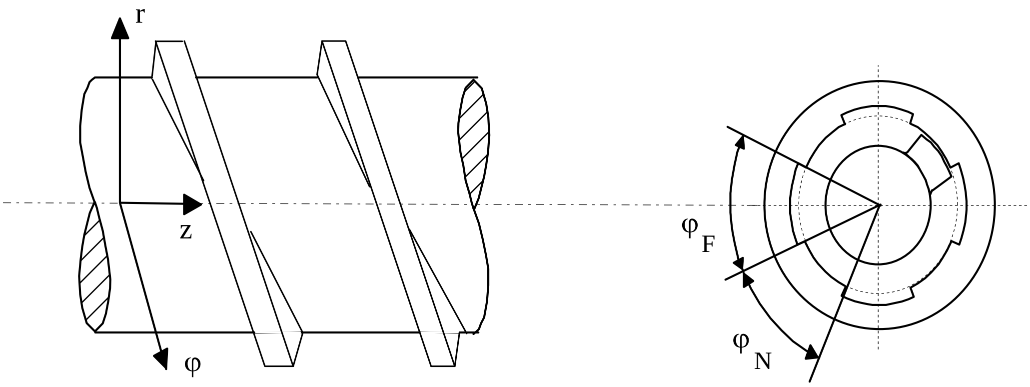

Figure 76- Coordinate system

Obtaining this equation is possible because the dependence of the average effective friction coefficient in relation to the angle of transport of solids (φ) is small. The transport angle decreases as the channel progresses, as pressure increases and the block of solids becomes more and more compact. In this way, the calculation of this angle is an interactive process, being necessary firstly to obtain its initial value (φ_0) and the flow rate (Q) [RAUT 82a]:

$$\varphi_0 = \arcsin\left[-\frac{\frac{D_i\ f_c^2}{D_c\,f_{ef}}}{1+f_c^2}+\sqrt{\left(\frac{\frac{D_i\ f_c^2}{D_c\,f_{ef}}}{1+f_c^2}\right)^2+\frac{1-\left(\frac{D_i\ f_c^2}{D_c\,f_{ef}}\right)^2}{1+f_c^2}}\right]-\theta_c \qquad \textbf{(246)}$$

$$Q = \rho_s\ \pi\ N\ D_c\ A_f\ \frac{tg\theta_c\ tg\varphi_0}{tg\theta_c + tg\varphi_0} \qquad \textbf{(247)}$$

where:

$$A_f = \frac{\pi}{4}\left(D_c^2 - D_i^2\right) - \frac{e\ H}{\sin\theta_c} \qquad \textbf{(248)}$$

of which: N is the rotation speed of the screw, θ_c the angle of inclination of the screw and D_i the internal diameter of the screw.

The transport angle can be obtained, at any point along the solids transport zone, from the following equation:

$$\phi = arctg\left[\frac{1}{\frac{D_c A_f \pi N}{Q}\rho_s - \cot g\theta_c}\right] \qquad \textbf{(249)}$$

where ρ_s is obtained for local pressure and temperature conditions.

Grünschloβ [GRÜ 84] developed a model that considers the existence of a cross flow of polymer granules in the grooves (Figures 77 and 78). Through a qualitative analysis Grünschloβ verified that this transversal flow occurred mainly when the value of h_N/b_N is low (Figure 78). This means that the determination of the value of the average effective friction coefficient will depend on this quotient, and two situations may occur: i) if h_N/b_N is greater than a critical value, the average effective friction coefficient will be obtained from equation 237; ii) otherwise, its value varies between the value given by equation 237 and f_c. It is precisely in this second situation, located at the end of the groove area, that greater pressure develops, which is why it is more important in the performance of the grooves. The practical studies of Grünschloβ allowed to build the model shown in Figure 79.

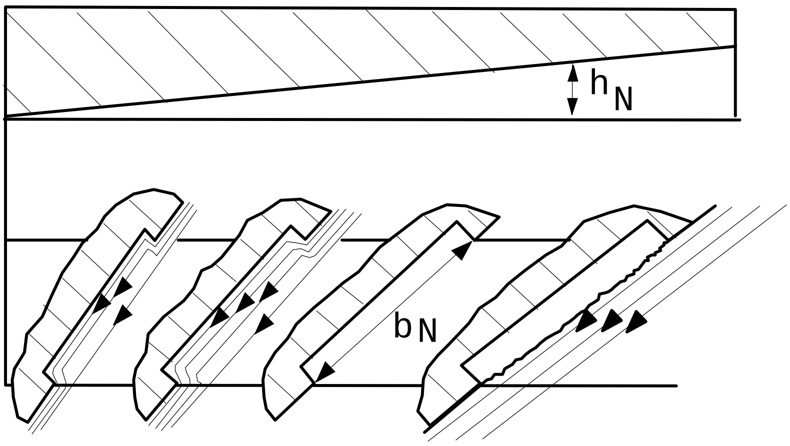

Figure 77- Transverse flow of granules in the grooves

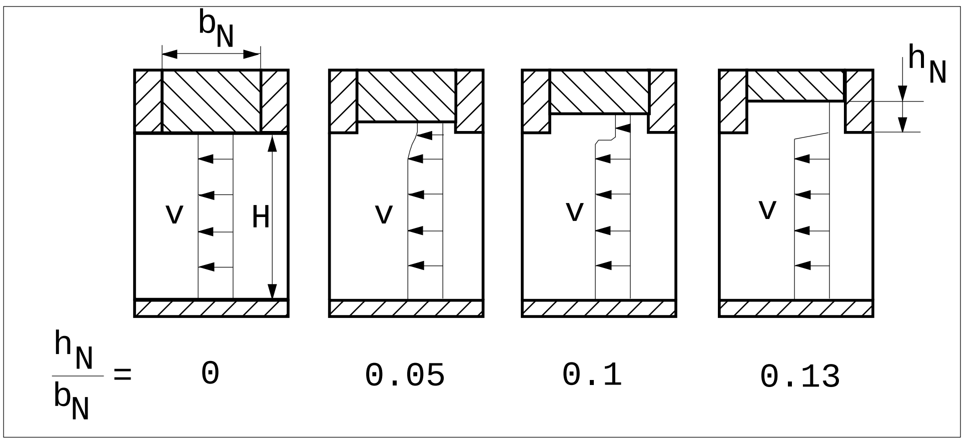

Figure 78- Velocity profiles in the screw channel and across the grooves

The derived model is based on the fact that the total power consumed to maintain the flow of granules, according to the process illustrated in the previous figure, naturally adjusts to a minimum value ($P_{Ges\ min}$).

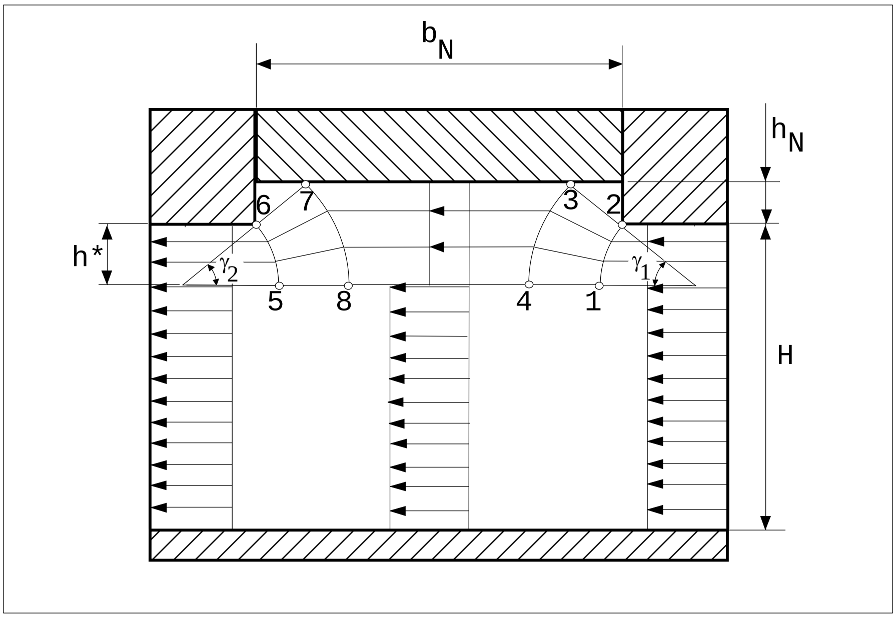

Figure 79- Model that illustrates the flow across the slots

The total power (P_{Ges}) is due to: deformations in zones 1-2-3-4 and 5-6-7-8, deflections in zones 1-2, 3-4, 5-6 and 7-8 and the friction in zones 1-4, 5-8, 2-3, 6-7, 3-7 and 4-8. Being obtained from the sum of all these components.

$$P_{Ges} = 4\,P_{1-2} + 2\,P_{1-2-3-4} + 2\,P_{1-4} + 2\,P_{2-3} + P_{3-7} + P_{4-8} \qquad \textbf{(250)}$$

where: $P_{1-2} = P_{3-4} = P_{5-6} = P_{7-8}$ are the dimensionless power consumptions due to deflections in zones 1-2, 3-4, 5-6 and 7-8; $P_{1-2-3-4} = P_{5-6-7-8}$ are the consumption of dimensionless power due to the deformations in zones 1-2-3-4 and 5-6-7-8; $P_{1-4} = P_{5-8}$ are the dimensionless power consumption due to internal friction in zones 1-4 and 5-8; $P_{2-3} = P_{6-7}$ are the dimensionless power consumption due to internal friction with the material stagnant in zones 2-3 and 6-7; P_{3-7} is the dimensionless power consumption due to friction in zone 3-7 and P_{4-8} is the dimensionless power consumption due to friction in zone 4-8.

These values depend on γ_1, γ_2 e h^*, and they can be obtained from the following equations, by considering $\gamma_1 = \gamma_2 = \gamma$.

$$P_{1-2} = \frac{h^*}{b_N}\frac{\sin^2(\omega-\varphi)}{tg\gamma}\left(\sqrt{1+\frac{tg^2\gamma}{\sin^2(\omega+\varphi)}}-1\right) \qquad \textbf{(251)}$$

$$P_{1-2-3-4} = \frac{h^*}{b_N}\ln\left(1+\frac{h_N}{h^*}\right) \qquad \textbf{(252)}$$

$$P_{1-4} = \frac{h_N^2}{2b_N \sin\gamma\left(h^* + \frac{h_N}{2}\right)} \tag{253}$$

$$P_{2-3} = \frac{h^* h_N}{b_N \sin\gamma\left(h^* + \frac{h_N}{2}\right)} \tag{254}$$

$$P_{3-7} = \frac{h^*}{h^* + h_N}\frac{f_{Na}}{f_{p-p}}\left(1 - \frac{2h_N}{b_N tg\gamma}\right) \tag{255}$$

$$P_{4-8} = \frac{h^*}{h^* + h_N}\left(1 + \frac{2h^*}{b_N}\left(\frac{1}{tg\gamma} - \frac{1}{\sin\gamma}\right) - \frac{2h_N}{b_N \sin\gamma}\right) \tag{256}$$

where h^* is the level of divergence of the grooves (Figure 79), γ is the angle of the deformation zone (Figure 79) and ω is the angle of inclination of the helix of the grooves (in the case of longitudinal grooves ω=0).

Thus P_{Ges} depends on two values γ e h^*, it is necessary to minimize the function P_{Ges} = f (γ,h^*,) using a numerical method of minimization. In this case, the method used for the determination of P_{Gesmin} was the Rosenbrok algorithm, which is a numerical method suitable for the optimization of functions of several variables.

It is then possible to obtain the value of the friction coefficient that acts in the groove area (f_e) through:

$$f_e = f_p^{'}\, P_{Ges\,\min} \tag{257}$$

Finally, the average effective friction coefficient acting on the cylinder can be calculated iteratively at any point in the groove area, replacing f'_p with f_e in expression 2:

$$f_{ef} = f_b + (f_e - f_b)\frac{B}{\pi D_b} \tag{258}$$

Application study of the models presented

Geometric data

The extruder to be used in the calculations has a square pitch screw with a diameter of 36 mm and an L/D ratio equal to 26. It also has the possibility of the optional inclusion of sections with different geometries, with the length of 4D (144 mm) and where the depth varies linearly from a maximum value (2mm) at the beginning of the grooves, until it is canceled at the exit. Table 4 shows the various configurations used in the grooves.

Polymer properties

The polymer used in the calculations is High Density Polyethylene (HDPE) whose properties relevant to the solids transport zone are given in table 5.

Table 4- Grooves configurations.

Configuration	N_N	b_N (mm)	N_N*b_N (mm)
1	12	5.0	60
2	10	6.0	60
3	8	7.5	60
4	6	10.0	60
5	4	15.0	60
6	12	4.0	48
7	12	6.0	72

Table 5- Coefficients of friction.

Friction coeficiente polymer-cylinder	0.45
Friction coeficiente polymer-screw	0.25
Internal friction coeficiente	0.669

Average friction coefficient

The results presented below show the influence of the calculation model and the number, width and depth of the grooves on the value of the average friction coefficient. The grooves geometries in Table 4 were used for the 4 calculation models considered. Figure 80 shows the variation of the average friction coefficient with the channel depth for the various calculation models and configuration 1 (Table 4).

As expected, the average friction coefficient obtained by the Goldacker and Rautenbach models is not influenced by the depth of the groove channel. While in the Potente model it varies continuously, and in the Grünschloβ model it only varies when the value of h_N/b_N is below a certain value (in this case 0.06). From this value the average friction coefficient is the same as in the Goldacker model, this is because the equation used is the same (equations 237 and 258) when P_{Gesmin} tends towards the unit.

The studies carried out made it possible to draw the following conclusions: i) in the Goldacker and Potente models, the average friction coefficient does not vary with the slot configurations; ii) in the Rautenbach model this variation is random, and for the number of grooves below 6 the average friction coefficient is lower than the polymer-cylinder friction coefficient; iii) the Grünschloβ model produces slight variations with the number of grooves; iv) the average friction coefficient is strongly influenced by the total width of the grooves (B), as can be seen in Table 6, all models include this factor, the increase in the average friction coefficient is proportional to the increase in B.

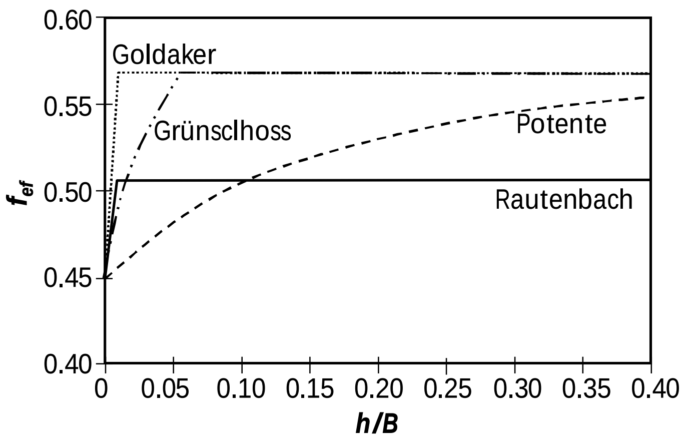

Figure 80- Coefficient of average friction versus depth of grooves

Table 6- Coefficient of friction as a function of B for the various models.

Model	***B* (mm)**	**f_{ef} (maximum)**
Goldacker	48/60/72	0.544/0.567/0.591
Potente	48/60/72	0.537/0.554/0.569
Rautenbach	48/60/72	0.491/0.505/0.519
Grünschloβ	48/60/72	0.544/0.568/0.591

Influence on the global process

A higher coefficient of average friction in the zone of transport of solids with grooves, implies a generation of greater pressure in this zone, and as a consequence a greater flow. For this reason, the models that provide a higher average friction coefficient (Goladcker and Grünschloβ) also result in a higher output and develop a higher pressure (Table 7).

Table 7- Flow rate obtained with the various models.

Model	**Q (kg/hr)**	**P_{max} (MPa)**
No grooves	8.06	48.2
Goldacker	8.32	80.1
Potente	8.07	56.1
Rautenbach	8.07	52.2
Grünschloβ	8.17	72.3

4.2. Mixing sections

Dispersive mixing sections

Among the solutions available, here, due to their practical importance, two types of sections are considered: Torpedo (Figure 81) and Maddock (Figures 82 and 83). Mixing sections like Maddock can have channels parallel to the axis (Figure 82) or inclined - Union Carbide (Figure 83). The equations to be used for these two cases are the same, as long as the angle of inclination, in the first case, is considered to be zero.

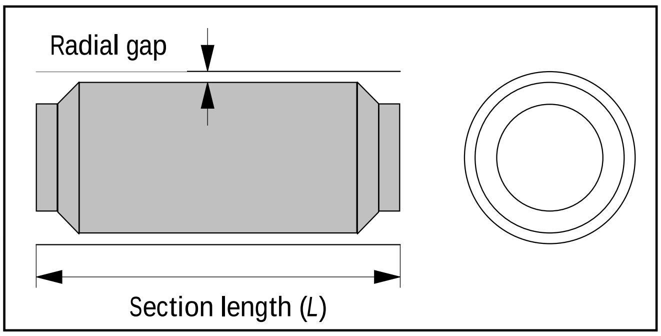

Figure 81- "Torpedo" mixing section

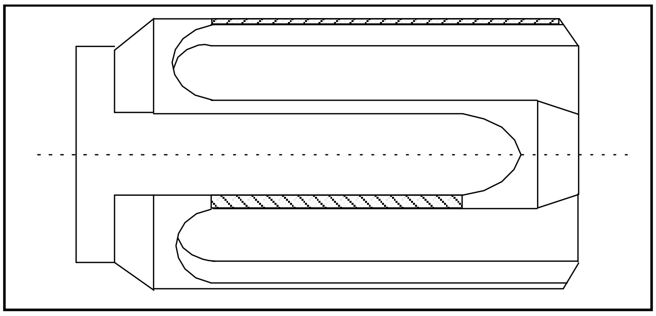

Figure 82- "Maddock" mixing section

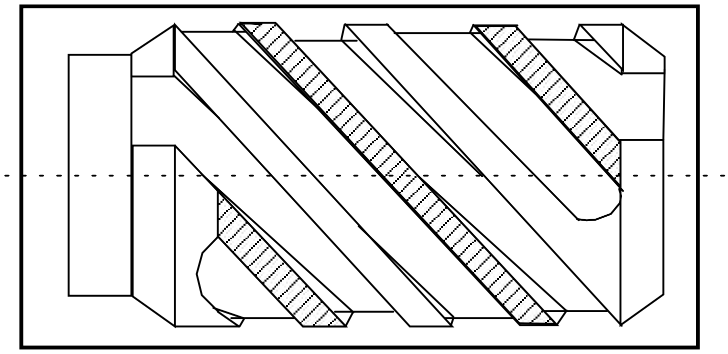

Figure 83- "Union Carbide" mixing section

The simplifications used to simulate the flow in this type of sections are identical to those used in normal screw sections [TAD 70], that is, it is considered that the cylinder rotates and the section is stopped and the unrolled channels are imagined (Figure 84).

According to Rauwendaal [RAU 86], considering that the effect of the screw's rotation velocity on viscosity cannot be neglected, the pressure drop in a torpedo section will be:

$$\Delta P = (q+r)^{1/3} + (q-r)^{1/3} \qquad \textbf{(259)}$$

where:

$$q = \frac{40 k_0^3 \, \Delta L \, Q}{\pi \, D_c \, \delta_T^3} \qquad \textbf{(260)}$$

$$r = \left(q^2 - t^2\right)^{1/3} \qquad \textbf{(261)}$$

$$t = \frac{-20 \tau_T^2 \, \Delta L^2}{9 \delta_T^2} \qquad \textbf{(262)}$$

$$\tau_T = k \left(\frac{V_b}{\delta_T} \right)^n \qquad \textbf{(263)}$$

where ΔL is the longitudinal section length (Figure 81), δ_T is the gap between the cylinder and the section, Q is the volumetric flow rate and τ_T is the shear stress in the gap.

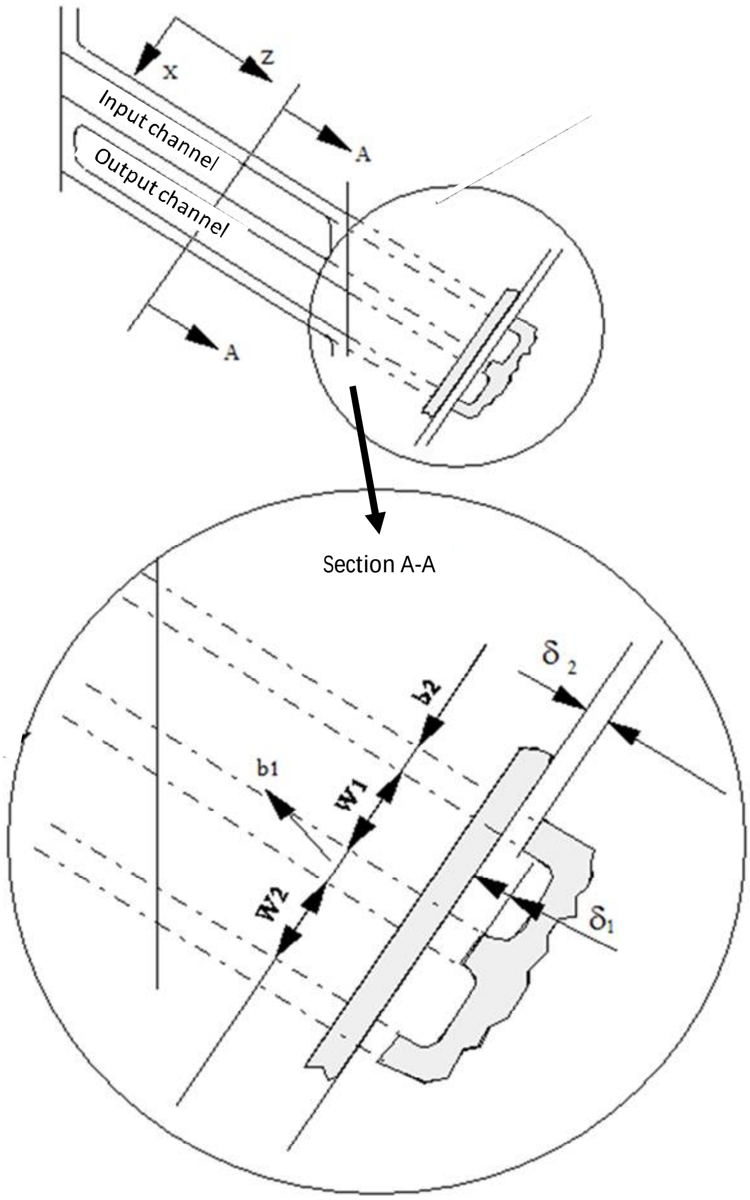

Figure 84- Geometric parameters of a "Maddock" section

For the geometry shown in Figure 84, Tadmor and Klein [TAD 70] proposed the following expressions:

$$\Delta P = P(0)\left[1-\overline{P}^*(1)\right] \quad \textbf{(264)}$$

$$\overline{P}^*(1) = \overline{P}^*(0) - \left(\frac{1-\Psi_4-\Psi_5}{\Psi_2}\right) + \frac{\Psi_1}{\Psi_2}\left[1-\overline{P}(1)\right] \quad \textbf{(265)}$$

$$\overline{P}^*(0) = \frac{\Psi_0 - 1}{\Psi_3} + 1 - \frac{R_1}{\Psi_3}\left(e^{-\sqrt{\alpha}} + \sqrt{\alpha} - 1\right) - \frac{R_2}{\Psi_3}\left(e^{\sqrt{\alpha}} - \sqrt{\alpha} - 1\right) \quad \textbf{(266)}$$

$$\overline{P}(1) = 1 - \frac{1}{\Psi_1}\left[\frac{\left(1-\frac{2\beta}{\alpha}\right)\left(1-e^{-\sqrt{\alpha}}\right)}{\sqrt{\alpha}\left(1+e^{-\sqrt{\alpha}}\right)} - \Psi_4 + \frac{\beta}{\alpha}\right] \quad \textbf{(267)}$$

Being $P(0)$ the pressure at the beginning of the input channel and Ψ_0, Ψ_1, Ψ_2, Ψ_3, Ψ_4, Ψ_5, α, β, R_1, R_2 and R_3 constants which depend on the geometry of the system and the operating conditions, the values of which can be calculated using the following equations:

$$\Psi_0 = \frac{\pi N D_c L}{2Q(0)}\left(\delta_1 - \delta_2\right) \quad \textbf{(268)}$$

$$\Psi_1 = \frac{W_1\ H_1^3\ P(0)\ F_{P1}\ \cos\varphi}{12\,\eta_1 Q(0)\ L} \quad \textbf{(269)}$$

$$\Psi_2 = \frac{W_2\ H_2^3\ P(0)\ F_{P2}\ \cos\varphi}{12\,\eta_2 Q(0)\ L} \quad \textbf{(270)}$$

$$\Psi_3 = \frac{P(0)L}{12\cos\phi Q(0)}\left(\frac{\delta_1^3}{\eta_3 b_1} + \frac{\delta_2^3}{\eta_4 b_2}\right) \quad \textbf{(271)}$$

$$\Psi_4 = \frac{\pi N D_c \sin\varphi\, W_1\ H_1\ F_{D1}}{2Q(0)} \quad \textbf{(272)}$$

$$\Psi_5 = \frac{\pi N D_c \sin\varphi\, W_2\ H_2\ F_{D2}}{2Q(0)} \quad \textbf{(273)}$$

$$\alpha = \Psi_3\left(\frac{1}{\Psi_1} + \frac{1}{\Psi_2}\right) \quad \textbf{(274)}$$

$$\beta = \frac{\Psi_3}{\Psi_2}\left(1 - \Psi_5 + \frac{\Psi_2\ \Psi_4}{\Psi_1}\right) \quad \textbf{(275)}$$

$$R_1 = \frac{1 - \frac{\beta}{\alpha}\left(1-e^{-\sqrt{\alpha}}\right)}{1-e^{-2\sqrt{\alpha}}} \quad \textbf{(276)}$$

$$R_2 = \frac{1 - \frac{\beta}{\alpha}\left(1-e^{-\sqrt{\alpha}}\right)}{1-e^{+2\sqrt{\alpha}}} \quad \textbf{(277)}$$

$$R_3 = \frac{\beta}{\alpha} \qquad \textbf{(278)}$$

where: D_c is the diameter of the cylinder, F_{D1} and F_{D2} are the form factors of the input and output channels, H_1 and H_2 are the depth of the input and output channels, L is the axial length of the section and η_1, η_2, η_3 e η_4 are the apparent viscosities in the inlet and outlet channels and on barriers 1 and 2.

Distributive mixing sections

Taking as an example a "Pineapple" mixing section (Figure 85), we will also try to predict the pressure drop and the temperature increase along the length of the device. For this purpose, the channels are considered to be rectangular, as shown in Figure 86 [PIT 82].

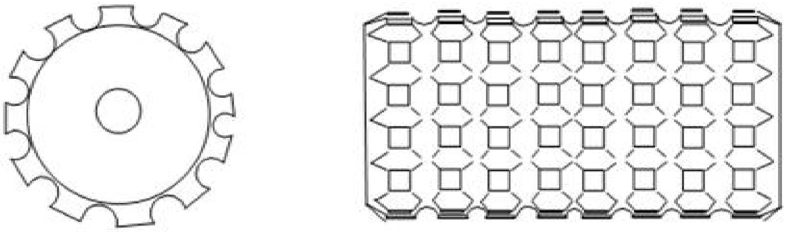

Figure 85- "Pineapple" mixing section

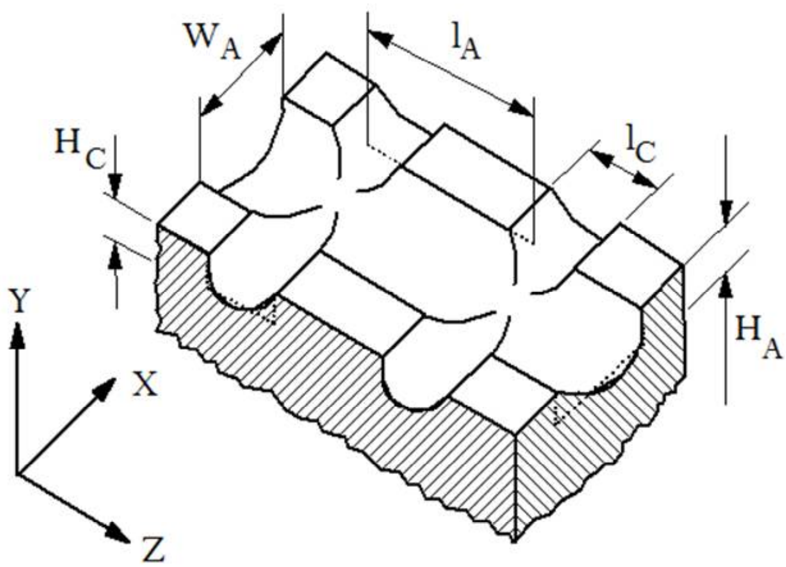

Figure 86- Simplified geometry of a "Pineapple" section

Thus, the total pressure drop in the device is [PIT 82]:

$$\Delta P = \Delta P_A + \Delta P_C \qquad \textbf{(279)}$$

$$\Delta P_A = \frac{12\,\bar{v}_A\,\bar{\eta}_A\,\bar{L}_A}{H_A^2\,F} \qquad \textbf{(280)}$$

$$\Delta P_C = \frac{12\,\overline{v}_C\,\overline{\eta}_C\,\overline{L}_C}{H_C^2\,F} \tag{281}$$

$$v_A = \frac{Q}{W_A\,H_A\,N_A} \tag{282}$$

$$v_C = \frac{Q}{2\,\pi\,R\,H_C} \tag{283}$$

$$\dot{\gamma}_A = \left(\dot{\gamma}_{PA}^2 + \dot{\gamma}_{DA}^2\right)^{1/2} \tag{284}$$

$$\dot{\gamma}_C = \left(\dot{\gamma}_{PC}^2 + \dot{\gamma}_{DC}^2\right)^{1/2} \tag{285}$$

$$\dot{\gamma}_{PA} = \frac{3\,\overline{v}_A}{H_A} \tag{286}$$

$$\dot{\gamma}_{PC} = \frac{\overline{v}_C}{H_C} \tag{287}$$

$$\dot{\gamma}_{DA} = \frac{10\,\pi}{3}\frac{R\,N}{H_A} \tag{288}$$

$$\dot{\gamma}_{DC} = \frac{2\,\pi\,R\,N}{H_C} \tag{289}$$

$$F = 1 - 0.6\frac{H_A}{W_A} \tag{290}$$

of which: ΔP_A is the total pressure drop in the axial channels, ΔP_C is the total pressure drop in the circumferential channels, $\overline{v}_A$ is the average speed in the axial channels, $\overline{v}_C$ is the average speed in the circumferential channels, $\overline{\eta}_A$ and $\overline{\eta}_C$ are the average viscosities in the axial and circumferential channels, calculated at shear rate $\dot{\gamma}_A$ and $\dot{\gamma}_C$, respectively, $\dot{\gamma}_{PA}$ and $\dot{\gamma}_{PC}$ are the shear rates in axial and circumferential channels due to pressure drop, $\dot{\gamma}_{DA}$ e $\dot{\gamma}_{DC}$ are the shear rates in axial and circumferential channels due to drag flow, L_A and L_C are the total lengths for each type of channels, obtained from l_A and l_C (Figure 86) and taking into account the number of channels in either direction, W_A and W_C are the widths for each type of channel, H_A and H_C are the depths for each type of channel, F the factor that takes into account the fact that the channel width is finite and R the external radius of the device

The average temperature is given by:

$$\overline{T} = \frac{T_{IN} + T_{OUT}}{2} + \Delta T \qquad \textbf{(291)}$$

where ΔT is calculated from:

$$\Delta T = \frac{H^2}{k\,V} \; \frac{\overline{\eta}_A \, \dot{\gamma}^2 \, \tau_A + \overline{\eta}_C \, \dot{\gamma}^2 \, \tau_C}{t_A + t_C} \qquad \textbf{(292)}$$

$$t_A = \frac{L_A}{\overline{v}_A} \qquad \textbf{(293)}$$

$$t_c = \frac{L_C}{\overline{v}_C} \qquad \textbf{(294)}$$

of which: V is the dimensionless number of viscous heating (it was found experimentally to be 25 for polyethylene and polystyrene) [PIT 82], T_{IN} is the melt temperature at the beginning of the section, T_{OUT} is the melt temperature at the end of the section and t_A e t_C are the mean residence times in the axial and circumferential channels, respectively.

4.3. Rotational barrel segment

Whit the aim of improving the performance of the plasticizing process Sikora and co-authors [SIK_R 98, SIK 06a, SIK 06b, SAS 08] proposed the use of a rotational barre segment in the metering zone of an extruder, *i.e.*, when the polymer is totally melted.

This is a new area of development that concerns with a rotational barrel segment (RBS) rotating in the same or opposite direction as the screw. The rotational barrel segment, fitted with intensifying grooves of torsional angle and torsional direction, can be a vital element of plasticizing system. It is a complete novelty that has not been described in literature or used in the existing extruders, except in some work developed by the team [SIK 06a, SIK 06b, SAS 08].

Changing the rotational speed of the grooved barrel segment as well as the direction of its rotation during the extrusion process will enable to influence the thermal, rheological, kinematic and dynamic conditions in the plasticizing system of the new extruder. Due to that behavior, it will be possible to efficiently control the extrusion process and to improve the quality of the products obtained because enhancing the above processes will result in the homogenization of the thermal and mechanical properties of materials and the structure of the products, without the need to use additional, expensive devices such as the gear pump and static mixer. This will be of utmost importance for polymer processing industry, as well as for food, cosmetics and pharmaceutical industries.

To implement the presence of the rotational barrel segment in the modeling program presented in this notes it is only necessary to take into account how the velocity is taking into account. Figure 87 shows the three different situations that can occur when an RBS is implemented in an extruder: a) the velocity of the RBS (N_b) is nil; b) the velocity of the RBS has the same direction than that of the screw (N_s) and c) the velocity of the RBS has a different direction than that of the screw.

In the first case the relative barrel velocity (V_b) results by transforming the rotational screw speed (N_s) in a linear velocity near the interior barrel velocity (this is: $V_b = \pi\, N_s\, D$, where D is the external screw diameter). In the second case the resulting (V'_b) velocity is reduced, while in the third the resulting velocity increases. This velocity will replace the velocity of the screw (V_c) in the location of the RBS.

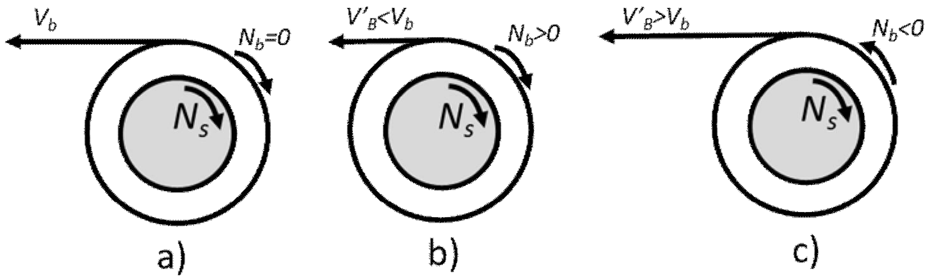

Figure 87- Definition of the relative barrel velocity (V'_b)

5. References

[AGA 96] J.F. Agassant, P. Avenas, J. Sergent, La Mise en Forme des Matiéres Plastiques, Lavoisier, 3rd edition, Paris (1996).

[AME 88] K. Amellal, B. Elbirli, Performance study of barrier screws in the transition zone, Polym. Eng. Sci., 28, 311 (1988).

[BAR 71] R. Barr, U.S. Patent, 3,698,541 (1971).

[BIG 73] D.M. Bigg, Mixing in a Single Screw Extruder, Ph. D. Thesis, University of Massachusetts (1973).

[BIG 74] D.M. Bigg, S. Middleman, Mixing in a Screw Extruder. A Model for Residence Time Distribution and Strain, Ind. Eng. Chem. Fundam., 13, pp. 66-71 (1974).

[BOE 90] D. Boes, A. Krämer, V. Lohrbäccher, A. Scheneiders, 30 Years of the Grooved Bush Extruder, Kunststoffe Germ. Plast., 80, pp. 659-664 (1990).

[BRO 70] R. L. Brown, J. C. Richards, Principles of Powder Mechanics, Pergamon Press, New York (1970)

[BRO 72] E. Broyer , Z. Tadmor, Solids Conveying in Screw Extruders – Part I: A modified Isothermal Model, Polym. Eng. Sci., 12, pp. 12-24 (1972).

[CAR 53] J.F. Carley, R.S. Mallouk, J.M. Mckelvey, Simplified flow theory for screw extruders, Ind. Eng. Chem., 45, 5, 974 (1953)

[CHU 71] C.I. Chung, Plasticating Single-Screw Extrusion Theory, Polym. Eng. Sci., 11, pp. 93-98 (1971).

[CHU 75] C.I. Chung, Maximum Pressure Developed by Solid Conveying Force in Screw Extruders, Polym. Eng. Sci., 15, pp. 29-34 (1975).

[CHU 10] C.I. Chung, Extrusion of Polymers: Theory & Practice, 2nd Edition, Hanser, Munich (2010).

[DAR 56] W.H. Darnell, E.A.J. Mol, Solids Conveying in Extruders, SPE J., 12, pp. 20-29 (1956).

[DEK 76] J. Dekker, Kunststoffe-Ger. Plast., 66, 130 (1976)

[DRA 70] R.F. Dray, D.L. Lawrence, U.S. Patent, 3,650,652 (1970).

[ELB 84] B. Elbirli, J.T. Lindt, S.R. Gottgetreu, S.M. Baba, Mathematical Modelling of Melting of Polymers in a Single-Screw Extruder, Polym. Eng. Sci., 24, pp. 988- 999 (1984).

[FEN 77] R.T. Fenner, Developments in the Analysis of Steady Screw Extrusion of Polymers, Polymer, 18, pp. 617-635 (1977).

[FEN 79] R.T. Fenner, Principles of Polymer Processing, McMillan, London (1979).

[GAS 09] A. Gaspar-Cunha, Modelling and Optimisation of Single Screw Extrusion, PhD Thesis, University of Minho, Guimarães, Lambert Academic Publishing, Koln (2009).

[GAS 14a] A. Gaspar-Cunha, J.A. Covas, The Plasticating Sequence in Barrier Extrusion Screws Part I: Modeling. Polym. Eng. and Sci., 54, pp. 1791–1803 (2014).

[GAS 14b] A. Gaspar-Cunha, J.A. Covas, The Plasticating Sequence In Barrier Extrusion Screws Part II: Experimental Assessment. Polym.-Plast. Technol. and Eng., 53, pp. 1456–1466 (2014).

[GAM 99] E. Gamache, P.G. Lafleur, C. Peiti, B. Vergnes, Measurement of the Coefficient of Dynamic Friction at Extrusion Processing Conditions, Polym, Eng, and Sci., 39, pp. 1604- 1613 (1999).

[GOL 71] E. Goldacker, Untersuchungen zur Inneren Reibung von Pulvern, Insbesondere in Hinblick auf Die Förderung in Extrudern, Diss. RWTH Aachen, 1971.

[GRÜ 84] E. Grünschloss, Calculation of the Mean Coefficient of Barrel Friction in Grooved Feed Sections, Kunsttoffe Germ. Plast., 74, pp. 405-409 (1984).

[HAN 96] C.D. Han, K.Y. Lee, N.C. Wheeler, Plasticating Single-Screw Extrusion of Amorphous Polymers: Development of a Mathematical Model and Comparison with Experiment, Polym. Eng. Sci., 36, pp. 1360-1376 (1996).

[HUA 93] H.X. Huang, Y.C. Peng, Theoretical Modelling of Dispersive Melting Mechanism of Polymers in an Extruder, Adv. Polym. Techn., 12, pp. 343-352 (1993).

[HYU 90] K.S. Hyun, M.A. Spalding, Bulk Density of Solid Polymer Resins as a Function of temperature and Pressure, Polym. Eng. Sci, 30, pp. 571- 576 (1990).

[ING 80] J.F. Ingen Housz, U.S. Patent, 4,218,146 (1980).

[ING 81] J.F. Ingen Housz, H.E.H. Meijer, Polym. Eng. Sci., 21, 352 (1981).

[KAC 72] L. Kacir, Z. Tadmor, Solids Conveying in Screw Extruders – Part III: The Delay Zone, Polym. Eng. Sci., 12, pp. 387-395 (1972).

[KAM 83] M. R. Kamal, V. Tan, and F. Kashani, The Thermal Conductivity and Diffusivity of Polyethylene Solids and Melts,' Adv. Polym. Technol., 3, pp. 89–98 (1983).

[KIM 72] H.T. Kim, U.S. Patent, 3,867,079 (1972).

[LEE 90] K.Y. Lee, C.D. Han, Analysis of the Performance of Plasticating Single-Screw Extruders with a New Concept of Solid-Bed Deformation, Polym. Eng. Sci., 30, pp. 665-676 (1990).

[LIN 85] J.T. Lindt, B. Elbirli, Effect of the Cross-Channel Flow on the Melting Performance of a Single-Screw Extruder, Polym. Eng. Sci, 25, pp. 412-418 (1985).

[MAD 59] B.H. Maddock, A Visual Analysis of Flow and Mixing in Extruder, Soc. Plast. Engs. J., 15, pp. 383-394 (1959).

[MAI 59] C. Maillefer, Swiss Patent, 363,149 (1959).

[McK 62] J.M. Mckelvey, Polymer Processing, John Wiley & Sons, New York (1962)

[MEN 67] G. Menges, P. Klenk, Kunststoffe-Ger. Plast., 57, 590 (1967)

[MIC 14] Michelangelli, O. P., Gaspar-Cunha, A., & Covas, J. A. (2014). The influence of pellet-barrel friction on the granular transport in a single screw extruder. Powder Technology, 264(9), 401–408.

[MIT 80] A.R. Mitchell, D.F. Griffiths, The Finite Difference Method in Partial Differential Equations, John Wiley & Sons, Chichester (1980).

[NED 82] R.M. Nedderman, S.B. Savage, U. Tuzun, G.T. Houlsby, Flow of granular materials. Part 1: discharge rates from hoppers: review, Chem. Eng. Sci., 37, 112, 1597 (1982)

[O´BR 92] K. O´Brian, Computer Modelling for Extrusion and Other Continuous Polymer Processes, Carl Hanser Verlag, Munich (1992).

[PIN 70] G. Pinto, Z. Tadmor, Mixing and Residence Time Distribution in Melt Screw Extruders, Polym. Eng. Sci., 10, pp. 279-288 (1970).

[PIT 82] J.F.T. Pittman, G.L. Pittman; Polymer Ext. III-PRI Conference, 19 (1982)

[POT 85] H. Potente, Methods of Calculating Grooved Extruder Feed Sections, Kunststoffe Germ. Plast., 75, pp. 439-441 (1985).

[POT 88] H. Potente, The Forced Feed Extruder Must be Reconsidered, Kunststoffe Germ. Plast., 78, pp. 355-363 (1988).

[POT 89] H. Potente, M. Koch, New Aspects in the Design of Extruders with a Forced Feeding Section, Int. Polym. Process., 4, pp. 208-218 (1989).

[RAUT 82a] R. Rautenbach, H. Peiffer, Model Calculation for the Design of the Grooved, Feed Section of Single-Screw Extruders, Kunststoffe Germ. Plast., 72, pp. 137-143 (1982).

[RAUT 82b] R. Rautenbach, H. Peiffer, Throughput and Torque Characteristics of Grooved Feed Sections in Single-Screw Extruders, Kunststoffe Germ. Plast., 72, pp. 262-266 (1982).

[RAU 86] C. Rauwendaal, Polymer Extrusion, Hanser Publishers, Munich (1986)

[SAS 08] E. Sasimowski, Characteristics of an extrusion process with a rotating sleeve of the barrel. Polimery, 53, 1, p. 47 (2008)

[SAS 14] E. Sasimowski, J.W. Sikora, B. Królikowski, Effectiveness of polyethylene extrusion in a single-screw grooved feed extruder, Polimery, 59, 6, pp. 505-510 (2014)

[SHA 88] P.A. Shamlou, Handling of Bulk Solids, Butterworth & Co. (1988)

[SIK 01] J.W. Sikora, The effect of the feed section groove taper angle on the performance of a single-screw extruder, Polymer Engineering and Science, 41, 9, pp. 1636-1643 (2001)

[SIK 06a] J.W. Sikora, E. Sasimowski, Verfahrenseinheit mit rotierendem Zylinderbereich. Kunststoffe, 96, 7, p. 104 (2006)

[SIK 06b] J.W. Sikora, E. Sasimowski, Processing Unit with Rotating Cylinder Segment. Kunststoffe International, 9, p. 1 (2006)

[SIK 13a] J.W. Sikora, B. Samujło, Impact of Feed Opening Width and Position on PVC Extrusion Process Effectiveness, International Polymer Processing, 9, 5, pp. 291-299 (2013)

[SIK 13b] J.W. Sikora, B. Samujło, J. Dzwonkowski, Influence of a Feed-Opening Section on the Output and Selected Mechanical Properties of a Poly(Vinyl Chloride) Extrudate, Advances in Polymer Technology, 33, 1, pp. 1-7 (2013)

[SIK 14] J. Sikora, B. Samujło, Investigation of the poly(vinyl chloride) extrusion process using a feed throat with a feed pocket" Polymer Engineering and Science, 54, 9, pp. 2037-2045 (2014)

[SIK_R 98] Sikora R., Sikora J. W.: Barrel of an extruder. Polish Patent No 185728 (1998)

[STE 95] M.J. Stevens, J.A. Covas, Extruder Principles and Operation, 2nd ed., Chapman & Hall, London (1995).

[TAD 67] Z. Tadmor, I.J. Duvdevani, I. Klein, Melting in Plasticating Extruders - Theory and Experiments, Polym. Eng. Sci., 7, pp.198- 217 (1967).

[TAD 70] Z. Tadmor, I. Klein, Engineering Principles of Plasticating Extrusion, Van Nostrand Reinhold, New York (1970).

[TAD 72] Z. Tadmor, E. Broyer, Solids Conveying in Screw Extruders – Part II: Non Isothermal Model, Polym. Eng. Sci., 12, pp. 378-386 (1972).

[TAD 06] Z. Tadmor, C.C. Gogos, Principles of Polymer Processing, 2nd Edition, Wiley-Interscience, New Jersey (2006)

[WAL 66] D.M. Walker, An Approximate Theory for Pressures and Arching in Hoppers, Chem. Eng. Sci., 21, pp. 975-997 (1966).

[WHI 90] J.L. White, Twin Screw Extrusion; Technology and Principles, Hanser, Munich (1990).

[ZIE 83] O.C. Zienkiewicz, K. Morgan, Finite Elements and Approximation, John Wiley & Sons, New York (1983).